FINAL REPORT

METEOROID HAZARDS IN DEEP SPACE

Prepared under Contract NAS 9-8104

May 1, 1970

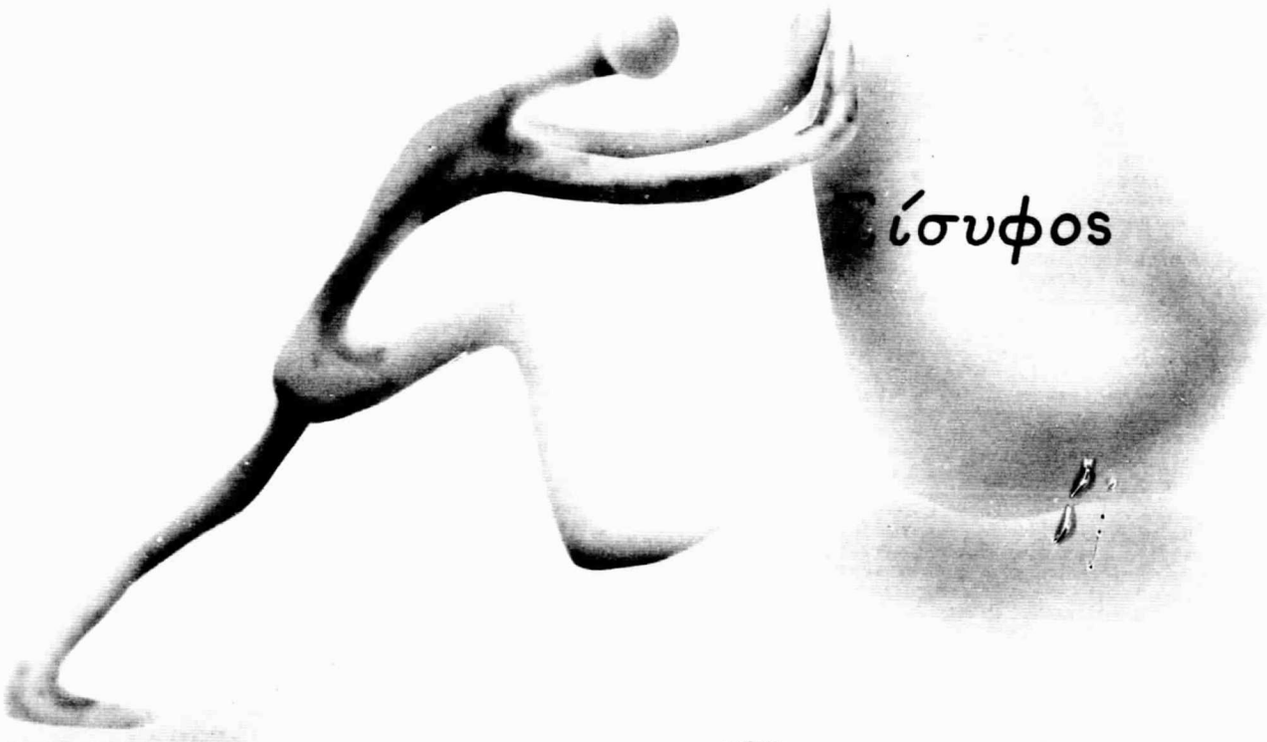

S. Chandra
S. Neste
R. Soberman
G. Zomber

SPACE SCIENCES LABORATORY

GENERAL ELECTRIC
SPACE DIVISION

FINAL REPORT

METEOROID HAZARDS IN DEEP SPACE

Prepared under Contract NAS 9-8104

May 1, 1970

S. Chandra
S. Neste
R. Soberman
G. Zomber

TABLE OF CONTENTS

1.0 Introduction (Statement of Work)

The purpose of the Deep Space Meteoroid Hazard Measurements Program is to describe the tasks required of the contractor and to present the technical framework within which they will be performed.

1.1 Background

The meteoroid population in interplanetary space is inferred from the results of earth based observations of meteors in the atmosphere, direct measurements by sensors on orbital satellites, and from measurements of the reflected and refracted sunlight from the asteroids and cosmic dust. Meteoroid measurements in deep space to date have been limited to the results obtained from small sensors placed on a few U.S. and Soviet probes. The information obtained is pertinent to cosmic dust and any attempt to sample the population of larger meteoroids is hampered by the need for very large and heavy sensors. Thus, the largest meteoroid detected by the Pegasus satellites which deployed 2000 square feet of sensor area in earth orbit was approximately 10^{-6} grams or 0.15 mm in diameter. Undoubtedly, larger meteoroids could have been detected if the sensor threshold could have been increased which was precluded by payload limitations.

The detection and measurement of meteoroid properties by an optical system using reflected sunlight overcomes the weight and detection threshold limitations of the conventional impact sensors by permitting a large detection area to system weight ratio.

1.2 Objectives

Part I (Design Study)

a. Formulation of the equations for a Sisyphus system of generalized geometry and performance of an error analysis to consider the effects of misalignment of the optical systems and errors in measuring transit times through the fields of view.

b. Analytical consideration of a Sisyphus system consisting of two operating optical detection systems, to determine what parameters of a traversing meteoroid can be determined.

c. Improvement of the illuminated particle simulation system and demonstration to produce a spot representative of the light scattered by a 1 mm diameter meteoroid travelling at 15 km/sec at a range of 1 km.

d. Performance of optical tests on available electroformed aluminum mirrors to determine the accuracy with which they must be con-

structed and the feasibility of using them in an operational system.

e. Investigation of problems introduced by low values of signal to noise ratio and detection thresholds required to minimize triggering by false signals.

Part II (Breadboard Fabrication)

a. Construction of a three channel breadboard model incorporating the Sisyphus concept and demonstration of its ability to detect simulated meteoroids.

a.1 It was not necessary to demonstrate the telemetry signal conditioning and shift register in the breadboard stage. However, it was required to examine the problems inherent in these subsystems and to describe them analytically. Only signal conditioning, telemetry and power need be considered in terms of accuracy, bit requirements, etc., that are necessary to return the sensor output data to Earth in sufficient detail to perform the analysis determined in Part I (Design Study).

a.2 The breadboard model need not be configured mechanically to any specific spacecraft application but must be capable of recording simulated meteoroids. It would show that a prototype instrument can be constructed (utilizing the same electrical and optical properties) which possesses physical characteristics consistent with spacecraft experiment packaging.

1.3 Period of Performance

The period of performance for the above work was 15 months, starting 24 June 1968.

1.4 Modifications

1.4.1 The statement of work was modified to include:

a. A careful evaluation of the state of the art of light-weight plastic and metallic mirrors to determine realizable surface accuracies and their resulting image aberrations.

b. A detailed trade-off study in which optical aberrations introduced by fast wide angle optics must be considered in opposition to electronic or statistical uncertainties introduced by slower, narrower angle optics (aperture being held fixed).

c. Assembly of the Sisyphus breadboard with a complete set of optimum light-weight optics similar in size to the type proposed for the Jupiter F/G mission (GE Proposal GE N-11031, 1968); this set of optics to be tested experimentally for edge-of-field spot size and spot intensity, and the results of the test presented.

d. Test of the breadboard complete with optics against simulated meteoroids of the size, velocity, and range which would be anticipated in flight. The simulation to be carried out with a lighting background equivalent in intensity to the expected background for the Jupiter F/G mission.

e. A detailed report on the performance of the breadboard including the light-weight optics.

f. A final report containing a detailed error analysis.

1.4.2 The period of performance was extended to 3 May 1970.

2.0 Work Accomplished

Following is the Final Report of work performed during the contract, and results obtained. An attempt has been made to organize the report in accordance with the Work Statement.

2.1 Sisyphus Mathematics

The equations for a Sisyphus system of generalized geometry are provided in Appendix 1. Also given is a two-cone solution which shows that once a reliable flux rate is established, two optical systems can still provide useful information.

2.2 Instrument Orientation and Viewing Angle

Effects of orientation and viewing angle were investigated in detail. The results are given in Appendix 2.

2.3 Laboratory Simulation

Simulation of the illuminated particle was performed rather simply, using a CW laser. The laser beam passes through a small focusing telescope and is deflected by a mirror mounted on a motor shaft. Target is a sheet of Bristol board, viewed by the Sisyphus optics. Rotating the mirror then permits sweeping of the laser light spot through the Sisyphus fields of view at various velocities. 15 km/s at 1 km range = 15 rad/s or about 144 rps. Physical limitations prevented actual measurement at 1 km range. The distance which could be accommodated in the laboratory was about 20 feet. In order to simulate particle brightness, neutral density filters were used. Optical spacing was reduced to six (6) inches; closer spacing was not feasible due to physical limitations.

2.4 Optics

2.4.1 General Description of the Optical Fabrication Technique

The optics consisted of mirrors produced at Zolomatics, Inc., Hollywood, California by replication technique, This is an inexpensive method for producing replicas of mirrors. In this technique, aluminum replicas are electro-deposited directly on the master mold. The aluminum mirror is then coated with an epoxy resin of closely-matched thermal characteristics; a precisely formed aluminum backing dish is placed over the epoxy-coated mirror surface. After the epoxy resin has cured, the sandwich is separated from the master under vacuum by applying slight pressure.

The advantage of the replication technique is that the resulting optical components are very light and, even in relatively small quantities, are less expensive than optical components individually ground and polished by conventional methods.

This cost advantage becomes possible because the general shape of the supporting backing can be formed to within a thousandth of an inch (about fifty times the wavelength of the visible light) by stamping and annealing or on a lathe, while the expensive job of bringing the shape to within a fraction of a wavelength is eliminated by the replication technique in which, in essence, the residual irregularities of the backing are filled in with the bonding material.

The reduction in weight is achieved by reducing the thickness of the backing to a minimum commensurate with the structural (mechanical and vibration) requirements. Fabrication of light-weight optics using replication involves three aspects:

a. fabrication of light-weight backing to correct radius of curvature and shape (to a thousandth of an inch)

b. grinding of the glass masters

c. replication of a coating on the masters to achieve the required optical quality figure.

In the case of the Sisyphus optical system, however, the major consideration was the fact that the replication techniques make it possible to meet the extraordinarily stringent weight requirements for Pioneer F/G. Accordingly, a test program was undertaken to develop and perfect the technique of making such replicated mirrors on very thin aluminum backing using an easily-tested spherical mirror design.

The results presented in this report are based upon the developmental, light-weight, spherical mirrors provided by Zolomatics and used for the breadboard system.

2.4.2 Sisyphus Breadboard Optics

a. Physical description

The breadboard optics consist of spherical mirrors replicated over a backing dish formed of very thin aluminum sheet (0.020 inch thickness). These mirrors have a diameter of 6 inches; the radius of curvature is 7.669 inches (therefore, focal length = 3.835 inches). The optical surfaces of the mirrors have a microinch thick gold coating to improve the reflectivity for light in the visible region of the spectrum.

Weight of these mirrors varied between 36 and 38 grams.

b. Development of the backing

The initial attempts were made with stamped aluminum backing dishes which did not have any reinforcing structure. These turned out to be too flimsy and easily deformable because of their very small thickness. Therefore, to improve strength without adding significantly to the weight, it was decided to bend the edge of the mirror to form a rim. The mirror formed in this manner has greater structural stability against deformation. However, these mirrors still have anomalities because of the stresses in the aluminum sheets due to unidirectional rolling in the manufacture of the aluminum sheets. As a result of these stresses, some of the spherical mirrors used for the breadboard actually have a somewhat spheroidal shape, and the images were astigmatic. These internal stresses will be removed from the final version of the optics for Pioneer by repeated stamping and annealing cycles.

c. Optical performance tests of the breadboard optics

As stated earlier, the breadboard optics consisted of 6-inch diameter, 3.835 inch focal length spherical mirrors. As is well known, the two conjugate foci of a spherical mirror coincide at the center of curvature of the mirror. In other words, if the spherical mirror is perfect, a very small object at the center of curvature of the mirror is perfectly imaged back at the center of curvature. (The image quality that we are concerned with in the present context is much lower than the diffraction effects of finite aperture size. Consequently, we shall not make any mention of such diffraction effects in this report). Therefore, we used this principle for testing of the spherical mirrors as described on the following page.

The schematic set-up is illustrated in figure 2.4.2.c. Light from a light source, S, passes through a very small aperture, A, (1 mm diameter) and is collected by an f/0.95 one-inch focal length Angenieux lens, L, and then brought to focus at C. The image of the aperture, A, is reduced sixteen times and, due to high quality of the Angenieux lens, becomes essentially a point (~60 microns) at C. Because of the small f-ratio (f/0.95) of the lens, the fan of rays spreading from C is wide enough to cover the entire spherical mirror, M, when placed in such a way that point C is at its center of curvature. The whole set-up was mounted on a precision optical bench. The mirror was mounted at its center (vertex) on a goniometer head to provide precise angular adjustment along the horizontal and vertical planes. The goniometer head was then mounted on a vertical post whose height was micro-adjustable. Finally, the vertical post was on a precision carriage to provide micro-displacements in the longitudinal direction (along the optical axis). With the help of these adjustments, the spherical mirror to be tested was accurately aligned such that the center of curvature of the mirror was at point C, and the chief ray was parallel to (and coincident with) the optical axis of the mirror. Under these conditions, the spherical mirror forms the image, C', of C back onto itself. Due to reciprocity relationship, this image is then formed at I in the plane of aperture. In order to permit inspection of the image, I, the mirror was tilted very slightly with respect to the chief ray so that return image did not fall exactly over aperture A. If the mirror were perfect, the return image, I, would be equal to the size of the aperture, A. However, because of distortions in the surface of the mirror, the image spot size was much larger and could be easily visualized due to the large magnification realized through the Angenieux lens arrangement. When reduced to the image plane at C', the minimum spot size was 0.6 mm (~ 3 milliradians).

The very first mirrors received from Zolomatics, Inc. had, of course, a very much larger spot size. However, the rate of improvement, with successive mirrors received, confirmed the expectation that further improvements in the backing, by repeated annealing, will further reduce the spot size to a corresponding figure of about one milliradian, which was the goal when designing the optical system for the Pioneer mission.

d. Effect of low temperature on the mirrors

The effect of low temperature on the mirrors was examined by dipping one sample mirror in liquid nitrogen for about ten minutes and then allowing it to attain the room temperature. During the low

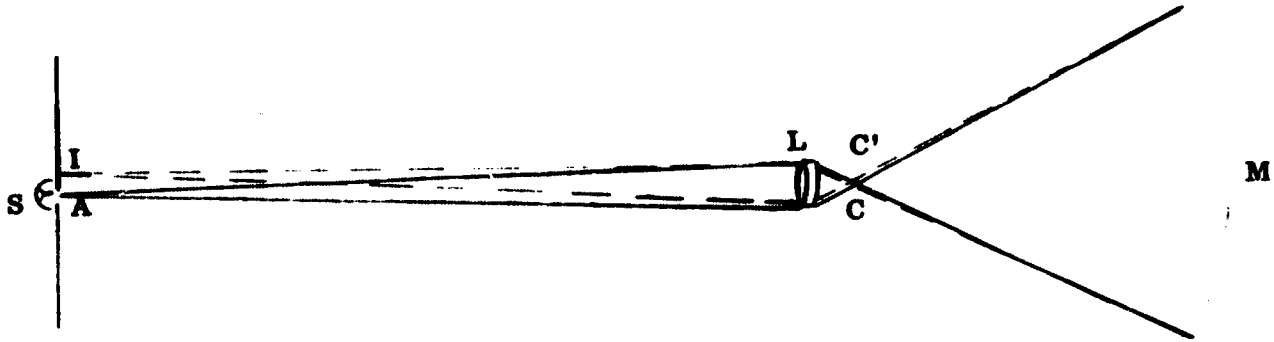

Figure 2.4.2.c Schematic of the Optical Set-up used for Testing of the Mirrors

temperature phase, there was a considerable amount of atmospheric water vapor condensation on the mirror. However, as the mirror once again attained the room temperature, the surface appearance and the reflectivity of the mirror was fully restored. During the low temperature test, as soon as the ice-coating cleared, no appreciable change in aberration was seen (relative to room temperature).

2.5 False Alarm Rate

False alarm rate at low signal-to-noise ratios was investigated, both theoretically and empirically. Details are provided in Appendix 3. The results show that a false alarm rate of 1 per month can be obtained with a S/N ratio of about 3.2 for a system of three optical channels:

a. System false alarm rate must not be greater than about one per month, i.e., about 2.5×10^6 seconds mean time between false events.

b. At 500 khz bandwidth, the circuit can respond to half-sine pulses; thus, noise pulses can occur at approximately 5×10^5/sec. Thus, the false alarm probability must be

$$P_{FA} \leq \frac{1}{2.5 \times 10^6 \cdot 5 \times 10^5} = 0.8 \times 10^{-12}$$

c. For a system response of 2 usec, a 3.2 usec pulse width (now required for coincidence) needs at least 1.6 noise pulses, i.e., 2 pulses overlapping. Thus, if P = probability of a pulse occurring, then $P^{1.6}$ = probability of overlap and $(P^{1.6})^3 = P^{4.8}$ = probability of overlapping pulses in three independent channels simultaneously.

d. $P_{FA \text{ each channel}} = \sqrt[4.8]{0.8 \times 10^{-12}}$

$$\doteq 3 \times 10^{-3}$$

but $$P_{FA} = e^{-1/2 (T/n)^2}$$

$$T/n \doteq 3.2$$

2.6 Breadboard Results

The breadboard model of Sisyphus was constructed. It was demonstrated on the 30th of January 1970. A large error in Z-axis velocity was obtained. As a result, a detailed error analysis was directed by the customer. This error analysis was performed (see Appendix 4); it shows

that the Z-axis velocity accuracy is extremely sensitive to relatively small values of angular misalignment of the optics. In the breadboard model, spherical mirrors were used whose fields and optical axes were difficult to determine (and, therefore, align). It is estimated that this accounts for the Z-axis error measured during the demonstration.

3.0 Conclusions and Recommendations

3.1 Conclusions

It has been established, both mathematically and through the breadboard design implementation, that the tri-optic measurement of small illuminated moving particles is practical. The resulting data can be interpreted without ambiguity.

3.2 Recommendations

Design and build flight-qualified hardware to obtain much-needed information on meteoroid matter and flux, in support of space probes and the manned space program.

This study was performed to lay the groundwork for the Pioneer F/G Asteroid/Meteoroid Experiment. The limitations of size, weight and power on the Pioneer spacecraft were stringent. For future missions, it has been shown desirable to increase the size of the optics, the spacing between optics, and the bandwidth and counting rate in the electronics. Such improvements will result in measurement of a larger range of particle sizes at greater distances and with increased accuracy.

APPENDIX 1

A. Light Reflection from Particles

In this section, we justify the approximation which was made in the equation (3)

$$I = \frac{I_O \, r \, \pi \, a^2}{5 \, \pi \, R^2 \, s^2} = \frac{I_\odot r}{5 s^2} \left[\frac{a}{R}\right]^2 \qquad \text{(A-1)}$$

where I is the reflected sunlight power incident on the optics; I_O is the solar illumination power at 1 a.u.; s is the distance from the sun in a.u.; r is the reflectivity coefficient of the object; a is the radius of the particle; and R is the distance from the object to the detector.

We have previously indicated that we shall not be dealing with particles less than 50 microns in diameter for reasons of configuration and detector sensitivity. Above this size, we can approximate particles as "large objects" since the diameter is at least 1 order of magnitude greater than the light wavelengths of interest. Put in another fashion, the Mie size parameter $\left(\frac{2 \pi a}{\lambda}\right)$ is greater than 350 and large body optical theory can be applied.

We state here a theorem which indicates that although we shall be treating spheres specifically, most of what is said will apply equally well to the natural effluent particles. This theorem states that "the scattering pattern caused by reflection on large convex particles with random orientation is identical with the scattering pattern by reflection on large spheres of the same material and having the same surface condition." The proof of this theorem depends in part upon another which states that "the average geometric cross section of a convex particle with random orientation is 1/4 its surface area." Rigorous proofs for both of the above theorems are contained in van de Hulst (1957). For a polished totally reflecting particle where the reflection is specular, the reflected power or intensity can be written as

$$I = \frac{I_O \, \bar{G}}{4 \pi \, R^2 s^2} \qquad \text{(A-2)}$$

where $\bar{G}$ is the average geometrical cross section of the particle which, from the above theorem, is 1/4 of the total surface area. For a sphere, $G = \pi a^2$. Thus, for a sphere, equation (A-2) becomes

$$I = \frac{I_O}{4 s^2} \left(\frac{a}{R}\right)^2 . \qquad \text{(A-3)}$$

If we have a particle from which the light reflection is diffuse, then the exact form of the reflection depends upon the nature of the surface. We shall assume that we can treat the particles as being partially reflective with a reflectivity coefficient r and that the portion of the light which is reflected obeys Lambert's law. This would indicate that the surface brightness would be the same in all directions independent of

the direction from which it is illuminated. The scattering pattern of a sphere whose surface elements follow Lambert's law has been computed and tabulated (van de Hulst, 1957). Compared to polished particles, we have an additional factor so that equation (A-2) becomes

$$I = \frac{I_0 \bar{G} f(\gamma)}{4 \pi R^2 s^2} \qquad \text{(A-4)}$$

where $f(\gamma) = \frac{8}{3\pi} (\sin \gamma - \gamma \cos \gamma)$. Table A-1 gives $f(\gamma)$ for various values of γ. We see that for $\gamma \approx 90^\circ$, we have $f(\gamma) \approx .8$. Substituting this into equation (A-4) and multiplying by the reflectivity coefficients, we see that for partially reflecting spheres whose surfaces obey Lambert's law, we arrive at equation (A-1).

Table A-1. Scattering by a White, Diffusely Reflecting Sphere Following Lambert's Law.

γ	$f(\gamma)$	γ	$f(\gamma)$	γ	$f(\gamma)$
0°	0	70°	0.443	140°	2.134
10°	0.0015	80°	0.630	150°	2.349
20°	0.0119	90°	0.849	160°	2.527
30°	0.0395	100°	1.093	170°	2.628
40°	0.0917	110°	1.355	180°	2.667
50°	0.1742	120°	1.624		
60°	0.2907	130°	1.888		

B. Mathematics of the Aligned Sisyphus System

The solution for the Sisyphus System consisting of three cones is presented below. The cones are assumed to have equal half angles and parallel axes. Furthermore, the lines joining their apexes lie in a plane perpendicular to their axes.

In the course of the solution, it is necessary to distinguish between the cones. As a matter of convention, the first cone through which the particle passes will be labelled cone 1. If the triangle formed by the line joining the apexes is traversed in a clockwise direction as seen looking back into the detector, the next apex encountered will be designated as the apex of cone 2. The remaining cone is then cone 3.

Right hand coordinate systems are established for each cone as shown in Figure B-1. All corresponding axes are parallel. The coordinate axes are such that in cone 1 the X_3 axis coincides with the axis of the cone and its sense is positive in a direction from the apex into the field of view. Axis X_2 lies in the plane of the apexes and its positive direction is from cone 1 to cone 2. Axis X_1 lies in the apex plane and forms a right hand orthogonal system with X_2 and X_3. Denoting by α the half cone angle, there results in each cone coordinate system:

$$X_1 = R \tan \alpha \cos \varphi$$
$$X_2 = R \tan \alpha \sin \varphi$$
$$X_3 = R$$

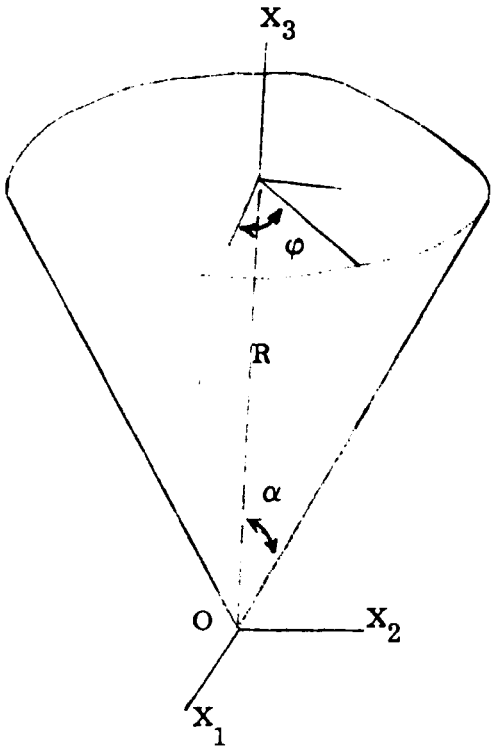

Figure B-1

A new variable, X_{ijk}, is now defined where:

i = 1, 2, 3 for X_1, X_2, X_3
j = 1, 2, 3 for cones 1, 2 or 3
k = 1 denotes an entrance point
    2 denotes an exit point

The equations of an entrance or exit point then are:

$$X_{1jk} = R_{jk} \tan \alpha \cos \varphi_{jk}$$

$$X_{2jk} = R_{jk} \tan \alpha \sin \varphi_{jk}$$

$$X_{3jk} = R_{jk} \qquad \text{(B-1)}$$

The components of velocity are V_{ij}. Let the axes of the cones be parallel. That is:

$$X_{i1} \parallel X_{i2} \parallel X_{i3}$$

then

$$V_{i1} = V_{i2} = V_{i3} = V_i .$$

In each cone system of coordinates there is:

$$X_{ij2} - X_{ij1} = V_i (\tau_{j2} - \tau_{j1}) \qquad \text{(B-2)}$$

where τ_{jk} is a time.

Let there exist another coordinate system whose axes are parallel to those of the cones. Denote this system by $\bar{X}$. Then:

$$\bar{X}_{ij1} - \bar{X}_{i11} = V_i (\tau_{j1} - \tau_{11}) \qquad \text{(B-3)}$$

Now

$$X_{ijk} = \bar{X}_{ijk} + C_{ij} \qquad \text{(B-4)}$$

where the C_{ij} are constants dependent upon the geometry of the system and the origin of the $\bar{X}_{ijk}$ system.

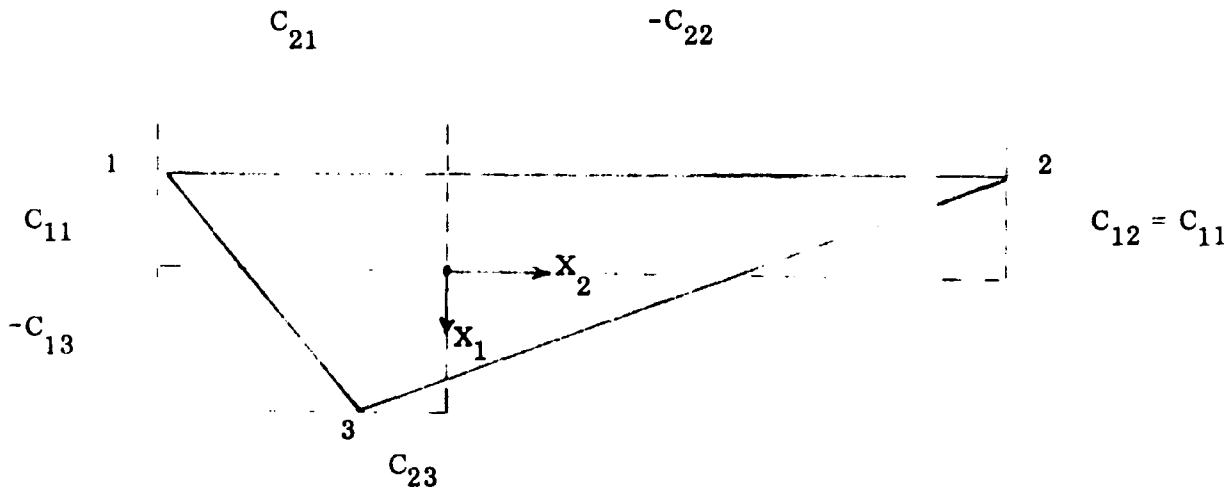

Figure B-2

Then (B-2) becomes

$$\bar{\bar{X}}_{ij2} - \bar{\bar{X}}_{ij1} = V_i (\tau_{j2} - \tau_{j1}) \tag{B-5}$$

Adding (B-3) to (B-5), there is:

$$\bar{\bar{X}}_{ij2} - \bar{\bar{X}}_{i11} = V_i (\tau_{j2} - \tau_{11}) \tag{B-6}$$

Both (B-3) and (B-6) can be written as:

$$\bar{\bar{X}}_{ijk} = \bar{\bar{X}}_{i11} + V_i (\tau_{jk} - \tau_{11}) \tag{B-7}$$

Using (B-1) in (B-7) yields:

$$\begin{aligned}
R_{jk} \tan\alpha \cos\varphi_{jk} &= R_{11} \tan\alpha \cos\varphi_{11} + V_1 (\tau_{jk} - \tau_{11}) + C_{1j} - C_{11} \\
R_{jk} \tan\alpha \sin\varphi_{jk} &= R_{11} \tan\alpha \sin\varphi_{11} + V_2 (\tau_{jk} - \tau_{11}) + C_{2j} - C_{21} \\
R_{jk} &= R_{11} + V_3 (\tau_{jk} - \tau_{11}) + C_{3j} - C_{31}
\end{aligned} \tag{B-8}$$

Using the last equation in the first two yields:

$$\begin{aligned}
&\left[R_{11} + V_3 (\tau_{jk} - \tau_{11}) + C_{3j} - C_{31}\right] \tan\alpha \cos\varphi_{jk} = \\
&\qquad R_{11} \tan\alpha \cos\varphi_{11} + V_1 (\tau_{jk} - \tau_{11}) + C_{1j} - C_{11} \\
&\left[R_{11} + V_3 (\tau_{jk} - \tau_{11}) + C_{3j} - C_{31}\right] \tan\alpha \sin\varphi_{jk} = \\
&\qquad R_{11} \tan\alpha \sin\varphi_{11} + V_2 (\tau_{jk} - \tau_{11}) + C_{2j} - C_{21}
\end{aligned} \tag{B-9}$$

Squaring and adding yields:

$$\left[R_{11} + V_3(\tau_{jk} - \tau_{11}) + C_{3j} - C_{31}\right]^2 \tan^2 \alpha =$$
$$\left[R_{11} \tan \alpha \cos \varphi_{11} + V_1(\tau_{jk} - \tau_{11}) + (C_{1j} - C_{11})\right]^2 +$$
$$\left[R_{11} \tan \alpha \sin \varphi_{11} + V_2(\tau_{jk} - \tau_{11}) + (C_{2j} - C_{21})\right]^2 \quad \text{(B-10)}$$

Equation (B-10) corresponds to five equations where j = 1; k = 2 and j = 2, 3; k = 1, 2. The five unknowns are R_{11}, φ_{11}, V_1, V_2 & V_3. It is convenient at this time to change the names of some of the variables and constants. Thus, letting:

$$\begin{aligned} d_{ij} &= (C_{ij} - C_{i1})/\tan \alpha \\ h_{jk} &= (\tau_{jk} - \tau_{11})/\tan \alpha \\ v_3 &= V_3 \tan \alpha \\ r &= R_{11} \\ \lambda &= \varphi_{11} \end{aligned} \quad \text{(B-11)}$$

Equation (B-10) then becomes:

$$(r + v_3 h_{jk} + d_{3j} \tan \alpha)^2 = (r \sin \lambda + V_2 h_{jk} + d_{2j})^2 +$$
$$(r \cos \lambda + V_1 h_{jk} + d_{1j})^2 \quad \text{(B-12)}$$

Squaring yields:

$$h_{jk}^2 (V_1^2 + V_2^2 - v_3^2) + 2r h_{jk} (V_1 \cos \lambda + V_2 \sin \lambda - v_3) +$$
$$2r (d_{1j} \cos \lambda + d_{2j} \sin \lambda - d_{3j} \tan \alpha) +$$
$$2h_{jk} (d_{1j} V_1 + d_{2j} V_2 - d_{3j} \tan \alpha \, v_3) +$$
$$(d_{1j}^2 + d_{2j}^2 - d_{3j}^2 \tan^2 \alpha) = 0 \quad \text{(B-13)}$$

Now

$$d_{i1} = (C_{i1} - C_{i1})/\tan \alpha = 0$$

so

$$h_{12}^2 (V_1^2 + V_2^2 - v_3^2) + 2r h_{12} (V_1 \cos \lambda + V_2 \sin \lambda - v_3) = 0$$

and so:

$$r = - \frac{V_1^2 + V_2^2 - v_3^2}{2 (V_1 \cos \lambda + V_2 \sin \lambda - v_3)} \, h_{12} \quad \text{(B-14)}$$

Using (B-14) in (B-13) yields:

$$\left[\left\{ h_{jk}^2 - h_{12}\, h_{jk} \right\} - \frac{h_{12}\,(d_{1j} \cos\lambda + d_{2j} \sin\lambda - d_{3j} \tan\alpha}{V_1 \cos\lambda + V_2 \sin\lambda - v_3} \right] (V_1^2 + V_2^2 - v_3^2) +$$

$$2h_{jk}\,(d_{1j}\,V_1 + d_{2j}\,V_2 - d_{3j} \tan\alpha\, v_3) +$$

$$(d_{1j}^2 + d_{2j}^2 - d_{3j}^2 \tan^2\alpha) = 0 \qquad \text{(B-15)}$$

Here $k = 1, 2 \qquad j = 2, 3$

Equations (B-15) are four equations in four unknowns λ, V_1, V_2, v_3.

Now, in (B-15) subtracting $k = 1$ from $k = 2$ yields:

$$-(h_{j2} + h_{j1} - h_{12})(V_1^2 + V_2^2 - v_3^2) = 2\,(d_{1j}\,V_1 + d_{2j}\,V_2 - d_{3j} \tan\alpha\, v_3) \qquad \text{(B-16)}$$

Letting

$$\begin{aligned} a &= (h_{21} + h_{22} - h_{12})/h_{12} \\ b &= (h_{31} + h_{32} - h_{12})/h_{12} \end{aligned} \qquad \text{(B-17)}$$

Equation (B-16) yields:

$$-\frac{1}{2}\,(V_1^2 + V_2^2 - v_3^2) = \frac{1}{ah_{12}}\,(d_{12}\,V_1 + d_{22}\,V_2 - d_{32} \tan\alpha\, v_3) =$$

$$\frac{1}{bh_{12}}\,(d_{13}\,V_1 + d_{23}\,V_2 - d_{33} \tan\alpha\, v_3) \qquad \text{(B-18)}$$

Now, if the apexes all lie in the plane $X_3 = 0$,

$$d_{3j} = 0 \qquad \text{(B-19)}$$

so

$$\left(d_{23} - d_{22}\,\frac{b}{a}\right) V_2 = \left(d_{12}\,\frac{b}{a} - d_{13}\right) V_1$$

and

$$V_1 = \frac{d_{23} - d_{22}\,\frac{b}{a}}{d_{12}\,\frac{b}{a} - d_{13}}\; V_2 \qquad \text{(B-20)}$$

Since the $\bar{X}_2$ axis is oriented parallel to the line joining cones 1 and 2, there results:

$$d_{12} = 0 \qquad \text{(B-21)}$$

Let

$$m_1 = d_{13}/d_{22}$$
$$m_2 = d_{23}/d_{22}$$
$$d = -d_{22}$$

From equation (B-20)

$$V_1 = -\frac{1}{m_1}\left(m_2 - \frac{b}{a}\right) V_2 \tag{B-23}$$

Define a new variable, η, such that

$$V_2 = \frac{2da}{h_{12}}\,\eta \tag{B-24}$$

Then

$$V_1 = \frac{2d}{m_1 h_{12}}\,(b - am_2)\,\eta \tag{B-25}$$

From equation (B-18)

$$v_3^2 = \left(\frac{2d}{h_{12}}\right)^2 \left\{\left[\left(\frac{b - m_2 a}{m_1}\right)^2 + a^2\right] \eta^2 - \eta\right\} \tag{B-26}$$

Let

$$p_3 = \left(\frac{b - am_2}{m_1}\right)^2 + a^2 \tag{B-27}$$

so

$$v_3^2 = \left(\frac{2d}{h_{12}}\right)^2 (p_3\,\eta - 1)\,\eta \tag{B-28}$$

Using (B-18) in (B-15) yields

$$\frac{h_{12}}{h_{j1}\,h_{j2}}\,\frac{d_{1j}\cos\lambda + d_{2j}\sin\lambda}{V_1\cos\lambda + V_2\sin\lambda - v_3}\,(d_{1j}\,V_1 + d_{2j}\,V_2) = -\left[\frac{d_{1j}^2 + d_{2j}^2}{2\,h_{j1}\,h_{j2}}\,(h_{j2} + h_{j1} - h_{12}) + (d_{1j}\,V_1 + d_{2j}\,V_2)\right] \tag{B-29}$$

Substituting j = 2 and j = 3 yields:

$$\frac{h_{12}}{h_{21}\,h_{22}}\;\frac{d_{22}\,\sin\lambda\;d_{22}\,a\,\eta}{\left(\frac{d_{23}}{d_{13}}\right)\left(-a+\frac{d_{22}}{d_{23}}\,b\right)\eta\cos\lambda+a\,\eta\sin\lambda-\frac{v_3\,h_{12}}{d}}=$$

$$-\left\{\frac{d_{22}^{\,2}}{2\,h_{12}\,h_{22}}\;a\,h_{12}+2\,\frac{d\,d_{22}}{h_{12}}\;a\,\eta\right\} \qquad \text{(B-30)}$$

or

$$\frac{h_{12}}{h_{21}\,h_{22}}\;\frac{\eta\sin\lambda}{\left(\frac{m_2}{m_1}\right)\left(\frac{b}{m_2}-a\right)\eta\cos\lambda+a\,\eta\sin\lambda-\frac{v_3\,h_{12}}{2d}}=$$

$$-\frac{h_{12}}{2\,h_{21}\,h_{22}}+\frac{2\,a\,\eta}{h_{12}} \qquad \text{(B-31)}$$

and

$$\frac{h_{12}}{h_{31}\,h_{32}}\;\frac{(d_{13}\cos\lambda+d_{23}\sin\lambda)\left[d_{23}\left(\frac{d_{22}}{d_{23}}\,b-a\right)+d_{23}\,a\right]\eta}{\left(\frac{d_{23}}{d_{13}}\right)\left(\frac{d_{22}}{d_{23}}\,b-a\right)\eta\cos\lambda+a\,\eta\sin\lambda-\frac{v_3\,h_{12}}{2d}}=$$

$$-\left\{\frac{d_{13}^{\,2}+d_{23}^{\,2}}{2\,h_{31}\,h_{32}}\;b\,h_{12}+\left[d_{23}\left(\frac{d_{22}}{d_{23}}\,b-a\right)+a\,d_{23}\right]\frac{2d}{h_{12}}\;\eta\right\} \qquad \text{(B-32)}$$

or

$$\frac{h_{12}}{h_{31}\,h_{32}}\;\frac{(m_1\cos\lambda+m_2\sin\lambda)\,\eta}{\left(\frac{m_2}{m_1}\right)\left(\frac{b}{m_2}-a\right)\eta\cos\lambda+a\,\eta\sin\lambda-\frac{v_3\,h_{12}}{2d}}=$$

$$-\left\{\frac{(m_1^{\,2}+m_2^{\,2})}{2\,h_{31}\,h_{32}}\;h_{12}-\frac{2\,\eta}{h_{12}}\right\} \qquad \text{(B-33)}$$

So by letting

$$\begin{aligned} f &= 4\, h_{21}\, h_{22}/h_{12}^2 \\ g &= 4\, h_{31}\, h_{32}/h_{12}^2 \\ v_3' &= v_3\, h_{12}/2d \\ A &= \frac{1}{m_1}(b - m_2 a) \end{aligned} \tag{B-34}$$

equations (B-31) and (B-33) become

$$\frac{\eta \sin \lambda}{A\,\eta \cos \lambda + a\,\eta \sin \lambda - v_3'} = \frac{f\,\eta - 1}{2} \tag{B-35}$$

and

$$\frac{\eta\,[m_1 \cos \lambda + m_2 \sin \lambda]}{A\,\eta \cos \lambda + a\,\eta \sin \lambda - v_3'} = \frac{g\,\eta - (m_1^2 + m_2^2)}{2} \tag{B-36}$$

Solving (B-35) and (B-36) for $\sin \lambda$ and $\cos \lambda$ yields:

$$\sin \lambda \quad \frac{v_3'\,(1 - f\,\eta)\, m_1}{\eta \left\{ \left[2\, m_1 + m_1 a + (m_1^2 + m_2^2)\, A - m_2 A \right] + \left[(m_2 A - m_1 a)\, f - Ag \right] \eta \right\}} \tag{B-37}$$

and

$$\cos \lambda \quad \frac{-\, v_3' \left[m_2\,(1 - f\,\eta) + g\,\eta - (m_1^2 + m_2^2) \right]}{\eta \left\{ \left[2\, m_1 + m_1 a + (m_1^2 + m_2^2)\, A - m_2 A \right] + \left[(m_2 A - m_1 a)\, f - Ag \right] \eta \right\}} \tag{B-38}$$

Thus,

$$\tan \lambda = \frac{m_1\,(f\,\eta - 1)}{g\,\eta - m_2\,(f\,\eta - 1) - (m_1^2 + m_2^2)} \tag{B-39}$$

Squaring $\sin \lambda$ and $\cos \lambda$ then adding yields:

$$\begin{aligned} &\left\{ \left[2\, m_1 + m_1 a - A m_2 + A\,(m_1^2 + m_2^2) \right] + \left[(m_2 A - m_1 a)\, f - Ag \right] \eta \right\}^2 \eta = \\ &\quad (p_3\,\eta - 1) \left\{ \left[(m_1^2 + m_2^2)\, f^2 - 2\, m_2\, fg + g^2 \right] \eta^2 - \right. \\ &\quad 2 \left[(m_1^2 + m_2^2)\, f - m_2 g - m_2 f\,(m_1^2 + m_2^2) + g\,(m_1^2 + m_2^2) \right] \eta + \\ &\quad \left. \left[(m_1^2 + m_2^2) - 2\, m_2\,(m_1^2 + m_2^2) + (m_1^2 + m_2^2)^2 \right] \right\} \end{aligned} \tag{B-40}$$

Letting

$$p_1 = (m_1 a - m_2 A) f + Ag$$

$$p_2 = \{ 2 m_1 + m_1 a - A m_2 + A (m_1^2 + m_2^2) \}$$

$$p_3 = \left(\frac{b - m_2 a}{m_1} \right)^2 + a^2$$

$$p_4 = (m_1^2 + m_2^2) f^2 - 2 m_2 f + g^2$$

$$p_5 = 2 \left[(m_1^2 + m_2^2) f - m_2 g - m_2 f (m_1^2 + m_2^2) + g (m_1^2 + m_2^2) \right]$$

$$p_6 = (m_1^2 + m_2^2) - 2 m_2 (m_1^2 + m_2^2) + (m_1^2 + m_2^2)^2 \qquad \text{(B-41)}$$

yields

$$(p_2 - p_1 \eta)^2 \eta = (p_3 \eta - 1) (p_4 \eta^2 - p_5 \eta + p_6) \qquad \text{(B-42)}$$

or

$$A_3 \eta^3 + A_2 \eta^2 + A_1 \eta + A_0 = 0 \qquad \text{(B-43)}$$

where

$$A_3 = p_1^2 - p_3 p_4$$

$$A_2 = -2 p_1 p_2 + p_3 p_5 + p_4$$

$$A_1 = p_2^2 - p_3 p_6 - p_5$$

$$A_0 = p_6 \qquad \text{(B-44)}$$

Thus far, the problem has been reduced to the solution of a cubic equation. Two problems remain to be solved. They are:

I The cubic gives three roots. They must be investigated to determine the correct one.

II Having the correct root, there must be a way of determining whether v_3 is positive or negative.

To study these problems, a condition is imposed stating that the particle enters cone 1. Referring to Figure B-3 where A is the plane tangent to cone 1 at P, the entrance point, and $\bar{n}$ is the normal to the plane directed into the cone, the condition states that

$$\bar{v} \cdot \bar{n} \geq 0 \qquad \text{(B-45)}$$

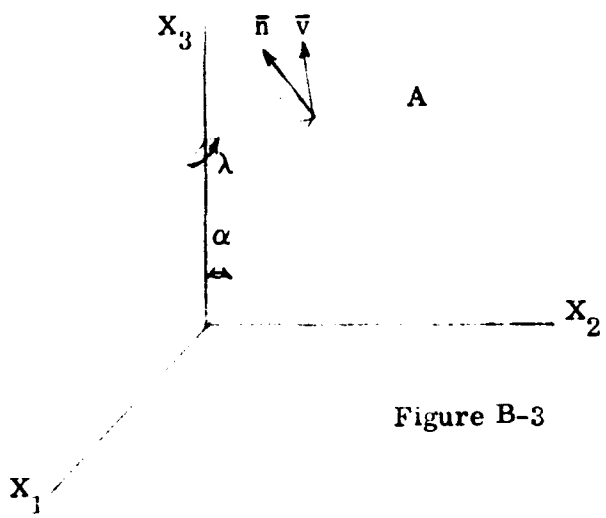

Figure B-3

Now

$$\bar{n} = -|\bar{n}| \cos\alpha \cos\lambda \,\hat{i} - |\bar{n}| \cos\alpha \sin\lambda \,\hat{j} + |\bar{n}| \sin\alpha \,\hat{k} \qquad \text{(B-46)}$$

So (B-46) becomes:

$$-V_1 \cos\lambda - V_2 \sin\lambda + v_3 \geq 0 \qquad \alpha \leq \frac{\pi}{2}$$

or

$$V_1 \cos\lambda + V_2 \sin\lambda - v_3 \leq 0 \qquad \text{(B-47)}$$

Now from (B-14)

$$r = -\frac{(V_1^2 + V_2^2 - v_3^2)\, h_{12}}{2\,(V_1 \cos\lambda + V_2 \sin\lambda - v_3)} \qquad \text{(B-14)}$$

but

$$V_1^2 + V_2^2 - v_3^2 = \left(\frac{2d}{h_{12}}\right)^2 \eta \qquad \text{(B-48)}$$

so

$$r = \left[\frac{\left(\frac{2d}{h_{12}}\right)^2 h_{12}}{2\,(-V_1 \cos\lambda - V_2 \sin\lambda + v_3)}\right] \eta$$

The quantity in the brackets is positive, so for

$$r \geq 0 \qquad \eta \geq 0 \qquad \text{(B-49)}$$

Thus, all negative roots of (B-43) may be discarded as giving negative ranges.

To obtain the sign of v_3, equations (B-23), (B-24), (B-37) and (B-38) are used in the entrance condition (B-47). Then

$$\frac{v_3 m_1}{p_2 - p_1 \eta} \geq 0 \qquad \text{(here } m_1 > 0\text{)} \tag{B-50}$$

So let

$$\frac{v_3}{p_2 - p_1 \eta} = \left| c(\eta) \right| \tag{B-51}$$

where $c(\eta)$ is some function of η whose value is unimportant since only the sign of v_3 is desired.

Then

$$v_3 = \left| c(\eta) \right| (p_2 - p_1 \eta) \tag{B-52}$$

Thus, if $p_2 - p_1 \eta > 0$, then

$$v_3 = + \frac{2d}{h_{12}} \sqrt{(p_3 \eta - 1)\eta}$$

if $p_2 - p_1 \eta < 0$, then

$$v_3 = - \frac{2d}{h_{12}} \sqrt{(p_3 \eta - 1)\eta}$$

and if $p_2 - p_1 \eta = 0$, then

$$v_3 = 0 \tag{B-53}$$

Now, if $v_3 \neq 0$, $\sin \lambda$ and $\cos \lambda$ can be determined from (B-37) and (B-38). This uniquely fixes λ. The value of r can be determined from (B-14).

If, however, $v_3 = 0$, a problem arises in determining $\sin \lambda$ and $\cos \lambda$. Returning to the entrance condition

$$V_1 \cos \lambda + V_2 \sin \lambda \leq 0 \tag{B-54}$$

Now, if $\tan \lambda \neq \infty$, then

$$(V_1 + V_2 \tan \lambda) \cos \lambda \leq 0 \tag{B-55}$$

This yields

$$\cos \lambda \; \frac{d}{h_{12}\left\{(g - m_2 f)\,\eta + m_2 - (m_1^2 + m_2^2)\right\}} \leq 0 = -\left|c_1(\eta)\right| \tag{B-56}$$

Thus

$$\cos \lambda = -\left|c_1(\eta)\right| \frac{h_{12}\left\{(g - m_2 f)\,\eta + m_2 - (m_1^2 + m_2^2)\right\}}{d} \tag{B-57}$$

The value of $c_1(\eta)$ is unimportant since (B-57) serves only to fix the sign of $\cos \lambda$ and hence the quadrant of λ. The value of λ can be obtained from (B-39).

Now, if $\tan \lambda = \infty$, use

$$(V_1 \cot \lambda + V_2) \sin \lambda \leq 0 \tag{B-58}$$

or

$$V_2 \sin \lambda \leq 0 = -\left|c_2(\eta)\right| \tag{B-59}$$

Thus

$$\sin \lambda = -\left|c_2(\eta)\right| \frac{1}{V_2} \tag{B-60}$$

Once η is uniquely defined, all other quantities are uniquely defined.

The problem remains to uniquely determine η from the three possibilities. It has been shown that negative values of η yield negative ranges. Also, from

$$v_3 = \frac{2d}{h_{12}} \sqrt{(p_3 \eta - 1)\,\eta} \tag{B-30}$$

we obtain that $(p_3 \eta - 1)\,\eta \geq 0$ for a real velocity.

Intuitively, there appears to be only one physically meaningful solution. It remains only to complete the mathematical proof. Attempts have been made to complete this proof but thus far they have been unsuccessful. There remains, however, an alternate means of attacking the problem. This is to build into a computer program the logic to test for the existence of more than one solution. If this should occur, an error message would be printed and further computation terminated. This capability has been inserted into a computer program designed to perform the calculations outlined above. Thus far, in all cases tested, the problem has not arisen.

C. Mathematics for a Sisyphus System of Generalized Geometry

The previous solution for the Sisyphus system (Appendix B) made the rather restricting assumption that the optic axes of the fields of view were exactly parallel. Since it is quite probable that the experimental package will encounter vibration, strain, and thermal variation, we must consider the possibility that the system may become misaligned. We must, therefore, possess the ability to accurately reduce any data which may be returned from such a misaligned system. This capability does exist and the mathematical derivation is presented below.

At a first glance it may appear redundant to present separate solutions for both the aligned and misaligned systems since it would seem that the first is but a special case of the second. However, the complex nature of the misaligned solution requires that an iterative method be applied in order to obtain numerical values. The particular computer program being used demands an initial estimate for the values of the unknown quantities. This estimate is obtained by using the results from the aligned solution. Thus, in order to obtain the complete solution, both the aligned and misaligned aspects of the system must be considered. Also, in view of the more complex geometry presented by the misaligned case, it was necessary to adopt a more versatile notation as is described below and illustrated in Figure C-1. However, it did not seem beneficial to revise the notation and computer program used for the aligned case.

Consider the Sisyphus system as defining three identical cones of half angle α. Let us denote the first cone entered by the particle as cone 1. If the triangle formed by the line joining the apexes is traversed in a clockwise direction as seen looking back into the detector, the next apex encountered will be designated as the apex of cone 2. The remaining cone is cone 3.

We can establish a right-hand coordinate system as shown in Figure 1. The X_2 axis lies in the plane of the apexes and joins apexes 1 and 2, being positive in the direction from 1 to 2. Axis X_1 lies in the plane of the apexes. The X_3 axis is in the general direction of the cone's view such that it forms a right-handed coordinate system with X_1 and X_2.

The vector from the base of the i^{th} cone to the particle's entrance into that cone is designated ρ_i and the vector to the particle's exit is σ_i. The corresponding angles of entrance and exit in the plane of the apexes are φ_i and ψ_i. Times of entrance and exit at the i^{th} cone are designated τ_{ij} where j is 1 for an entrance point and 2 for an exit point. The vector v is an arbitrary velocity vector.

Two angles are required to specify the orientation of a misaligned cone, as shown in Figure 2. The X' system of coordinates can be pictured as a rotation of the original system by γ about the X_3 axis followed by a rotation of θ about this new X_1' axis. Here, both γ and θ are positive in the counterclockwise direction. Relating the two coordinate systems, we have

$$X = AX'$$

where

$$A = \begin{pmatrix} \cos\gamma & -\cos\theta\sin\gamma & \sin\theta\sin\gamma \\ \sin\gamma & \cos\theta\cos\gamma & -\sin\theta\cos\gamma \\ 0 & \sin\theta & \cos\theta \end{pmatrix}$$

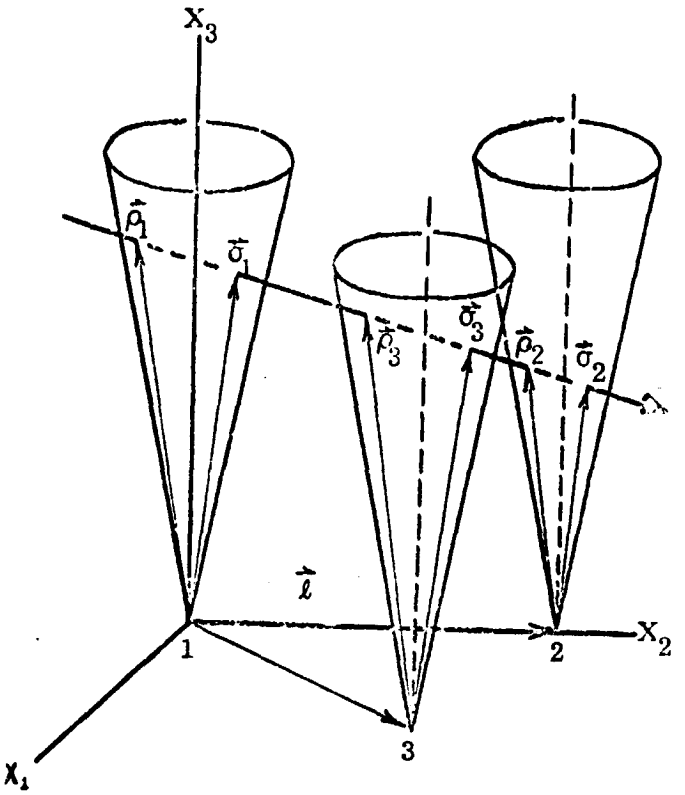

Figure C-1. Sisyphus Geometry (for convention only)

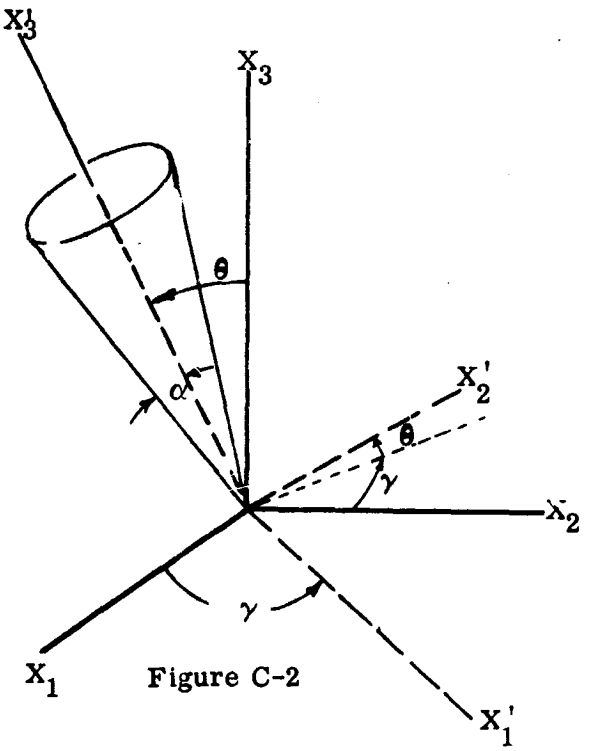

Figure C-2

The vector equations describing the particle's trajectory through the Sisyphus system can be written as

$$\vec{\sigma}_1 = \vec{\rho}_1 + \vec{v}\, t_{12} \qquad \text{(C-1.1)}$$
$$\vec{\rho}_3 = \vec{\rho}_1 + \vec{v}\, t_{31} - i\vec{n} \qquad \text{(C-1.2)}$$
$$\vec{\sigma}_3 = \vec{\rho}_1 + \vec{v}\, t_{32} - i\vec{n} \qquad \text{(C-1.3)}$$
$$\vec{\rho}_2 = \vec{\rho}_1 + \vec{v}\, t_{21} - \vec{\ell} \qquad \text{(C-1.4)}$$
$$\vec{\sigma}_2 = \vec{\rho}_1 + \vec{v}\, t_{22} - \vec{\ell} \qquad \text{(C-1.5)}$$

where $v = V_1 \hat{i} + V_2 \hat{j} + V_3 \hat{k}$ and t_{ij} is the time interval from the entrance into the first cone to the entrance ($j = 1$) or the exit ($j = 2$) of the i^{th} cone.

Taking components, we get the following 15 equations:

$\hat{i}$ components

$$\sigma_1 (\sin\alpha \cos\psi_1 \cos\gamma_1 - \sin\alpha \sin\psi_1 \sin\gamma_1 \cos\theta_1 + \cos\alpha \sin\gamma_1 \sin\theta_1) =$$
$$\rho_1 (\sin\alpha \cos\varphi_1 \cos\gamma_1 - \sin\alpha \sin\varphi_1 \sin\gamma_1 \cos\theta_1 + \cos\alpha \sin\gamma_1 \sin\theta_1)$$
$$+ V_1 t_{12} \qquad \text{(C-2.1)}$$

$$\rho_3 (\sin\alpha \cos\varphi_3 \cos\gamma_3 - \sin\alpha \sin\varphi_3 \sin\gamma_3 \cos\theta_3 + \cos\alpha \sin\gamma_3 \sin\theta_3) =$$
$$\rho_1 (\sin\alpha \cos\varphi_1 \cos\gamma_1 - \sin\alpha \sin\varphi_1 \sin\gamma_1 \cos\theta_1 + \cos\alpha \sin\gamma_1 \sin\theta_1)$$
$$+ V_1 t_{31} - m \sin\lambda \qquad \text{(C-2.2)}$$

$$\sigma_3 (\sin\alpha \cos\psi_3 \cos\gamma_3 - \sin\alpha \sin\psi_3 \sin\gamma_3 \cos\theta_3 + \cos\alpha \sin\gamma_3 \sin\theta_3) =$$
$$\rho_1 (\sin\alpha \cos\varphi_1 \cos\gamma_1 - \sin\alpha \sin\varphi_1 \sin\gamma_1 \cos\theta_1 + \cos\alpha \sin\gamma_1 \sin\theta_1)$$
$$+ V_1 t_{32} - m \sin\lambda \qquad \text{(C-2.3)}$$

$$\rho_2 (\sin\alpha \cos\varphi_2 \cos\gamma_2 - \sin\alpha \sin\varphi_2 \sin\gamma_2 \cos\theta_2 + \cos\alpha \sin\gamma_2 \sin\theta_2) =$$
$$\rho_1 (\sin\alpha \cos\varphi_1 \cos\gamma_1 - \sin\alpha \sin\varphi_1 \sin\gamma_1 \cos\theta_1 + \cos\alpha \sin\gamma_1 \sin\theta_1)$$
$$+ V_1 t_{21} \qquad \text{(C-2.4)}$$

$$\sigma_2 (\sin\alpha \cos\psi_2 \cos\gamma_2 - \sin\alpha \sin\psi_2 \sin\gamma_2 \cos\theta_2 + \cos\alpha \sin\gamma_2 \sin\theta_2) =$$
$$\rho_1 (\sin\alpha \cos\varphi_1 \cos\gamma_1 - \sin\alpha \sin\varphi_1 \sin\gamma_1 \cos\theta_1 + \cos\alpha \sin\gamma_1 \sin\theta_1)$$
$$+ V_1 t_{22} \qquad \text{(C-2.5)}$$

$\hat{j}$ components

$$\sigma_1 (\sin\alpha \cos\psi_1 \sin\gamma_1 + \sin\alpha \sin\psi_1 \cos\theta_1 \cos\gamma_1 - \cos\alpha \sin\theta_1 \cos\gamma_1) =$$
$$\rho_1 (\sin\alpha \cos\varphi_1 \sin\gamma_1 + \sin\alpha \sin\varphi_1 \cos\theta_1 \cos\gamma_1 - \cos\alpha \sin\theta_1 \cos\gamma_1)$$
$$+ V_2 t_{12} \qquad \text{(C-3.1)}$$

$$\rho_3 (\sin\alpha \cos\varphi_3 \sin\gamma_3 + \sin\alpha \sin\varphi_3 \cos\theta_3 \cos\gamma_3 - \cos\alpha \sin\theta_3 \cos\gamma_3) =$$
$$\rho_1 (\sin\alpha \cos\varphi_1 \sin\gamma_1 + \sin\alpha \sin\varphi_1 \cos\theta_1 \cos\gamma_1 - \cos\alpha \sin\theta_1 \cos\gamma_1)$$
$$+ V_2 t_{31} - m \cos\lambda \qquad \text{(C-3.2)}$$

$$\sigma_3 (\sin\alpha \cos\psi_3 \sin\gamma_3 + \sin\alpha \sin\psi_3 \cos\theta_3 \cos\gamma_3 - \cos\alpha \sin\theta_3 \cos\gamma_3) =$$
$$\rho_1 (\sin\alpha \cos\varphi_1 \sin\gamma_1 + \sin\alpha \sin\varphi_1 \cos\theta_1 \cos\gamma_1 - \cos\alpha \sin\theta_1 \cos\gamma_1)$$
$$+ V_2 t_{32} - m \cos\lambda \qquad \text{(C-3.3)}$$

$$\rho_2 (\sin\alpha \cos\varphi_2 \sin\gamma_2 + \sin\alpha \sin\varphi_2 \cos\theta_2 \cos\gamma_2 - \cos\alpha \sin\theta_2 \cos\gamma_2) =$$
$$\rho_1 (\sin\alpha \cos\varphi_1 \sin\gamma_1 + \sin\alpha \sin\varphi_1 \cos\theta_1 \cos\gamma_1 - \cos\alpha \sin\theta_1 \cos\gamma_1)$$
$$+ V_2 t_{21} - \ell \qquad \text{(C-3.4)}$$

$$\sigma_2 (\sin\alpha \cos\psi_2 \sin\gamma_2 + \sin\alpha \sin\psi_2 \cos\theta_2 \cos\gamma_2 - \cos\alpha \sin\theta_2 \cos\gamma_2) =$$
$$\rho_1 (\sin\alpha \cos\varphi_1 \sin\gamma_1 + \sin\alpha \sin\varphi_1 \cos\theta_1 \cos\gamma_1 - \cos\alpha \sin\theta_1 \cos\gamma_1)$$
$$+ V_2 t_{22} - \ell \qquad \text{(C-3.5)}$$

$\hat{k}$ components

$$\sigma_1 (\sin\alpha \sin\psi_1 \sin\theta_1 + \cos\alpha \cos\theta_1) =$$
$$\rho_1 (\sin\alpha \sin\varphi_1 \sin\theta_1 + \cos\alpha \cos\theta_1) + V_3 t_{12} \qquad \text{(C-4.1)}$$

$$\rho_3 (\sin\alpha \sin\varphi_3 \sin\theta_3 + \cos\alpha \cos\theta_3) =$$
$$\rho_1 (\sin\alpha \sin\varphi_1 \sin\theta_1 + \cos\alpha \cos\theta_1) + V_3 t_{31} \qquad \text{(C-4.2)}$$

$$\sigma_3 (\sin\alpha \sin\psi_3 \sin\theta_3 + \cos\alpha \cos\theta_3) =$$
$$\rho_1 (\sin\alpha \sin\varphi_1 \sin\theta_1 + \cos\alpha \cos\theta_1) + V_3 t_{32} \qquad \text{(C-4.3)}$$

$$\rho_2 (\sin\alpha \sin\varphi_2 \sin\theta_2 + \cos\alpha \cos\theta_2) =$$
$$\rho_1 (\sin\alpha \sin\varphi_1 \sin\theta_1 + \cos\alpha \cos\theta_1) + V_3 t_{2i} \qquad \text{(C-4.4)}$$

$$\sigma_2 (\sin\alpha \cos\psi_2 \sin\theta_2 + \cos\alpha \cos\theta_2) =$$
$$\rho_1 (\sin\alpha \sin\varphi_1 \sin\theta_1 + \cos\alpha \cos\theta_1) + V_3 t_{22} \qquad \text{(C-4.5)}$$

Multiplying equations (2.1) by $\cos\gamma_1$ and (3.1) by $\sin\gamma_1$ and adding, we obtain

$$\sigma_1 \sin\alpha \cos\psi_1 = \rho_1 \sin\alpha \cos\varphi_1 + V_1 t_{12} \cos\gamma_1 + V_2 t_{12} \sin\gamma_1 \qquad \text{(C-5.1)}$$

$$\rho_3 \sin\alpha \cos\varphi_3 = \rho_1 [\sin\alpha \cos\varphi_1 \cos(\gamma_1 - \gamma_3)$$
$$- \sin\alpha \sin\varphi_1 \cos\theta_1 \sin(\gamma_1 - \gamma_3) + \cos\alpha \sin\theta_1 \sin(\gamma_1 - \gamma_3)]$$
$$+ t_{31} (V_1 \cos\gamma_3 + V_2 \sin\gamma_3) - m (\sin\lambda \cos\gamma_3 + \sin\gamma_3 \cos\lambda) \qquad \text{(C-5.2)}$$

$$\sigma_3 \sin\alpha \cos\psi_3 = \rho_1 [\sin\alpha \cos\varphi_1 \cos(\gamma_1 - \gamma_3)$$
$$- \sin\alpha \sin\varphi_1 \cos\theta_1 \sin(\gamma_1 - \gamma_3) + \cos\alpha \sin\theta_1 \sin(\gamma_1 - \gamma_3)]$$
$$+ t_{32} (V_1 \cos\gamma_3 + V_2 \sin\gamma_3) - m (\sin\lambda \cos\gamma_3 + \sin\gamma_3 \cos\lambda) \qquad \text{(C-5.3)}$$

$$\rho_2 \sin\alpha \cos\varphi_2 = \rho_1 [\sin\alpha \cos\varphi_1 \cos(\gamma_1 - \gamma_2)$$
$$- \sin\alpha \sin\varphi_1 \cos\theta_1 \sin(\gamma_1 - \gamma_2) + \cos\alpha \sin\theta_1 \sin(\gamma_1 - \gamma_2)]$$
$$+ t_{21} (V_1 \cos\gamma_2 + V_2 \sin\gamma_2) - \ell \sin\gamma_2 \qquad \text{(C-5.4)}$$

$$\sigma_2 \sin\alpha \cos\psi_2 = \rho_1 [\sin\alpha \cos\varphi_1 \cos(\gamma_1 - \gamma_2)$$
$$- \sin\alpha \sin\varphi_1 \cos\theta_1 \sin(\gamma_1 - \gamma_2) + \cos\alpha \sin\theta_1 \sin(\gamma_1 - \gamma_2)]$$
$$+ t_{22} (V_1 \cos\gamma_2 + V_2 \sin\gamma_2) - \ell \sin\gamma_2 \qquad \text{(C-5.5)}$$

Now, multiply (2.1) by $(-\sin\gamma_1)$ and (3.1) by $\cos\gamma_1$ etc., and add:

$$\sigma_1 (\sin\alpha \sin\psi_1 \cos\theta_1 - \cos\alpha \sin\theta_1) =$$
$$\rho_1 (\sin\alpha \sin\varphi_1 \cos\theta_1 - \cos\alpha \sin\theta_1) - t_{12} (V_1 \sin\gamma_1 - V_2 \cos\gamma_1) \qquad \text{(C-6.1)}$$

$$\rho_3 (\sin\alpha \sin\varphi_3 \cos\theta_3 - \cos\alpha \sin\theta_3) =$$
$$\rho_1 [\sin\alpha \cos\varphi_1 \sin(\gamma_1 - \gamma_3) + \sin\alpha \sin\varphi_1 \cos\theta_1 \cos(\gamma_1 - \gamma_3)$$
$$- \cos\alpha \sin\theta_1 \cos(\gamma_1 - \gamma_3)] - t_{31} (V_1 \sin\gamma_3 - V_2 \cos\gamma_3)$$
$$+ m (\sin\lambda \sin\gamma_3 - \cos\lambda \cos\gamma_3) \qquad \text{(C-6.2)}$$

$$\sigma_3 (\sin\alpha \sin\psi_3 \cos\theta_3 - \cos\alpha \sin\theta_3) =$$
$$\rho_1 [\sin\alpha \cos\varphi_1 \sin(\gamma_1 - \gamma_3) + \sin\alpha \sin\varphi_1 \cos\theta_1 \cos(\gamma_1 - \gamma_3)$$
$$- \cos\alpha \sin\theta_1 \cos(\gamma_1 - \gamma_3)] - t_{32} (V_1 \sin\gamma_3 - V_2 \cos\gamma_3)$$
$$+ m (\sin\lambda \sin\gamma_3 - \cos\lambda \cos\gamma_3) \qquad \text{(C-6.3)}$$

$$\rho_2 (\sin\alpha \sin\varphi_2 \cos\theta_2 - \cos\alpha \sin\theta_2) =$$
$$\rho_1 [\sin\alpha \cos\varphi_1 \sin(\gamma_1 - \gamma_2) + \sin\alpha \sin\varphi_1 \cos\theta_1 \cos(\gamma_1 - \gamma_2)$$
$$- \cos\alpha \sin\theta_1 \cos(\gamma_1 - \gamma_2)] - t_{21} (V_1 \sin\gamma_2 - V_2 \cos\gamma_2)$$
$$- \ell \cos\gamma_2 \qquad \text{(C-6.4)}$$

$$\sigma_2 (\sin\alpha \cos\psi_2 \cos\theta_2 - \cos\alpha \sin\theta_2) =$$
$$\rho_1 [\sin\alpha \cos\varphi_1 \sin(\gamma_1 - \gamma_2) + \sin\alpha \sin\varphi_1 \cos\theta_1 \cos(\gamma_1 - \gamma_2)$$
$$- \cos\alpha \sin\theta_1 \cos(\gamma_1 - \gamma_2)] - t_{22} (V_1 \sin\gamma_2 - V_2 \cos\gamma_2)$$
$$- \ell \cos\gamma_2 \qquad \text{(C-6.5)}$$

Multiplying (4.1) by $\sin\theta_1$ and adding it to (6.1) multiplied by $\cos\theta_1$, etc. yields

$$\sigma_1 \sin\alpha \sin\psi_1 = \rho_1 \sin\alpha \sin\varphi_1 - t_{12} (V_1 \sin\gamma_1 - V_2 \cos\gamma_1) \cos\theta_1$$
$$+ V_3 t_{12} \sin\theta_1 \qquad \text{(C-7.1)}$$

$$\rho_3 \sin\alpha \sin\varphi_3 = \rho_1 [\sin\alpha \cos\varphi_1 \sin(\gamma_1 - \gamma_3) \cos\theta_3$$
$$+ \sin\alpha \sin\varphi_1 (\sin\theta_1 \sin\theta_3 + \cos\theta_1 \cos\theta_3 \cos(\gamma_1 - \gamma_3)$$
$$+ \cos\alpha (\cos\theta_1 \sin\theta_3 - \sin\theta_1 \cos\theta_3 \cos(\gamma_1 - \gamma_3)]$$
$$- t_{31} [(V_1 \sin\gamma_3 - V_2 \cos\gamma_3) \cos\theta_3 - V_3 \sin\theta_3]$$
$$+ m \cos\theta_3 (\sin\lambda \sin\gamma_3 - \cos\gamma_3 \cos\lambda) \qquad \text{(C-7.2)}$$

$$\sigma_3 \sin\alpha \sin\psi_3 = \rho_1 [\sin\alpha \cos\varphi_1 \sin(\gamma_1 - \gamma_3) \cos\theta_3$$
$$+ \sin\alpha \sin\varphi_1 (\sin\theta_1 \sin\theta_3 + \cos\theta_1 \cos\theta_3 \cos(\gamma_1 - \gamma_3))$$
$$+ \cos\alpha (\cos\theta_1 \sin\theta_3 - \sin\theta_1 \cos\theta_3 \cos(\gamma_1 - \gamma_3))]$$
$$- t_{32} [(V_1 \sin\gamma_3 - V_2 \cos\gamma_3) \cos\theta_3 - V_3 \sin\theta_3]$$
$$+ m \cos\theta_3 (\sin\lambda \sin\gamma_3 - \cos\gamma_3 \cos\lambda) \qquad \text{(C-7.3)}$$

$$\rho_2 \sin\alpha \sin\varphi_2 = \rho_1 [\sin\alpha \cos\varphi_1 \sin(\gamma_1 - \gamma_2) \cos\theta_2$$
$$+ \sin\alpha \sin\varphi_1 (\sin\theta_1 \sin\theta_2 + \cos\theta_1 \cos\theta_2 \cos(\gamma_1 - \gamma_2))$$
$$+ \cos\alpha (\cos\theta_1 \sin\theta_2 - \sin\theta_1 \cos\theta_2 \cos(\gamma_1 - \gamma_2))]$$
$$- t_{21} [(V_1 \sin\gamma_2 - V_2 \cos\gamma_2) \cos\theta_2 - V_3 \sin\theta_2]$$
$$- \ell \cos\gamma_2 \cos\theta_2 \qquad \text{(C-7.4)}$$

$$\sigma_2 \sin\alpha \sin\psi_2 = \rho_1 \Big[\sin\alpha \cos\varphi_1 \sin(\gamma_1 - \gamma_2) \cos\theta_2 + \sin\alpha \sin\varphi_1 (\sin\theta_1 \sin\theta_2 + \cos\theta_1 \cos\theta_2 \cos(\gamma_1 - \gamma_2)) + \cos\alpha (\cos\theta_1 \sin\theta_2 - \sin\theta_1 \cos\theta_2 \cos(\gamma_1 - \gamma_2)) \Big] - t_{22} \Big[(V_1 \sin\gamma_2 - V_2 \cos\gamma_2) \cos\theta_2 - V_3 \sin\theta_2 \Big] - \ell \cos\gamma_2 \cos\theta_2 \quad \text{(C-7.5)}$$

Next, multiply (4.1) by $\cos\theta_1$ and (6.1) by $(-\sin\theta_1)$ etc. and add:

$$\sigma_1 \cos\alpha = \rho_1 \cos\alpha + t_{12} \Big[(V_1 \sin\gamma_1 - V_2 \cos\gamma_1) \sin\theta_1 + V_3 \cos\theta_1 \Big] \quad \text{(C-8.1)}$$

$$\rho_3 \cos\alpha = \rho_1 \Big[-\sin\alpha \cos\varphi_1 \sin(\gamma_1 - \gamma_3) \sin\theta_3 + \sin\alpha \sin\varphi_1 (\sin\theta_1 \cos\theta_3 - \cos\theta_1 \sin\theta_3 \cos(\gamma_1 - \gamma_3)) + \cos\alpha (\cos\theta_1 \cos\theta_3 + \sin\theta_1 \sin\theta_3 \cos(\gamma_1 - \gamma_3)) \Big] + t_{31} \Big[(V_1 \sin\gamma_3 - V_2 \cos\gamma_3) \sin\theta_3 + V_3 \cos\theta_3 \Big] - m \sin\theta_3 (\sin\lambda \sin\gamma_3 - \cos\lambda \cos\gamma_3) \quad \text{(C-8.2)}$$

$$\sigma_3 \cos\alpha = \rho_1 \Big[-\sin\alpha \cos\varphi_1 \sin(\gamma_1 - \gamma_3) \sin\theta_3 + \sin\alpha \sin\varphi_1 (\sin\theta_1 \cos\theta_3 - \cos\theta_1 \sin\theta_3 \cos(\gamma_1 - \gamma_3)) + \cos\alpha (\cos\theta_1 \cos\theta_3 + \sin\theta_1 \sin\theta_3 \cos(\gamma_1 - \gamma_3)) \Big] + t_{32} \Big[(V_1 \sin\gamma_3 - V_2 \cos\gamma_3) \sin\theta_3 + V_3 \cos\theta_3 \Big] - m \sin\theta_3 (\sin\lambda \sin\gamma_3 - \cos\lambda \cos\gamma_3) \quad \text{(C-8.3)}$$

$$\rho_2 \cos\alpha = \rho_1 \Big[-\sin\alpha \cos\varphi_1 \sin(\gamma_1 - \gamma_2) \sin\theta_2 + \sin\alpha \sin\varphi_1 (\sin\theta_1 \cos\theta_2 - \cos\theta_1 \sin\theta_2 \cos(\gamma_1 - \gamma_2)) + \cos\alpha (\cos\theta_1 \cos\theta_2 + \sin\theta_1 \sin\theta_2 \cos(\gamma_1 - \gamma_2)) \Big] + t_{21} \Big[(V_1 \sin\gamma_2 - V_2 \cos\gamma_2) \sin\theta_2 + V_3 \cos\theta_2 \Big] + \ell \cos\gamma_2 \sin\theta_2 \quad \text{(C-8.4)}$$

$$\sigma_2 \cos\alpha = \rho_1 \Big[-\sin\alpha \cos\varphi_1 \sin(\gamma_1 - \gamma_2) \sin\theta_2 + \sin\alpha \sin\varphi_1 (\sin\theta_1 \cos\theta_2 - \cos\theta_1 \sin\theta_2 \cos(\gamma_1 - \gamma_2)) + \cos\alpha (\cos\theta_1 \cos\theta_2 + \sin\theta_1 \sin\theta_2 \cos(\gamma_1 - \gamma_2)) \Big] + t_{22} \Big[(V_1 \sin\gamma_2 - V_2 \cos\gamma_2) \sin\theta_2 + V_3 \cos\theta_2 \Big] + \ell \cos\gamma_2 \sin\theta_2 \quad \text{(C-8.5)}$$

Equations (5), (7) and (8) constitute 15 equations in 15 unknowns - ρ_i , σ_i , V_i , φ_i , and ψ_i ; i = 1, 2, 3.

Eliminate σ_1 from (5.1) and (7.1) using (8.1), etc.:

$$\left.\begin{aligned} &\tan\alpha \cos\psi_1 \Big[\rho_1 \cos\alpha + t_{12} (V_1 \sin\gamma_1 - V_2 \cos\gamma_1) \sin\theta_1 + V_3 t_{12} \cos\theta_1 \Big] = \rho_1 \sin\alpha \cos\varphi_1 + t_{12} (V_1 \cos\gamma_1 + V_2 \sin\gamma_1) \\ &\tan\alpha \sin\psi_1 \Big[\rho_1 \cos\alpha + t_{12} (V_1 \sin\gamma_1 - V_2 \cos\gamma_1) \sin\theta_1 + V_3 t_{12} \cos\theta_1 \Big] = \rho_1 \sin\alpha \sin\varphi_1 - t_{12} (V_1 \sin\gamma_1 - V_2 \cos\gamma_1) \cos\theta_1 + V_3 t_{12} \sin\theta_1 \end{aligned}\right\} \quad \text{(C-9.1)}$$

$$\left.\begin{aligned} \tan\alpha \cos\varphi_3 \ [\text{RHS of (8.2)}] &= [\text{RHS of (5.2)}] \\ \tan\alpha \sin\varphi_3 \ [\text{RHS of (8.2)}] &= [\text{RHS of (7.2)}] \end{aligned}\right\} \qquad \text{(C-9.2)}$$

$$\left.\begin{aligned} \tan\alpha \cos\psi_3 \ [\text{RHS of (8.3)}] &= [\text{RHS of (5.3)}] \\ \tan\alpha \sin\psi_3 \ [\text{RHS of (8.3)}] &= [\text{RHS of (7.3)}] \end{aligned}\right\} \qquad \text{(C-9.3)}$$

$$\left.\begin{aligned} \tan\alpha \cos\varphi_2 \ [\text{RHS of (8.4)}] &= [\text{RHS of (5.4)}] \\ \tan\alpha \sin\varphi_2 \ [\text{RHS of (8.4)}] &= [\text{RHS of (7.4)}] \end{aligned}\right\} \qquad \text{(C-9.4)}$$

$$\left.\begin{aligned} \tan\alpha \cos\psi_2 \ [\text{RHS of (8.5)}] &= [\text{RHS of (5.5)}] \\ \tan\alpha \sin\psi_2 \ [\text{RHS of (8.5)}] &= [\text{RHS of (7.5)}] \end{aligned}\right\} \qquad \text{(C-9.5)}$$

By squaring and adding each of the pairs of equations, we obtain 5 equations in 5 unknowns - V_1, V_2, V_3, ρ_1, φ_1. These are equations (10).

$$\begin{aligned} &\tan^2\alpha \left\{ \rho_1 \cos\alpha + t_{12} \left[(V_1 \sin\gamma_1 - V_2 \cos\gamma_1) \sin\theta_1 + V_3 \cos\theta_1 \right] \right\}^2 = \\ &\rho_1^2 \sin^2\alpha + 2\rho_1 \sin\alpha \, t_{12} \left[\cos\varphi_1 (V_1 \cos\gamma_1 + V_2 \sin\gamma_1) \right. \\ &\quad - \sin\varphi_1 \left(\left[V_1 \sin\gamma_1 - V_2 \cos\gamma_1 \right] \cos\theta_1 - V_3 \sin\theta_1 \right) \Big] \\ &\quad + t_{12}^2 \left\{ (V_1 \cos\gamma_1 + V_2 \sin\gamma_1)^2 \right. \\ &\quad \left. + \left[(V_1 \sin\gamma_1 - V_2 \cos\gamma_1) \cos\theta_1 - V_3 \sin\theta_1 \right]^2 \right\} \end{aligned} \qquad \text{(C-10.1)}$$

$$\begin{aligned} &\tan^2\alpha \left\{ \rho_1 \left[-\sin\alpha \cos\varphi_1 \sin(\gamma_1 - \gamma_3) \sin\theta_3 \right. \right. \\ &\quad + \sin\alpha \sin\varphi_1 (\sin\theta_1 \cos\theta_3 - \cos\theta_1 \sin\theta_3 \cos(\gamma_1 - \gamma_3)) \\ &\quad + \cos\alpha (\cos\theta_1 \cos\theta_3 + \sin\theta_1 \sin\theta_3 \cos(\gamma_1 - \gamma_3)) \Big] \\ &\quad + t_{31} \left[(V_1 \sin\gamma_3 - V_2 \cos\gamma_3) \sin\theta_3 + V_3 \cos\theta_3 \right] \\ &\quad \left. - m \sin\theta_3 (\sin\lambda \sin\gamma_3 - \cos\lambda \cos\gamma_3) \right\}^2 \\ &= \left\{ \rho_1 \left[\sin\alpha \cos\varphi_1 \cos(\gamma_1 - \gamma_3) - \sin\alpha \sin\varphi_1 \cos\theta_1 \sin(\gamma_1 - \gamma_3) \right. \right. \\ &\quad \left. + \cos\alpha \sin\theta_1 \sin(\gamma_1 - \gamma_3) \right] + t_{31} (V_1 \cos\gamma_3 + V_2 \sin\gamma_3) \\ &\quad \left. - m (\sin\lambda \cos\gamma_3 + \sin\gamma_3 \cos\lambda) \right\}^2 \\ &+ \left\{ \rho_1 \left[\sin\alpha \cos\varphi_1 \sin(\gamma_1 - \gamma_3) \cos\theta_3 \right. \right. \\ &\quad + \sin\alpha \sin\varphi_1 (\sin\theta_1 \sin\theta_3 + \cos\theta_1 \cos\theta_3 \cos(\gamma_1 - \gamma_3)) \\ &\quad + \cos\alpha (\cos\theta_1 \sin\theta_3 - \sin\theta_1 \cos\theta_3 \cos(\gamma_1 - \gamma_3)) \Big] \\ &\quad - t_{31} \left[(V_1 \sin\gamma_3 - V_2 \cos\gamma_3) \cos\theta_3 - V_3 \sin\theta_3 \right] \\ &\quad \left. + m \cos\theta_3 (\sin\lambda \sin\gamma_3 - \cos\gamma_3 \cos\lambda) \right\}^2 \end{aligned} \qquad \text{(C-10.2)}$$

$$\begin{aligned} &\tan^2\alpha \left\{ \rho_1 \left[-\sin\alpha \cos\varphi_1 \sin(\gamma_1 - \gamma_3) \sin\theta_3 \right. \right. \\ &\quad + \sin\alpha \sin\varphi_1 (\sin\theta_1 \cos\theta_3 - \cos\theta_1 \sin\theta_3 \cos(\gamma_1 - \gamma_3)) \\ &\quad + \cos\alpha (\cos\theta_1 \cos\theta_3 + \sin\theta_1 \sin\theta_3 \cos(\gamma_1 - \gamma_3)) \Big] \\ &\quad + t_{32} \left[(V_1 \sin\gamma_3 - V_2 \cos\gamma_3) \sin\theta_3 + V_3 \cos\theta_3 \right] \\ &\quad \left. - m \sin\theta_3 (\sin\lambda \sin\gamma_3 - \cos\lambda \cos\gamma_3) \right\}^2 \\ &= \left\{ \rho_1 \left[\sin\alpha \cos\varphi_1 \cos(\gamma_1 - \gamma_3) - \sin\alpha \sin\varphi_1 \cos\theta_1 \sin(\gamma_1 - \gamma_3) \right. \right. \\ &\quad \left. + \cos\alpha \sin\theta_1 \sin(\gamma_1 - \gamma_3) \right] + t_{32} (V_1 \cos\gamma_3 + V_2 \sin\gamma_3) \\ &\quad \left. - m (\sin\lambda \cos\gamma_3 + \sin\gamma_3 \cos\lambda) \right\}^2 \end{aligned}$$

$$
\begin{aligned}
&+ \{ \rho_1 [\sin\alpha \cos\varphi_1 \sin(\gamma_1 - \gamma_3) \cos\theta_3 \\
&\quad + \sin\alpha \sin\varphi_1 (\sin\theta_1 \sin\theta_3 + \cos\theta_1 \cos\theta_3 \cos(\gamma_1 - \gamma_3)) \\
&\quad + \cos\alpha (\cos\theta_1 \sin\theta_3 - \sin\theta_1 \cos\theta_3 \cos(\gamma_1 - \gamma_3))] \\
&\quad - t_{32} [(V_1 \sin\gamma_3 - V_2 \cos\gamma_3) \cos\theta_3 - V_3 \sin\theta_3] \\
&\quad + m \cos\theta_3 (\sin\lambda \sin\gamma_3 - \cos\gamma_3 \cos\lambda) \}^2
\end{aligned} \tag{C-10.3}
$$

$$
\begin{aligned}
&\tan^2\alpha \{ \rho_1 [- \sin\alpha \cos\varphi_1 \sin(\gamma_1 - \gamma_2) \sin\theta_2 \\
&\quad + \sin\alpha \sin\varphi_1 (\sin\theta_1 \cos\theta_2 - \cos\theta_1 \sin\theta_2 \cos(\gamma_1 - \gamma_2)) \\
&\quad + \cos\alpha (\cos\theta_1 \cos\theta_2 + \sin\theta_1 \sin\theta_2 \cos(\gamma_1 - \gamma_2))] \\
&\quad + t_{21} [(V_1 \sin\gamma_2 - V_2 \cos\gamma_2) \sin\theta_2 + V_3 \cos\theta_2] \\
&\quad + \ell \cos\gamma_2 \sin\theta_2 \}^2
\end{aligned}
$$

$$
\begin{aligned}
&= \{ \rho_1 [\sin\alpha \cos\varphi_1 \cos(\gamma_1 - \gamma_2) - \sin\alpha \sin\varphi_1 \cos\theta_1 \sin(\gamma_1 - \gamma_2) \\
&\quad + \cos\alpha \sin\theta_1 \sin(\gamma_1 - \gamma_2)] + t_{21} (V_1 \cos\gamma_2 + V_2 \sin\gamma_2) \\
&\quad - \ell \sin\gamma_2 \}^2
\end{aligned}
$$

$$
\begin{aligned}
&+ \{ \rho_1 [\sin\alpha \cos\varphi_1 \sin(\gamma_1 - \gamma_2) \cos\theta_2 \\
&\quad + \sin\alpha \sin\varphi_1 (\sin\theta_1 \sin\theta_2 + \cos\theta_1 \cos\theta_2 \cos(\gamma_1 - \gamma_2)) \\
&\quad + \cos\alpha (\cos\theta_1 \sin\theta_2 - \sin\theta_1 \cos\theta_2 \cos(\gamma_1 - \gamma_2))] \\
&\quad - t_{21} [(V_1 \sin\gamma_2 - V_2 \cos\gamma_2) \cos\theta_2 - V_3 \sin\theta_2] \\
&\quad - \ell \cos\gamma_2 \cos\theta_2 \}^2
\end{aligned} \tag{C-10.4}
$$

$$
\begin{aligned}
&\tan^2\alpha \{ \rho_1 [- \sin\alpha \cos\varphi_1 \sin(\gamma_1 - \gamma_2) \sin\theta_2 \\
&\quad + \sin\alpha \sin\varphi_1 (\sin\theta_1 \cos\theta_2 - \cos\theta_1 \sin\theta_2 \cos(\gamma_1 - \gamma_2)) \\
&\quad + \cos\alpha (\cos\theta_1 \cos\theta_2 + \sin\theta_1 \sin\theta_2 \cos(\gamma_1 - \gamma_2))] \\
&\quad + t_{22} [(V_1 \sin\gamma_2 - V_2 \cos\gamma_2) \sin\theta_2 + V_3 \cos\theta_2] \\
&\quad + \ell \cos\gamma_2 \sin\theta_2 \}^2
\end{aligned}
$$

$$
\begin{aligned}
&= \{ \rho_1 [\sin\alpha \cos\varphi_1 \cos(\gamma_1 - \gamma_2) - \sin\alpha \sin\varphi_1 \cos\theta_1 \sin(\gamma_1 - \gamma_2) \\
&\quad + \cos\alpha \sin\theta_1 \sin(\gamma_1 - \gamma_2)] + t_{22} (V_1 \cos\gamma_2 + V_2 \sin\gamma_2) \\
&\quad - \ell \sin\gamma_2 \}^2
\end{aligned}
$$

$$
\begin{aligned}
&+ \{ \rho_1 [\sin\alpha \cos\varphi_1 \sin(\gamma_1 - \gamma_2) \cos\theta_2 \\
&\quad + \sin\alpha \sin\varphi_1 (\sin\theta_1 \sin\theta_2 + \cos\theta_1 \cos\theta_2 \cos(\gamma_1 - \gamma_2)) \\
&\quad + \cos\alpha (\cos\theta_1 \sin\theta_2 - \sin\theta_1 \cos\theta_2 \cos(\gamma_1 - \gamma_2))] \\
&\quad - t_{22} [(V_1 \sin\gamma_2 - V_2 \cos\gamma_2) \cos\theta_2 - V_3 \sin\theta_2] \\
&\quad - \ell \cos\gamma_2 \cos\theta_2 \}^2
\end{aligned} \tag{C-10.5}
$$

Further reduction of these equations to three equations in three unknowns is possible. However, these equations are more convenient for purposes of computer solution. These five equations in ρ_1, φ_1, V_1, V_2, and V_3 have been programmed for computer iteration using the Secant method for non-linear equations, which is a part of the GE-605 auxiliary library.

APPENDIX 2

SISYPHUS ORIENTATION AND VIEWING ANGLE

Summary

A number of combinations of viewing angle and orientation angle (angle between Sisyphus optical axis and the vehicle rotation axis) have been studied for the Sisyphus System. An optimum combination appears to be a viewing angle of 10^{o} and an orientation angle of 45^{o}. This is based on two considerations: (1) the necessity to have a sufficient number of stars to provide a regular program of instrument calibration, and (2) minimizing the number of star exclusion circuits required to record particle events in the presence of such stars.

Viewing angles larger than 10^{o} may produce unacceptable image degradation while angles smaller than this will increase the number of bright stars exceeding the threshold of the instrument, and thus increase the required number of star exclusion circuits.

Orientation angles of 45^{o} and 30^{o} were considered for various viewing angles. The number of star exclusion circuits required remained the same in each case. However, the 30^{o} angle does not permit regular instrument calibration (too few stars) and was, therefore, ruled undesirable. Larger orientation angles decrease overall sensitivity due to the poorer scattering angle while smaller angles get into the shadow of the vehicle.

Viewing Angles

In determining an optimum viewing angle, three values were studied, namely, 5^{o}, 7.5^{o}, and 10^{o}. Associated with each of these angles is a threshold curve which varies with galactic latitude. The number of stars brighter than each of these thresholds was determined and the results are illustrated in Figures 1, 2, and 3.

The position (celestial longitude) of the Pioneer vehicle and the Sisyphus orientation will determine which of these stars will be in the field of view at any time. Using Figure 4, Pioneer's position can be obtained at any time during the mission. Thus, it is possible to determine which stars will be in the field of view as a function of time from launch. This information is given in Figures 5, 6 and 7.

It can be seen that the number of stars in the field during a single rotation varies from 4 at a 10^{o} viewing angle to 12 at a viewing angle of 5 degrees. Since a system which requires more star exclusion circuits is obviously more complex, the 10^{o} field of view appears to be most desirable. Prior studies have shown that the counting rates for these angles should be the same. The particle radius sensitivity goes inversely as the first power of the viewing angle.

Orientation Angles

The previous conclusions cited in the Pioneer proposal were obtained considering an orientation angle of 45^{o}. However, since this required a 10^{o} - 15^{o} tilt of the instrument optics relative to the supporting structure, an angle of 30^{o} was also considered. This would reduce the mounting difficulty since no tilt would be required.

A viewing angle of 10^{o} was selected since it optimizes the number of stars. Therefore, the only effect of reducing the orientation angle from 45^{o} to 30^{o} was to decrease the total sky area covered and thus eliminate some stars. However, the number of stars eliminated appears to be too great since, as is shown in Figure 9, there is a period of approximately 180 days when there are no bright stars in the field of view and thus calibration is impossible.

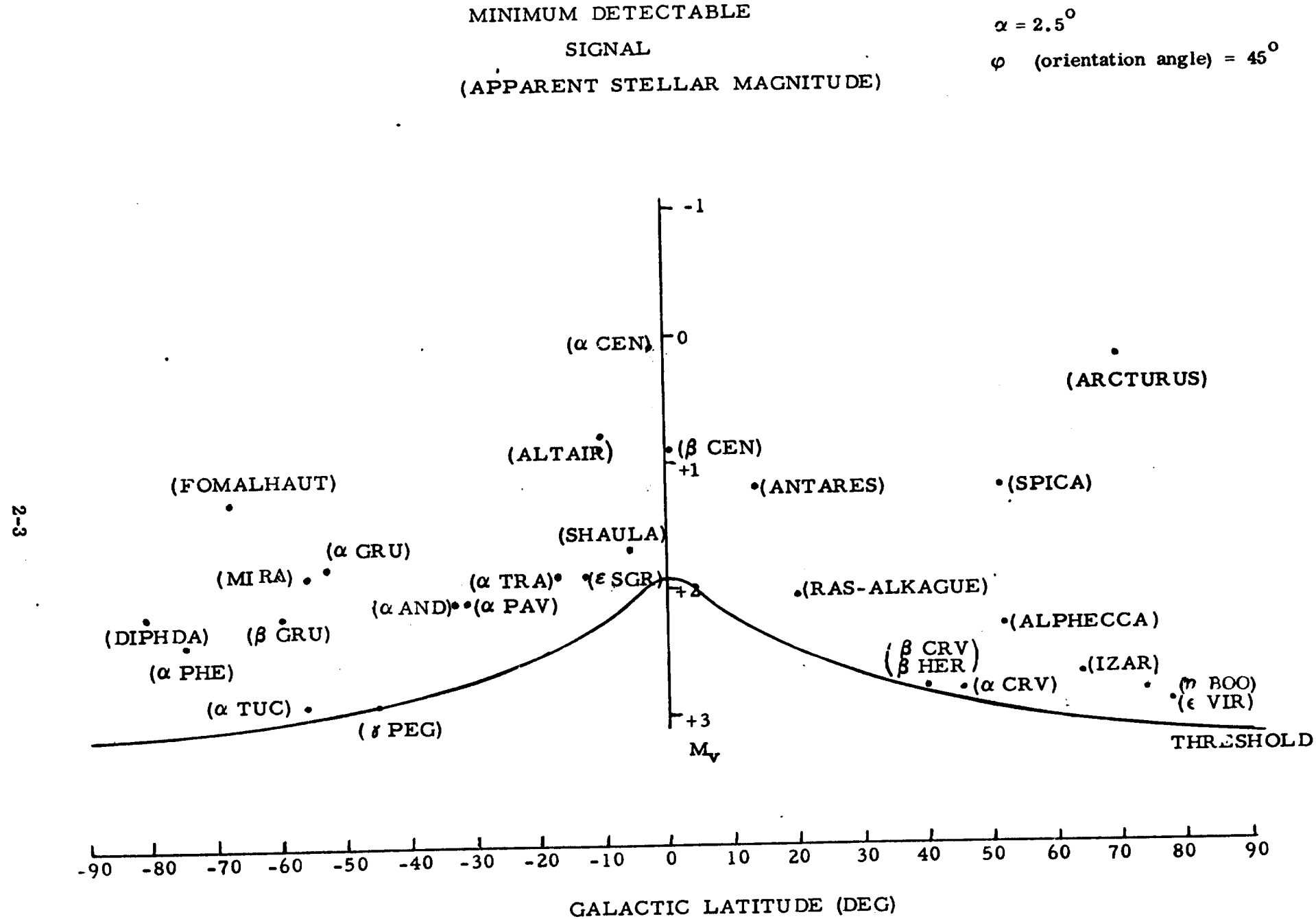
MINIMUM DETECTABLE
SIGNAL
(APPARENT STELLAR MAGNITUDE)
α = 2.5°
φ (orientation angle) = 45°
-1
0
+1
+2
+3
M_V
(α CEN)
(ARCTURUS)
(ALTAIR)
(β CEN)
(FOMALHAUT)
(ANTARES)
(SPICA)
(SHAULA)
(α GRU)
(MIRA)
(α TRA)
(ε SGR)
(RAS-ALKAGUE)
(α AND)
(α PAV)
(ALPHECCA)
(DIPHDA)
(β GRU)
(β CRV)
(β HER)
(IZAR)
(α PHE)
(α CRV)
(η BOO)
(ε VIR)
(α TUC)
(γ PEG)
THRESHOLD
-90 -80 -70 -60 -50 -40 -30 -20 -10 0 10 20 30 40 50 60 70 80 90
GALACTIC LATITUDE (DEG)

Figure 1.

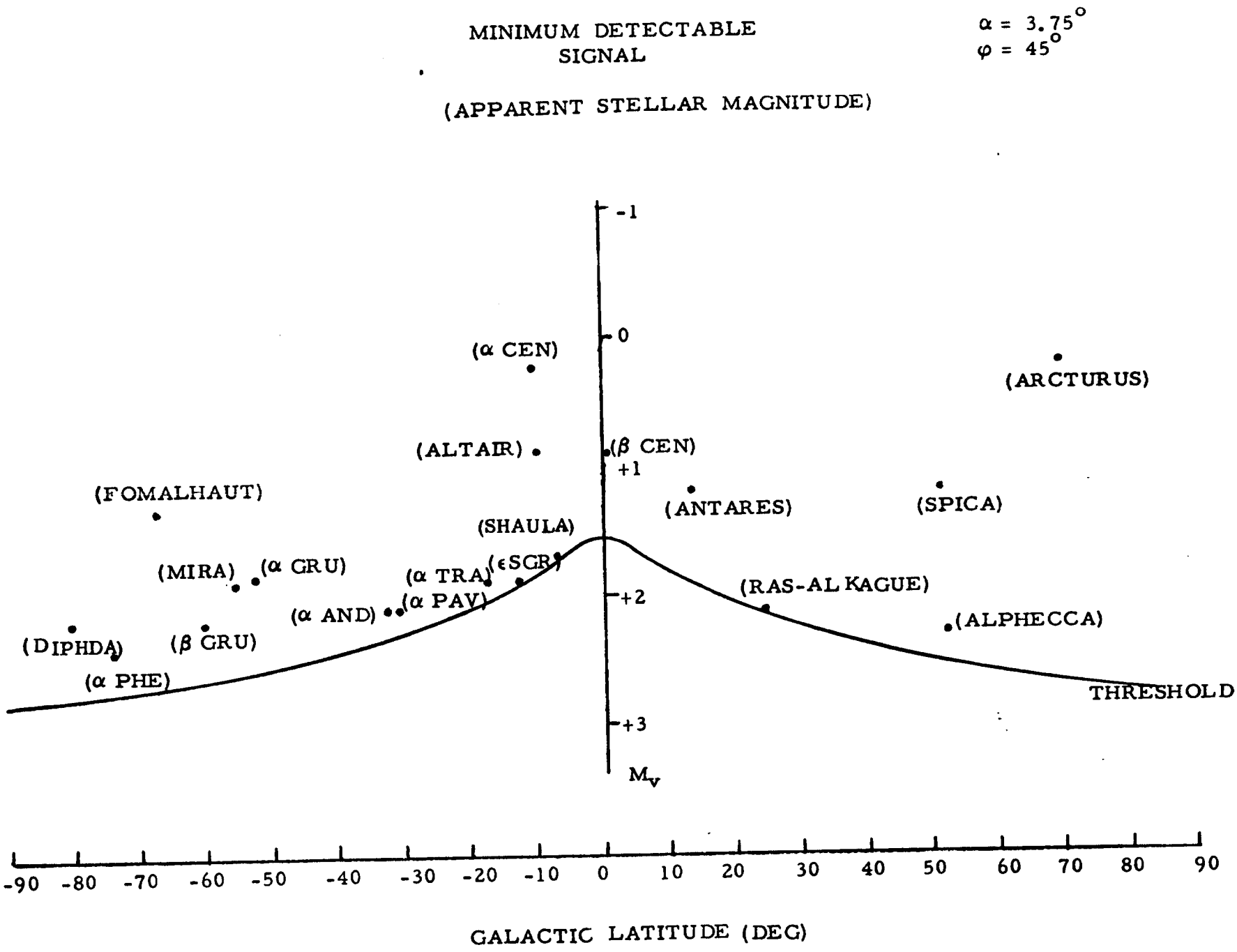
MINIMUM DETECTABLE SIGNAL
α = 3.75°
φ = 45°
(APPARENT STELLAR MAGNITUDE)
-1
0
+1
+2
+3
M_v
(α CEN)
(ARCTURUS)
(ALTAIR)
(β CEN)
(FOMALHAUT)
(ANTARES)
(SPICA)
(SHAULA)
(MIRA)
(α GRU)
(α TRA)
(εSGR)
(RAS-AL KAGUE)
(α AND)
(α PAV)
(ALPHECCA)
(DIPHDA)
(β GRU)
(α PHE)
THRESHOLD
-90 -80 -70 -60 -50 -40 -30 -20 -10 0 10 20 30 40 50 60 70 80 90
GALACTIC LATITUDE (DEG)

Figure 2.

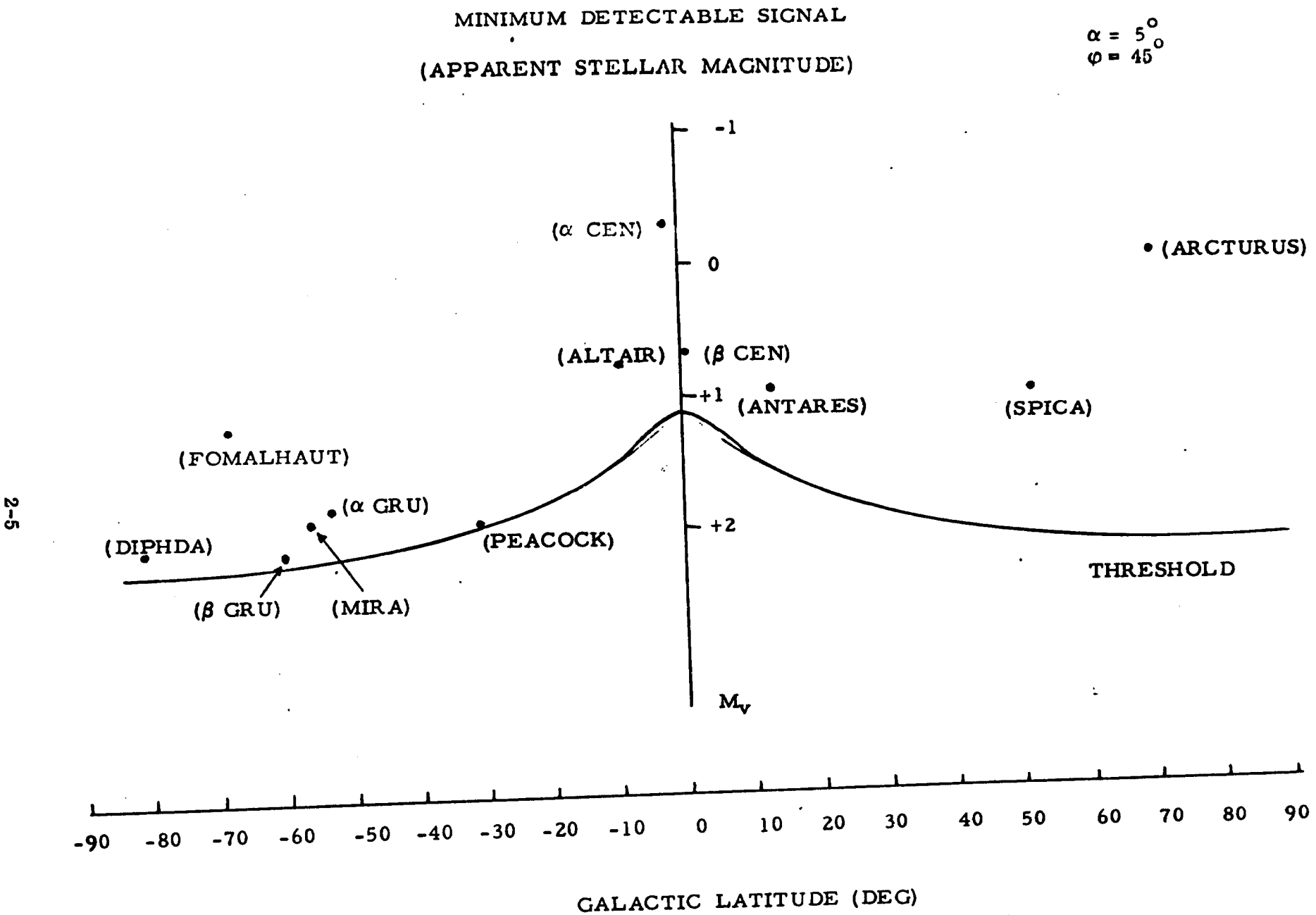
MINIMUM DETECTABLE SIGNAL
(APPARENT STELLAR MAGNITUDE)
α = 5°
φ = 45°
-1
0
+1
+2
M_V
(α CEN)
(ARCTURUS)
(ALTAIR)
(β CEN)
(ANTARES)
(SPICA)
(FOMALHAUT)
(α GRU)
(DIPHDA)
(PEACOCK)
THRESHOLD
(β GRU)
(MIRA)
-90 -80 -70 -60 -50 -40 -30 -20 -10 0 10 20 30 40 50 60 70 80 90
GALACTIC LATITUDE (DEG)

Figure 3.

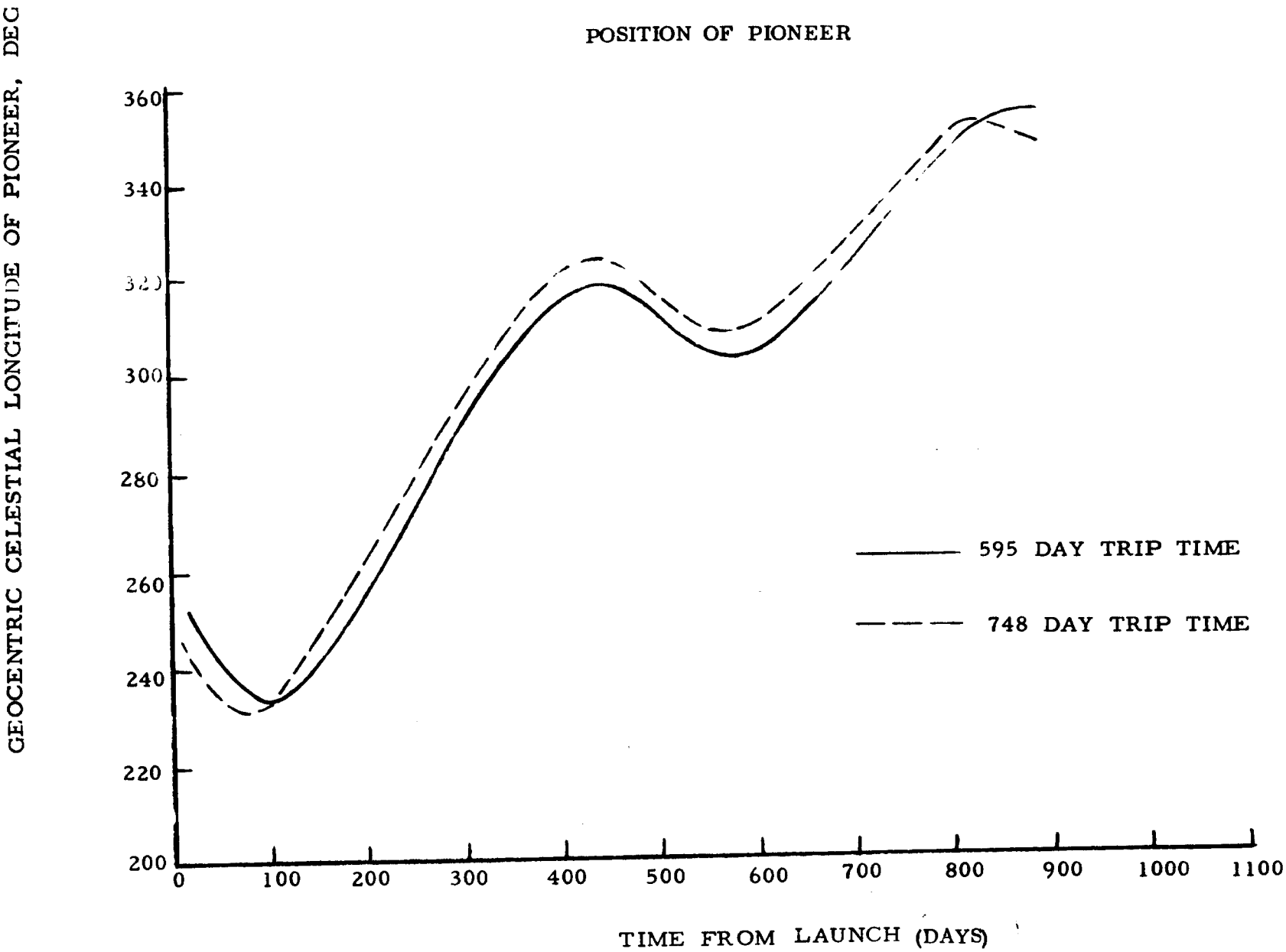
POSITION OF PIONEER
GEOCENTRIC CELESTIAL LONGITUDE OF PIONEER, DEG
360
340
320
300
280
260
240
220
200
0
100
200
300
400
500
600
700
800
900
1000
1100
595 DAY TRIP TIME
748 DAY TRIP TIME
TIME FROM LAUNCH (DAYS)

Figure 4.

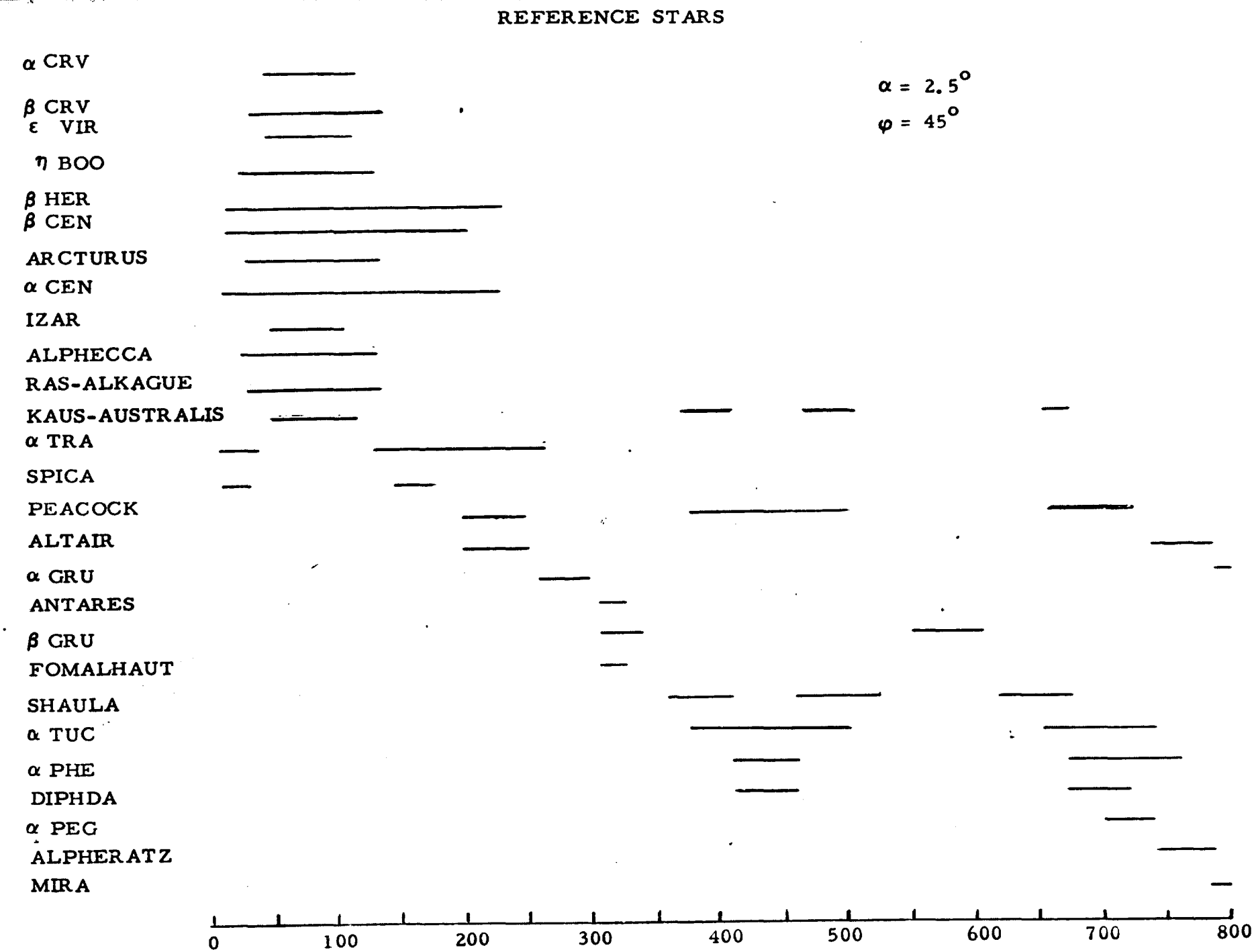
REFERENCE STARS
α CRV
β CRV
ε VIR
η BOO
β HER
β CEN
ARCTURUS
α CEN
IZAR
ALPHECCA
RAS-ALKAGUE
KAUS-AUSTRALIS
α TRA
SPICA
PEACOCK
ALTAIR
α GRU
ANTARES
β GRU
FOMALHAUT
SHAULA
α TUC
α PHE
DIPHDA
α PEG
ALPHERATZ
MIRA
α = 2.5°
φ = 45°
0
100
200
300
400
500
600
700
800
TIME FROM LAUNCH (DAYS)

Figure 5

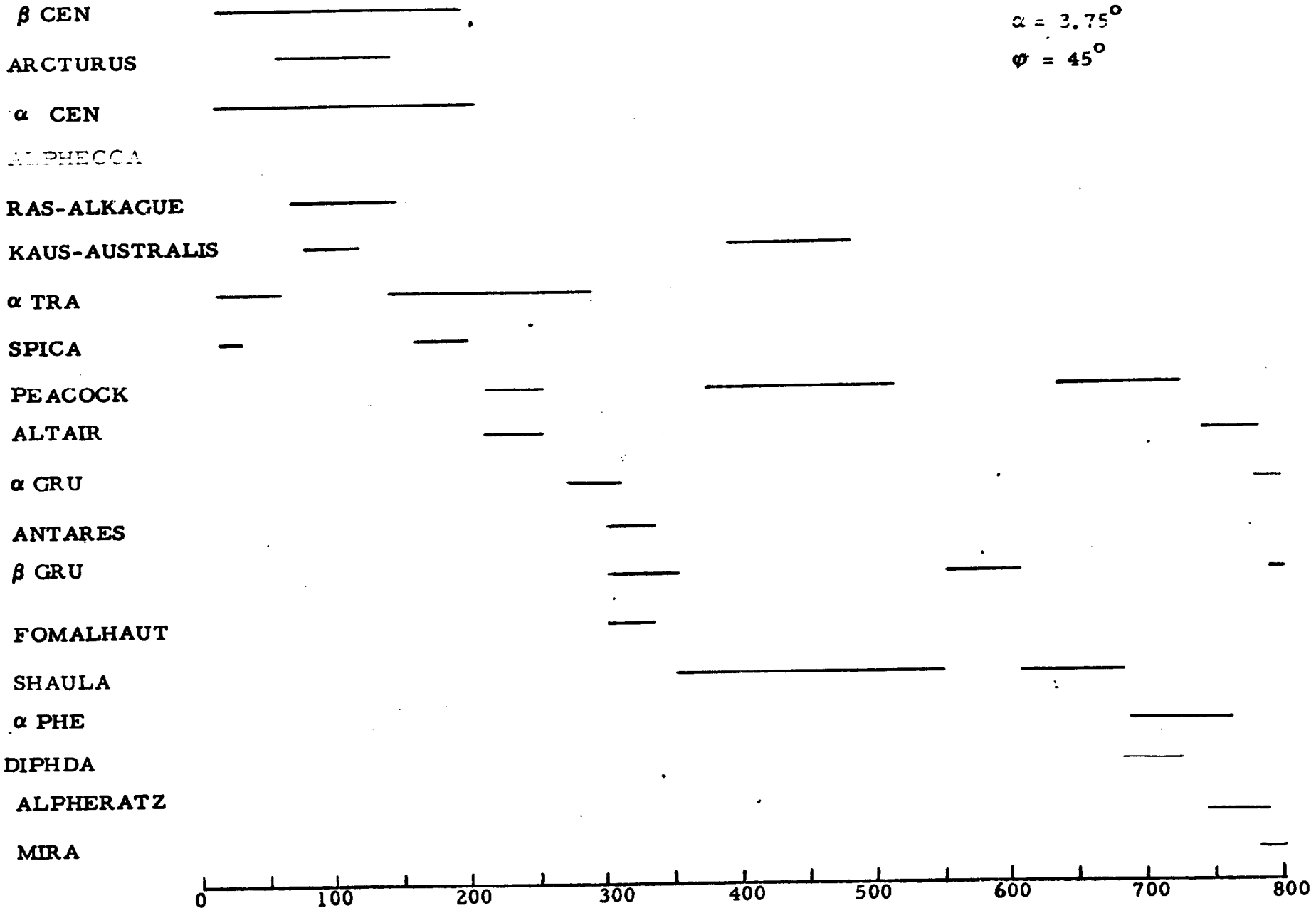
β CEN
ARCTURUS
α CEN
ALPHECCA
RAS-ALKAGUE
KAUS-AUSTRALIS
α TRA
SPICA
PEACOCK
ALTAIR
α GRU
ANTARES
β GRU
FOMALHAUT
SHAULA
α PHE
DIPHDA
ALPHERATZ
MIRA
α = 3.75°
φ = 45°
0
100
200
300
400
500
600
700
800
TIME FROM LAUNCH (DAYS)

Figure 6.

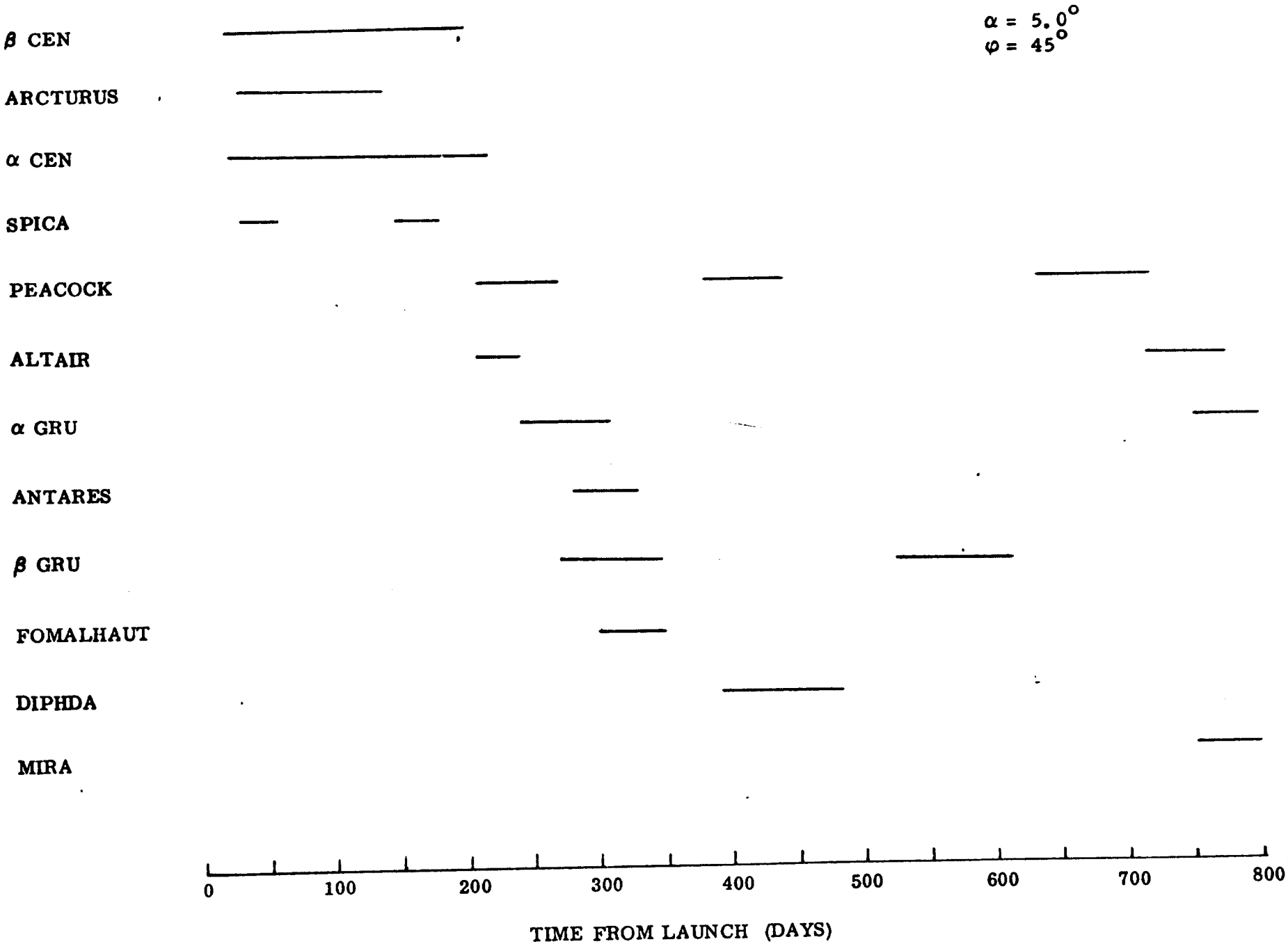
α = 5.0°
φ = 45°
β CEN
ARCTURUS
α CEN
SPICA
PEACOCK
ALTAIR
α GRU
ANTARES
β GRU
FOMALHAUT
DIPHDA
MIRA
0
100
200
300
400
500
600
700
800
TIME FROM LAUNCH (DAYS)

Figure 7.

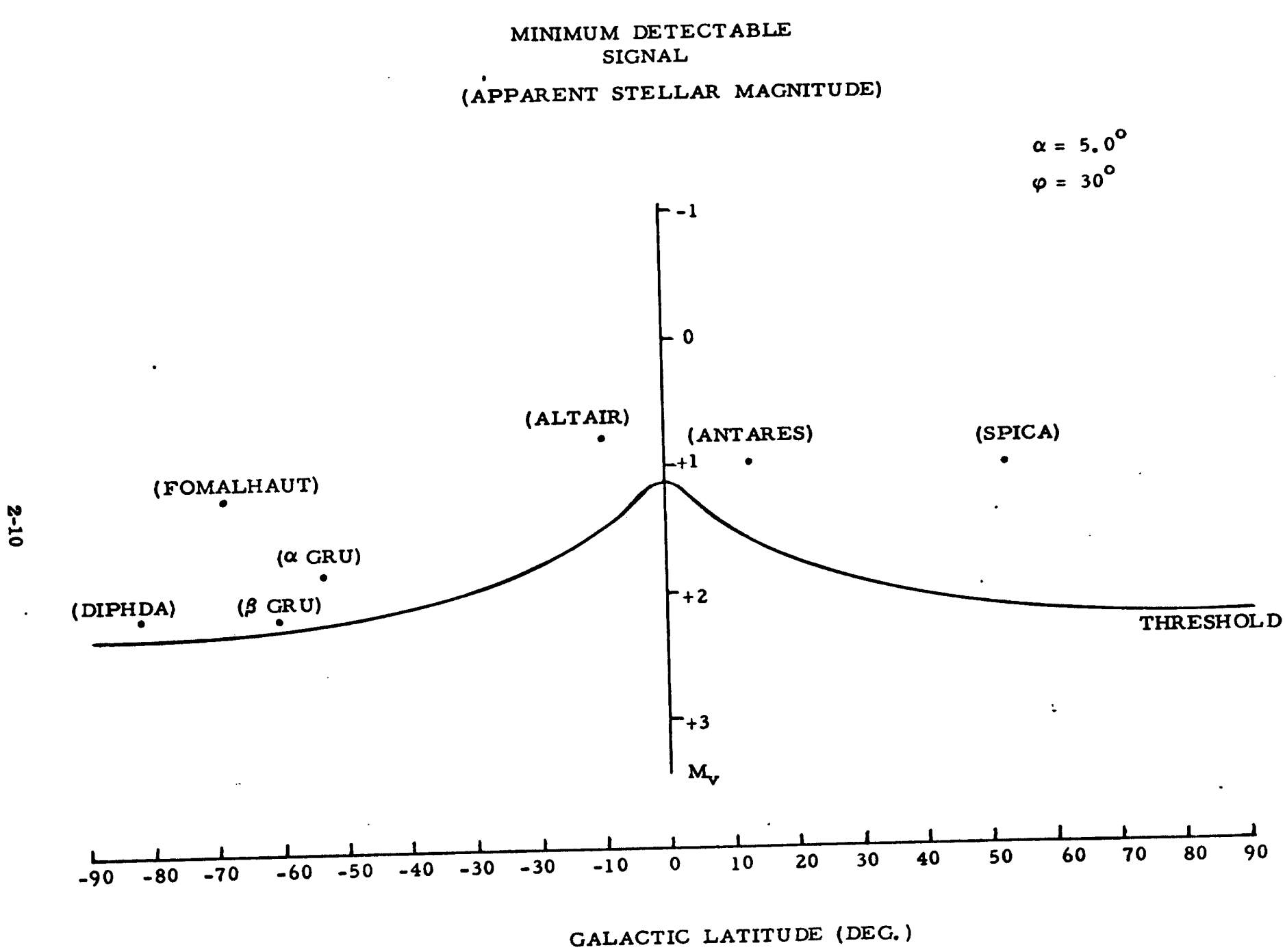
MINIMUM DETECTABLE
SIGNAL
(APPARENT STELLAR MAGNITUDE)
α = 5.0°
φ = 30°
-1
0
+1
+2
+3
M_v
(ALTAIR)
(ANTARES)
(SPICA)
(FOMALHAUT)
(α GRU)
(DIPHDA)
(β GRU)
THRESHOLD
-90 -80 -70 -60 -50 -40 -30 -30 -10 0 10 20 30 40 50 60 70 80 90
GALACTIC LATITUDE (DEG.)

Figure 8.

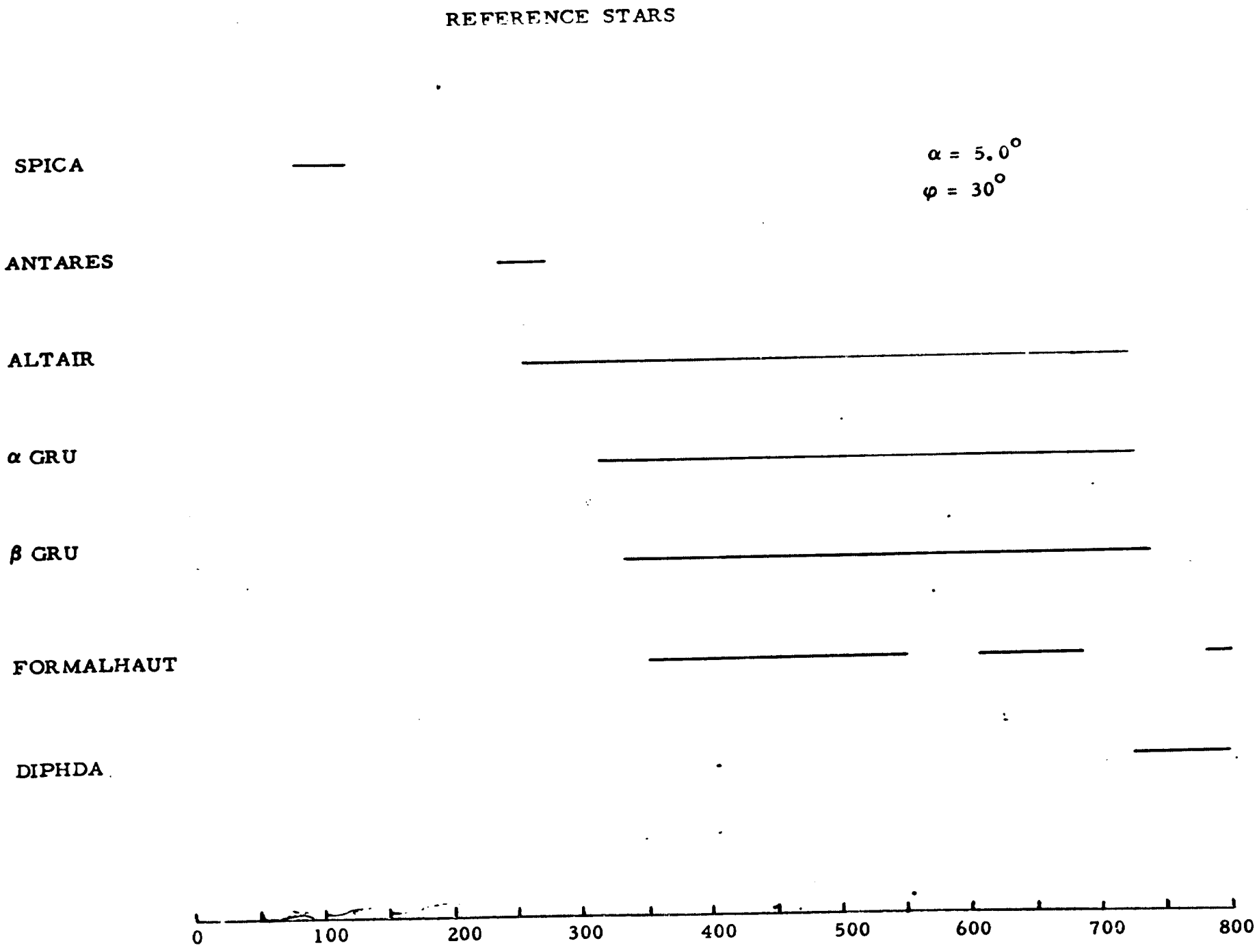
REFERENCE STARS
SPICA
ANTARES
ALTAIR
α GRU
β GRU
FORMALHAUT
DIPHDA
α = 5.0°
φ = 30°
0
100
200
300
400
500
600
700
800
TIME FROM LAUNCH (DAYS)

Figure 9.

Results

On the basis of the results from the cases considered, a viewing angle of 10^{o} and an orientation angle of 45^{o} seem to be the most desirable combination.

SISYPHUS FALSE ALARM RATE

I. INTRODUCTION

The Sisyphus system utilizes reflected or scattered solar radiation from a meteoroid for detection, trajectory and velocity measurements (Ref. 6). Three photoelectric detectors and associated optics which are separated by short base lines are pointed so that their optic axes are parallel and form the apexes of an equilateral triangle. The geometry of this system enables the trajectory of an object to be determined as it moves across the combined field of view of the detectors (see Fig. 1). While in the field of view, each photoelectric detector generates a signal from which transit times are obtained. The accuracy of such measurements is dependent upon the ability of the system to discriminate between noise (false alarms) and legitimate signals.

Discrimination between noise and signals can be obtained by three methods - (1) a threshold criteria, (2) a coincidence requirement, and (3) a pulse rejection technique. In the first approach, only those noise pulses which exceed a set threshold value will register as false alarms. In the second approach, coincidence signals from all three photoelectric detectors are required before a noise signal is registered while the third method requires, in addition, a minimum duration time for the pulse. Proper application of all three criteria should result in improved data return from the system which does not tax the available telemetry capacity.

II. EXPERIMENT

A. Objective

The first task in the development of the Sisyphus system is to investigate the effects of noise and threshold on discrimination of legitimate events and to demonstrate the degree of accuracy to which measurements can be made. To this end, the necessary laboratory equipment was designed, experimental data was obtained, and the results compared to the existing theories (Ref. 1, 2).

B. Circuit Design

1. Noise

To begin the investigation of the Meteoroid Detector, a noise background was needed to simulate a sky or star field. A "white noise" spectrum was selected because it supplied a "... wide, continuous frequency spectrum and its amplitude distribution simulates the characteristics of many natural phenomena ..." (Ref. 3).

Two white noise sources were considered. The first type used a regular carbon-base resistor. This type of resistor produced random voltage fluctuations across its terminals, known as Johnson Noise. The RMS voltage output across the resistor's terminals without an external current source may be expressed by:

FIGURE 1. Method of Particle Detection

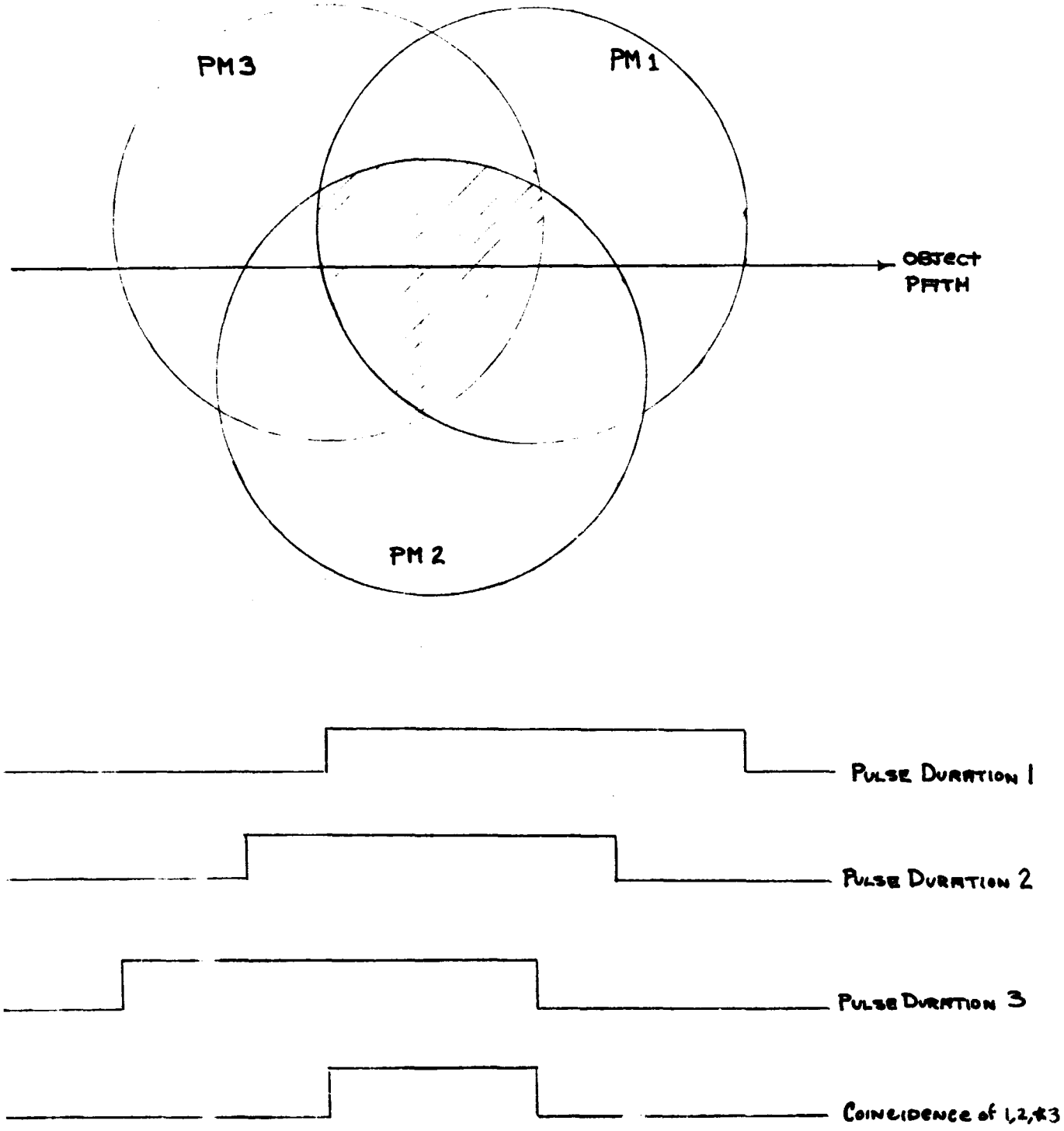

$$E_{RMS} = (4\,KCR\,\Delta F_{BW})^{1/2} \quad (1)$$

where K is the Boltzmann constant, C the temperature in degrees Kelvin, R the resistance and ΔF_{BW} the bandwidth frequency. For a sample case of 10 Megohm, 10^3 Hertz and 290° K (room temperature), the RMS voltage is

$$E_{RMS} = (4 \times 1.38 \times 10^{-23} \times 290 \times 10^6 \times 10^3)^{1/2} \cong 4 \text{ microvolts.}$$

This is well below the sensitivity of most instruments and, therefore, would have limited application. Even if the resistance and bandwidth frequency were squared and the ambient temperature raised an additional 100°C, the output E_{RMS} would only be approximately .15 volts. Consequently, the use of such a device would not be satisfactory.

The second approach to obtaining a suitable noise output resulted in the use of a photomultiplier tube (PM) as the noise source. The primary process of a PM is the absorption of quanta and the liberation of electrons. The fluctuations due to the discrete nature of this electronic charge is called Shot Noise. The RMS current from such a process may be expressed by the formula

$$I_{RMS} = 2\,e\,i\,\Delta F_{BW} \quad (2)$$

where e is 1.60×10^{-19} coulombs, i the average current, and ΔF_{BW} the bandwidth frequency. The RMS noise voltage for a PM may be defined as

$$E_{RMS} = I_{RMS} \times gain_{PM} \times R = gain_{PM} \times R \times (2\,e\,i\,\Delta F_{BW})^{1/2} \quad (3)$$

where i becomes the current found at the photocathode of the PM.

A comparison of Johnson and Shot noise may now be performed. If the $gain_{PM} = 10^6$, $i = 10^{-12}$ amperes, and the values for R, C and K from above, the Shot Noise output will be approximately 18 millivolts compared to the 4 microvolt output for Johnson Noise. This confirmed the use of a PM as a suitable noise source. The PM output was fed to a RMS voltmeter which was used both as a voltage measuring device and as an amplifier for input to the threshold circuit. Finally, it was found that only with proper shielding of the output, that is, using coaxial cables and light-tight covers, could the stray capacitances and 60 cycle noise be reduced within tolerable limits.

2. Threshold

A relatively simple threshold circuit was constructed as shown in Fig. 2. In essence, the transistors Q_1 and Q_2 act as switches. When Q_1 is on, Q_2 is

FIGURE 2. Schematic Diagram of a Threshold Circuit

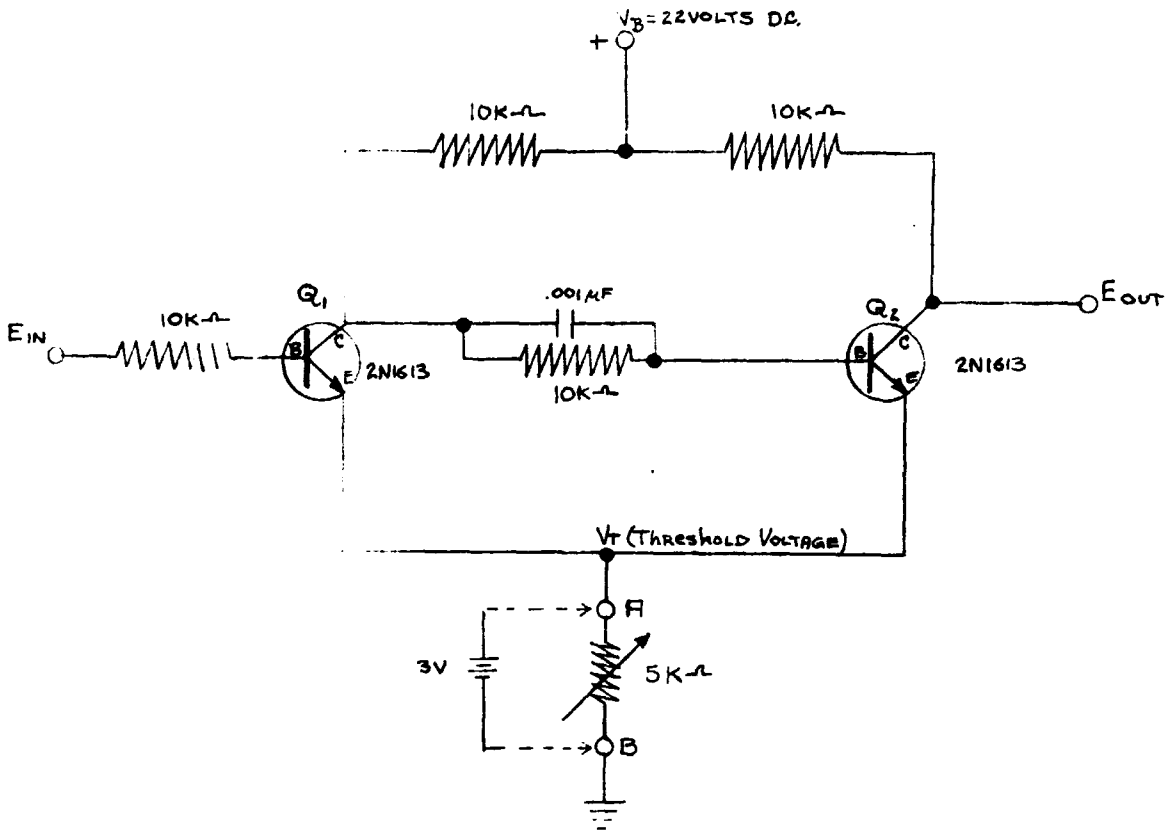

off and vice versa. The noise pulse (N) enters Q_1 at E_{in}; if $N < V_T$, Q_1 stays off while Q_2 stays on. The result is $E_{out} = V_T$. When $N \geq V_T$, Q_1 draws current to its collector, thereby turning off Q_2. This results in $E_{out} = V_B$. In other words, E_{out} will swing between V_T and V_B for a signal $N \geq V_T$. Q_2 also has the added effect of speeding up the switching rates of the threshold circuit.

In its original form, the circuit (see Fig. 2) included a 5K Ω potentiometer between terminals A and B. This potentiometer enabled the threshold V_T to be adjusted to various levels. This resistive load added an unwanted hysteresis effect thought to be of minimal importance at first. * It was found, however, that as soon as a noise pulse exceeded the threshold, the threshold would drop to a lower value, causing more noise pulses to exceed the new (lower) threshold. Also, recovery of the threshold to its normal position was inhibited. To eliminate this effect, the potentiometer was replaced by a 3 volt battery across terminals A and B. The equivalent threshold was measured to be 4 volts d.c.

3. Coincidence

To investigate coincidence of signals, as shown by Fig. 1, at least two threshold circuits, PMs and amplifiers, were needed. Design of the coincidence circuit required two diodes set in an "AND" position; that is, if one pulse from circuit 1 "and" another pulse from circuit 2 coincide, then a signal (E_c) would result). The final breadboard apparatus utilizing both threshold circuits and coincidence is shown in Fig. 3. In general, the amplitude of the coincidence signal will vary between V_T and V_B, similar to the threshold circuits.

4. Pulse Discrimination

The technique of pulse rejection can also be used in conjunction with the threshold criteria in order to reduce the false alarm problem. This method rejects all pulses which do not remain above the threshold for a preset length of time. Thus, even though a pulse satisfies the threshold criteria, it will not be accepted as legitimate unless the minimum time requirement is also satisfied.

The circuit employed to perform this rejection process is shown in Fig. 4. As can be seen from the figure, the circuit consists of two threshold circuits in series with an integrator. The integrator and the second threshold circuit make up the pulse discriminator. A noise signal entering the circuit must first satisfy the threshold criteria of circuit 1. The output of this threshold circuit is then passed on to the pulse discrimination circuit which tests the width of the pulse. If it is greater than or equal to 1/RC, the output of circuit 2 is $E_{out} = V_B$. If the pulse is too short, $E_{out} = V_T$. Thus, a false alarm will occur only if $N \geq V_T$ and the pulse width exceeds or equals 1/RC.

---

*In the more advanced stage of development of this system, hysteresis will be used.

FIGURE 3. Schematic Diagram of Both Threshold Circuits with Coincidence

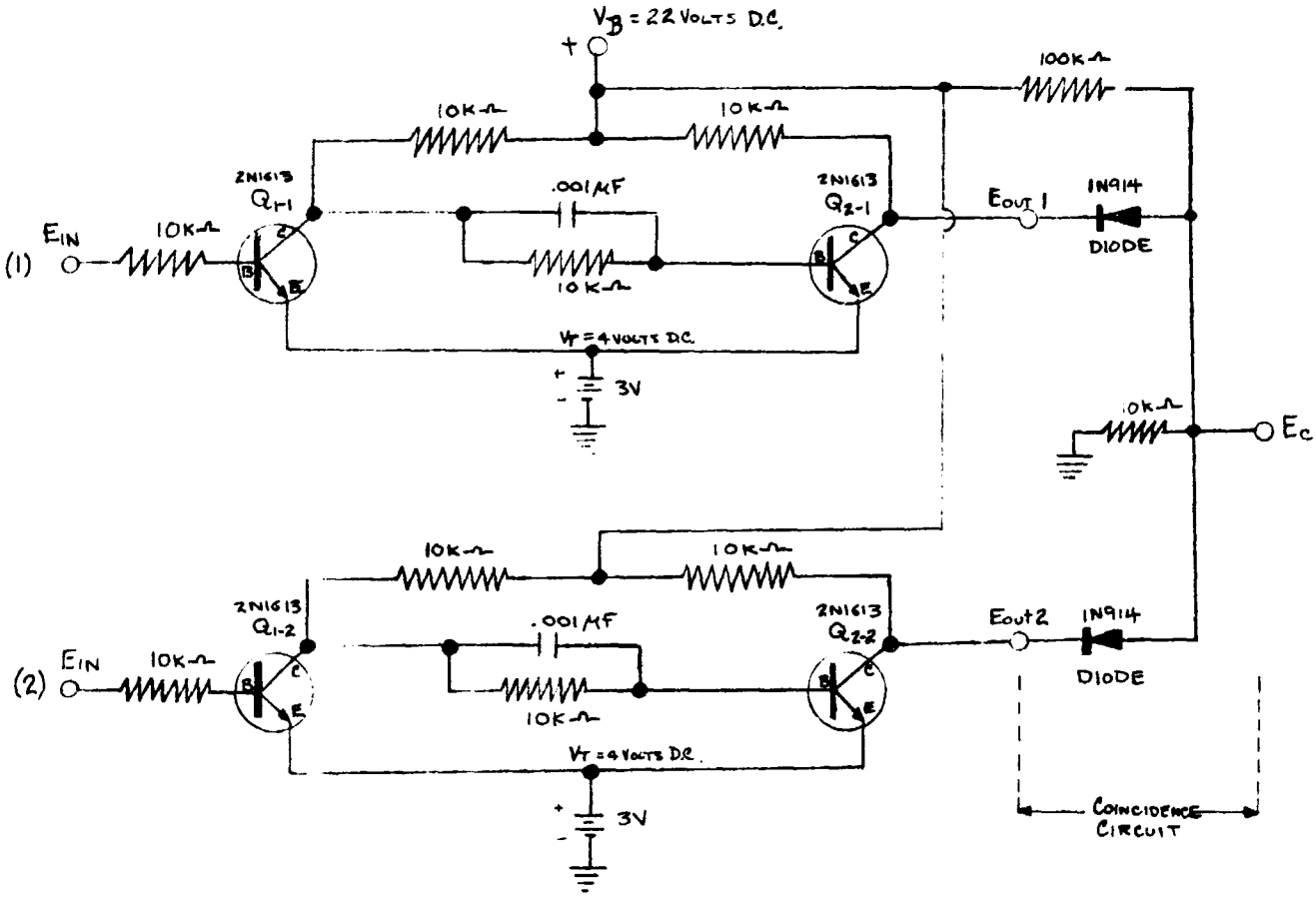

THRESHOLD CIRCUITS WITH PULSE DISCRIMINATION

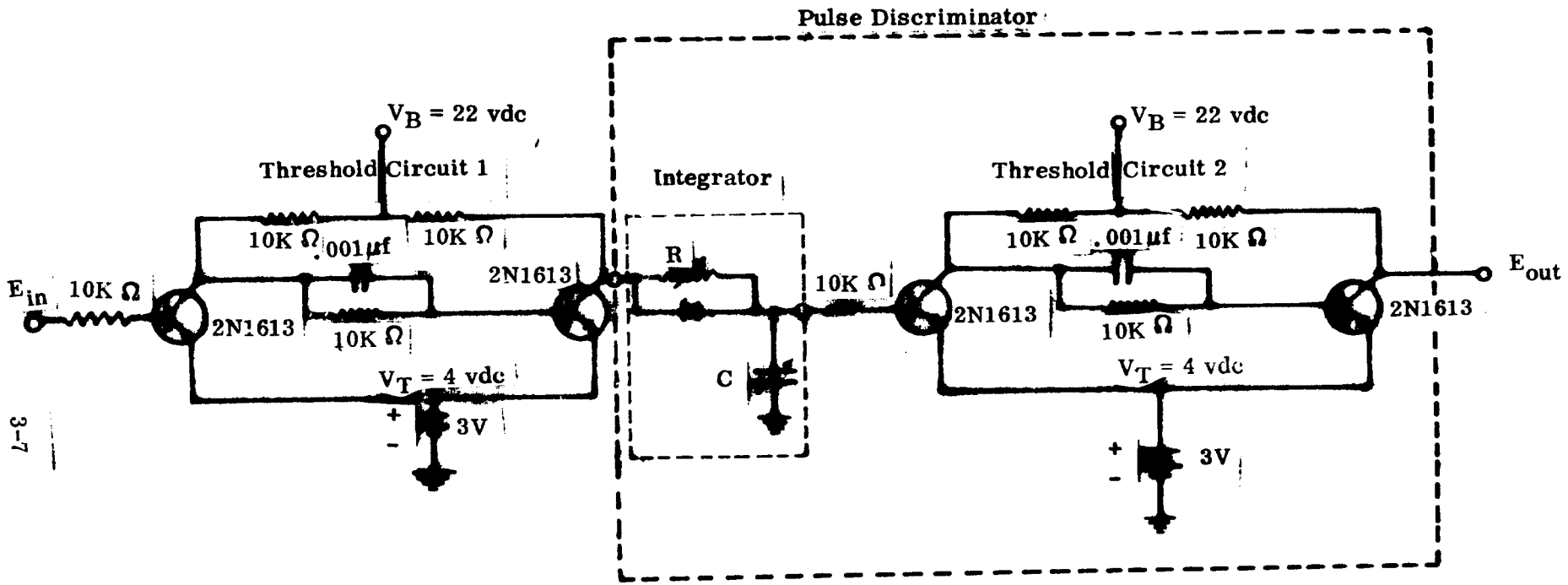

Figure 4

The probability of a false alarm can be further reduced by also requiring that the coincidence criteria be satisfied. The circuit, in this case, would be the same as that of Fig. 5 with threshold circuit 1 replaced by the coincidence circuit shown in Fig. 3.

5. Final Preparation of Equipment

The final assembly of the constructed test equipment required the addition of low level light sources to the PM windows and control of all unwanted stray light. The signal bandwidth (ΔF_{BW}) of each circuit was obtained by applying a sine wave of known amplitude at E_{in} and adjusting the input frequency until the half power point (-3 db) was reached. The noise equivalent bandwidth (ΔF_N) for a simple low pass RC circuit such as that used here may be expressed as $2 \Delta F_{BW}$. The time constant (τ) of each circuit is given by the expression

$$\tau = 1/(2 \pi \Delta F_{BW}) \tag{4}$$

The noise output of the PM (E_{RMS}) was amplified by the RMS volt meter. The RMS noise voltage (N) is given by the relationship

$$N = E_{RMS} \times \text{gain} \tag{5}$$

III. DISCUSSION

A. Theoretical Considerations

1. Threshold and Coincidence

The test equipment (as explained above) was designed on the principle that each time a noise signal exceeds the threshold (V_T), a false alarm pulse would occur (Fig. 5). In order to relate this concept into a useable form, the statistical fluctuations of the RMS noise voltage must be considered. The probability of detection of one false alarm is given by the Gaussian probability-density function (Ref. 4, 5).

$$P(n)\, dn = \frac{n}{N^2} \exp\left(-\frac{n^2}{2N^2}\right) dn \tag{6}$$

where "n" is the amplitude of the noise envelope and N the RMS value of the noise voltage. In order to determine the probability of a false alarm, P_{FA}, i.e., the probability of one noise pulse exceeding the threshold voltage (V_T), Eq. (6) is integrated between the limits of V_T and ∞. We now obtain

Figure 5. False Alarms Due to the Noise Voltage Exceeding Threshold

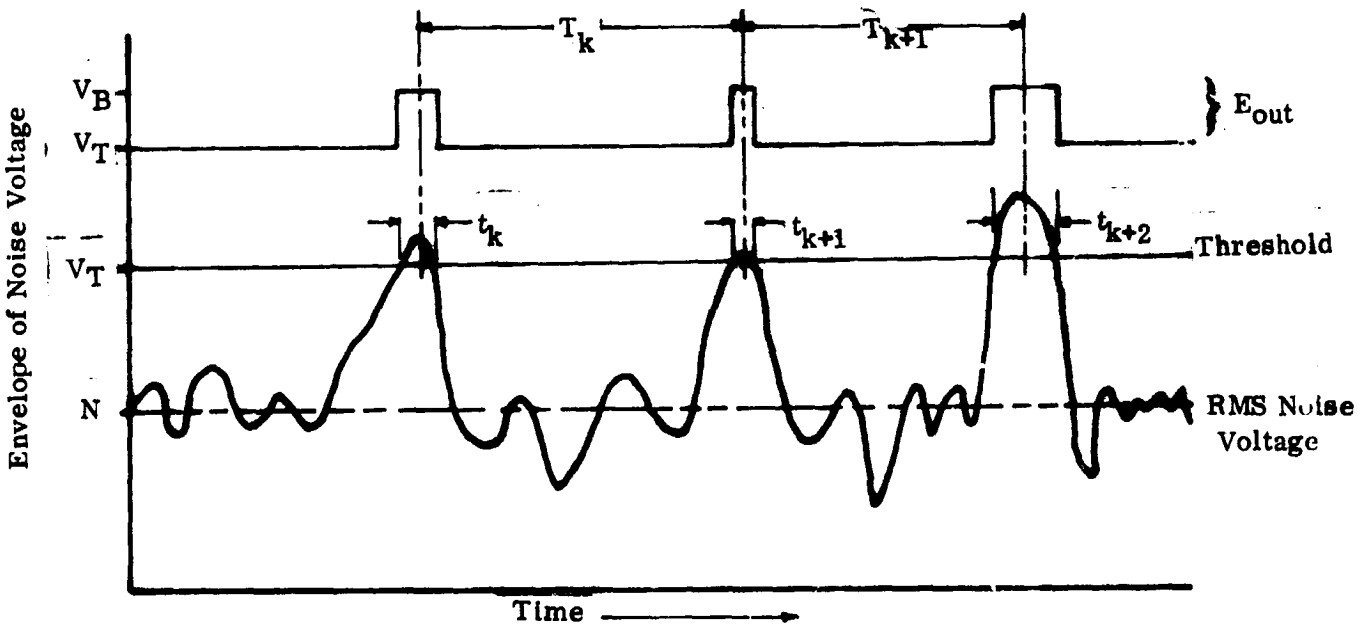

$$P_{FA} = \text{Probability } (V_T < n < \infty) = \int_{V_T}^{\infty} \frac{n}{N^2} \exp\left(-\frac{n^2}{2N^2}\right) dn$$

or

$$P_{FA} = \exp\left(-\frac{V_T^2}{2N^2}\right) \tag{7}$$

The relationship of Eq. (7) is one form of the Gaussian probability distribution, known as the Rayleigh probability distribution. The difference from the normal Gaussian is that the normalization of Eq. (6) is from V_T to ∞ and not $-\infty$ to ∞, as in the Gaussian distribution.

Substituting T (threshold voltage vdc) for V_T in Eq. (7), the final relationship, a power spectrum, is formed

$$P_{FA} = \exp\left(-\frac{1}{2}\left(\frac{T}{N}\right)^2\right) \tag{8}$$

In an earlier description (Ref. 6), T and N were defined in terms of power. Since our measurements in the laboratory will be made in terms of voltages, we shall henceforth define our threshold to noise ratio in terms of voltages. Given that ΔF_N, the noise equivalent bandwidth, defines the number of noise pulses possible per unit time, the false alarm rate (FAR) can now be obtained:

$$FAR = \Delta F_N \cdot P_{FA} = \Delta F_N \, e^{-1/2 \, (T/N)^2} \tag{9}$$

where T/N is the limiting factor in determining the FAR.

The probability of signal coincidence, given two independent circuits, may be expressed by the intersection of the two. Mathematically, it can be expressed as

$$P_c (1 \cap 2) = P_{FA}(1) \times P_{FA}(2) .$$

Therefore, Eq. (8) may be easily transformed to give

$$P_c = P_c (1 \cap 2) = e^{-1/2 \, (T/N)^2} \times e^{-1/2 \, (T/N)^2} = e^{-(T/N)^2} \tag{10}$$

To fully understand signal coincidence, the pulse shape must be considered. The actual pulse characteristics and shape duplicate a typical RC rise and decay curve. For the purpose of this discussion, since $\tau \ll 1$, the pulse will be considered rectangular; typical outputs of circuits 1 and 2 are shown in Figs. 6 and 7 (composite photograph). The outputs, as shown in Fig. 6, do not necessarily have the same pulse width. This is due to the fact that one or more pulses occurring close together could cause the threshold circuit to stay on for prolonged periods. This is especially true when $T/N \ll 1$. On the other hand, one noise pulse of high amplitude could also cause the same effect. Fig. 6-C shows the resultant or coincidence signal. The coincidence time squared (t_c^2) is just the product of the two circuits, or

$$t_c^2 = t_k \cdot t_j = (\tau_k + \epsilon_k) \cdot (\tau_j + \epsilon_j)$$

where ϵ is the signal width. Expanding, we get

$$t_c = (\tau_k \tau_j + \epsilon_k \tau_j + \epsilon_j \tau_k + \epsilon_j \epsilon_k)^{1/2} .$$

Coincidence of the signal pulses shown in Fig. 6-C can only occur when both pulses "happen to exist" at the same time. Predictions for rate of coincidence (ROC) may be readily obtained if their existence is due entirely to a random distribution. One such approach utilized DUTY CYCLE (D.C.), which may be defined as the percentage of time (t_k) a circuit is operable in contrast to the time it could have been operable (T_k). This may be written as

$$DC_1 = \frac{t_1}{T_k} \qquad \text{and} \qquad DC_2 = \frac{t_2}{T_k}$$

where the total on-time is equal to the number of pulses (N_i) times an available width τ, obtained from a given time period (T_k); therefore,

$$DC_1 = \frac{t_1}{T_k} = \frac{N_1 \tau_1}{T_k} \quad \text{and} \quad DC_2 = \frac{N_2 \tau_2}{T_k}$$

The actual percentage of on-time for a coincidence circuit is given by the product of the two duty cycles

$$DC_T = DC_1 \times DC_2 = \frac{N_1 \tau_1}{T_k} \times \frac{N_2 \tau_2}{T_k} = \frac{N_1 N_2 \tau_1 \tau_2}{T_k^2} \qquad (11)$$

2

Figure 6. Showing Signal Output of the Threshold Circuits with Coincidence

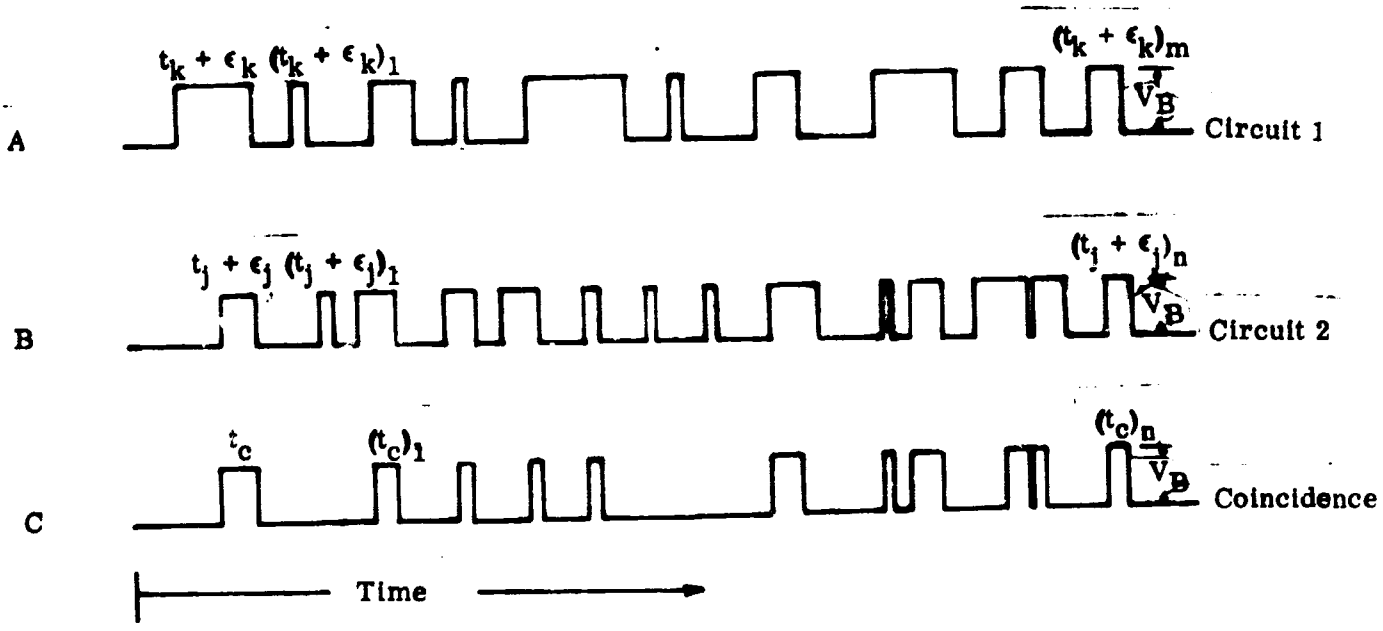

FIGURE 7. Composite Photograph Showing Typical Signal Output and Coincidence

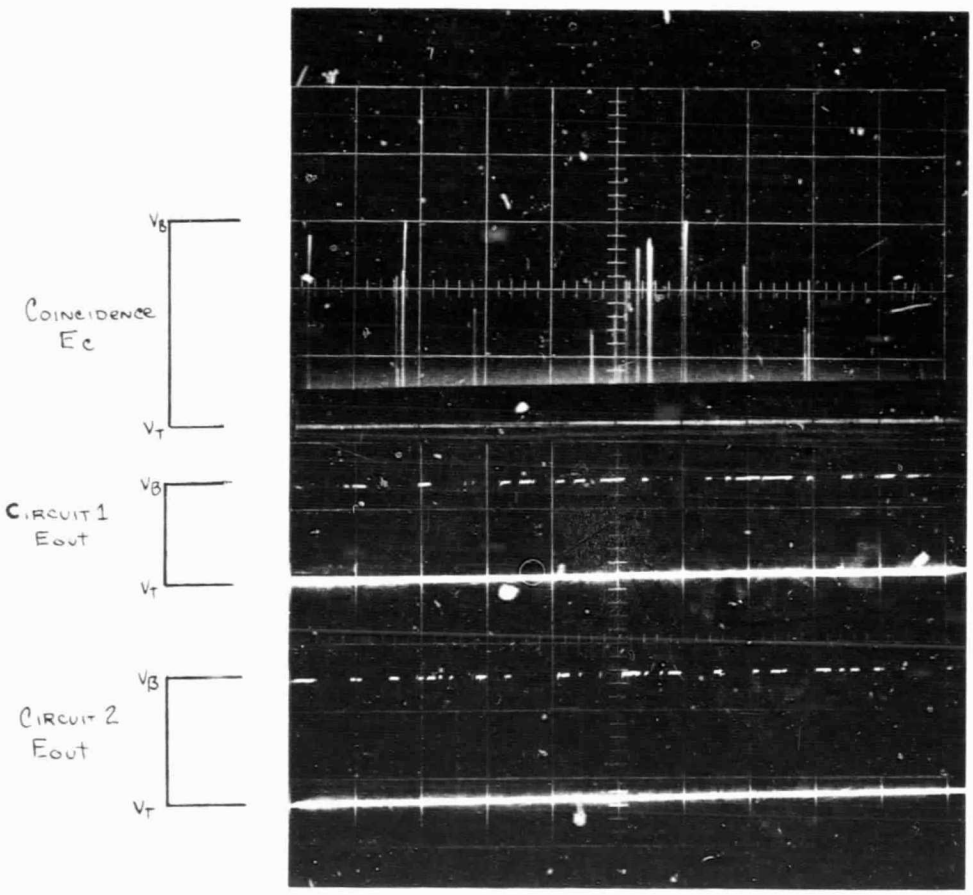

The actual ROC is then given as $ROC = DC_T/\tau$, where the τ used here must be the larger value, because the ROC should represent the minimum coincidence rate. In practice, the width of each pulse is a function of the noise amplitude and not τ (refer to Fig. 6). However, the minimum width per pulse must be at least equal to τ. Therefore, using $\tau = \tau_2$ because $\tau_2 > \tau_1$ (experimental results), we obtain

$$ROC = \frac{DC_T}{\tau_2} = \frac{N_1 N_2 \tau_1 \tau_2}{\tau_2 T_k^2} = \frac{N_1 N_2 \tau_1}{T_k^2} \qquad (12)$$

2. Threshold and Pulse Discrimination

The test equipment in this case was designed such that a false alarm pulse would occur each time the noise signal remained above the threshold for a predetermined length of time. In order to predict the false alarm rate for these conditions we must determine the probability that a noise pulse will be greater than or equal to a preset length of time and that it will also exceed the threshold.

The theory postulated is as follows. If pulses shorter than twice the time constant of the circuit are rejected, it is possible to simulate the false alarm rate of a broadband circuit by

$$FAR = \Delta F_N \, e^{-(T/N)^2} \qquad (13)$$

instead of

$$FAR = \Delta F_N \, e^{-1/2(T/N)^2} \, . \qquad (14)$$

As will be shown in the next section, the experimental results seem to verify this theory.

B. Evaluation of Results

The results of the experimental (measured) data and the theoretical (predicted) data have been compiled in Tables 1 and 2.

In comparing the results of each threshold circuit, one sees that a close correlation exists. Figs. 8 and 9 present these data in a graphical manner. The principal difference is in the slopes. It is believed that the divergence of the slopes is a function of the measured T/N ratio. The RMS noise voltage, together with the computed amplifier gain, could have been consistently too high throughout the measurement interval. The effect here would, in essence, shift the measured data and its slope upward.

TABLE ONE

EXPERIMENTAL DATA (SAMPLE SPACE 100 SECONDS)

NOISE PULSES PER SECOND

RMS NOISE VOLTAGE (MILLIVOLTS)	$(T/N)^2$	CIRCUIT NO. 1* PREDICTED	CIRCUIT NO. 1* MEASURED	CIRCUIT NO. 2** PREDICTED	CIRCUIT NO. 2** MEASURED	COINCIDENCES PREDICTED	COINCIDENCES MEASURED
2.20	12.415	32.81	19.00	31.81	11.1	NA	
.40	10.432	88.46	58.00	85.74	30.9	NA	
.60	8.889	191.30	130.10	185.40	85.0	NA	
.80	7.664	353.00	252.41	342.10	177.0	.87	.71
3.00	6.676	578.50	430.01	560.70	322.0	2.71	2.10
.20	5.868	866.70	681.00	840.10	489.0	6.51	5.40
.40	5.198	1211.00	960.40	1174.00	755.0	14.20	12.00
.60	4.636	1604.00	1283.00	1555.00	1036.0	25.90	23.00
.80	4.161	2034.00	1711.00	1972.00	1410.0	47.20	44.00
4.00	3.755	2492.00	2136.00	2416.00	1650.0	68.90	55.00
.20	3.406	2967.00	2534.00	2876.00	2100.0	104.10	106.00
.40	3.103	3452.00	3050.00	3346.00	2610.0	155.70	157.00
.60	2.839	3940.00	3498.00	3819.00	2854.0	195.30	205.00
.80	2.608	4424.00	3885.00	4288.00	3298.0	250.60	270.00
5.00	2.403	4900.00	4330.00	4750.00	3840.0	325.20	346.00
.20	2.222	5365.00	4790.00	5200.00	4100.0	384.10	430.00
.40	2.060	5816.00	5290.00	5638.00	4813.0	497.90	572.00
.60	1.916	6252.00	5394.00	6061.00	4956.0	522.80	740.00
.80	1.786	6672.00	6105.00	6467.00	5201.0	621.00	875.00
6.00	1.669	7074.00	6660.00	6857.00	5453.0	710.40	1037.00
.20	1.563	7459.00	6993.00	7230.00	6113.0	835.90	NA
.40	1.467	7827.00	7134.00	7587.00	6230.0	869.20	
.60	1.379	8177.00	7300.00	7926.00	6790.0	969.50	
.80	1.299	8511.00	7850.00	8250.00	7038.0	1080.40	
7.00	1.226	8828.00	8220.00	8557.00	7387.0	1187.70	
.20	1.159	9130.00	8600.00	8849.00	7703.0	1295.60	
.40	1.097	9416.00	8850.00	9127.00	8801.0	1385.00	
.60	1.040	9688.00	9100.00	9391.00	8100.0	1441.80	
.80	.987	9947.00	9405.00	9642.00	8790.0	1617.00	
8.00	.938	10190.00	9650.00	9880.00	8805.0	1662.00	
.20	.893	10420.00	9800.00	10100.00	9023.0	1729.60	
.40	.851	10540.00	10010.00	10320.00	9400.0	1840.50	
.60	.812	10850.00	10020.00	10520.00	9629.0	1887.10	
.80	.775	11050.00	10035.00	10710.00	9930.0	1949.00	
9.00	.741	11240.00	10040.00	10900.00	10043.0	1972.20	

*FN = 16.3 kc; τ = 19.56; threshold = 4 volts dc; gain = 516

**FN = 15.8 kc; τ = 20.10; threshold = 4 volts dc; gain = 516

NA = not available

TABLE TWO

RMS NOISE VOLTAGE (MV)	$(T/N)^2$	FALSE ALARM RATE	
		PREDICTED	MEASURED
3.0	8.33	5	8
3.6	6.10	46	55
4.2	4.70	189	205
5.2	3.32	755	725
6.4	2.50	1720	1400

Figure 8. Threshold Circuit No. 1 False Alarm Rate

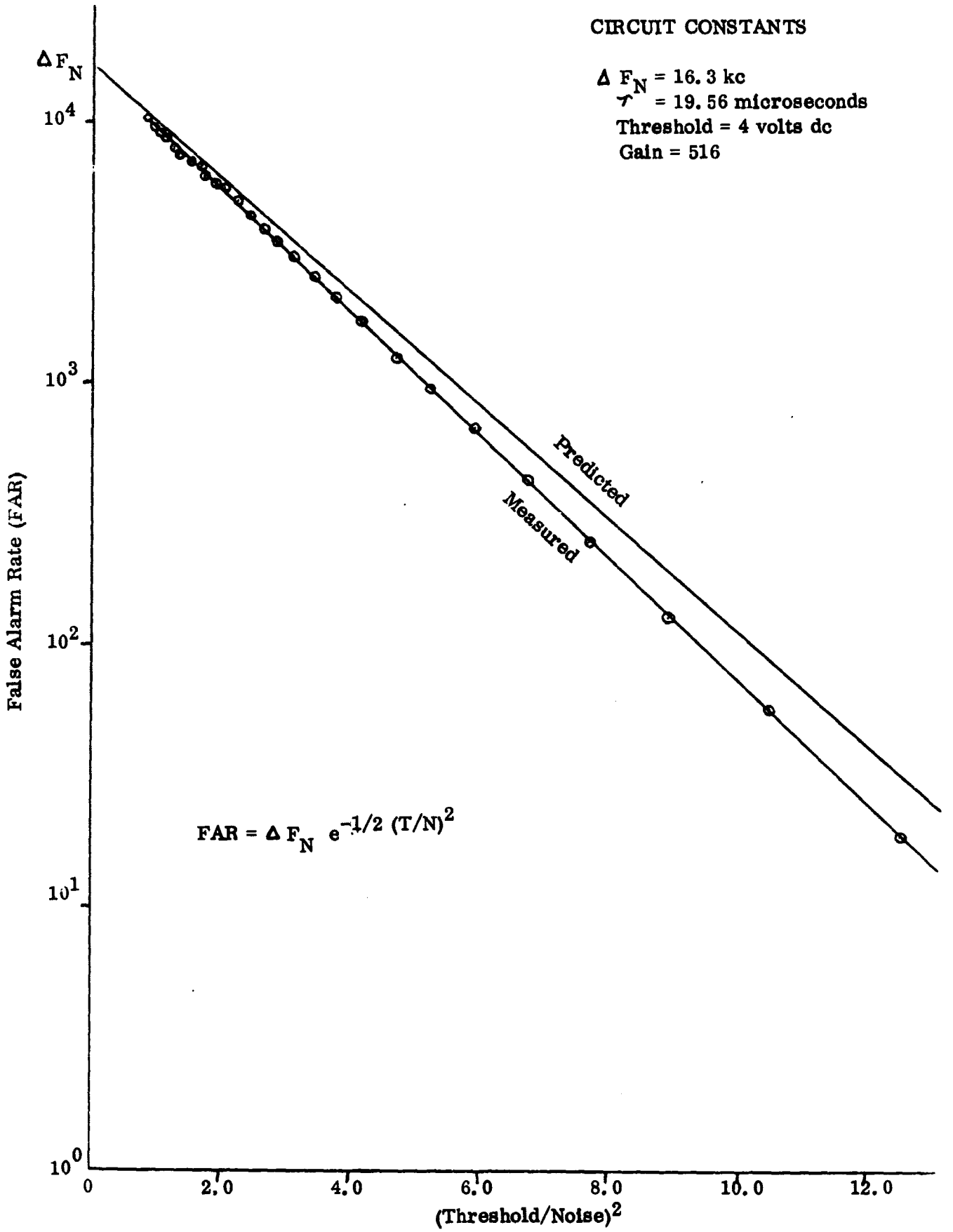

Figure 9. Threshold Circuit No. 2 False Alarm Rate

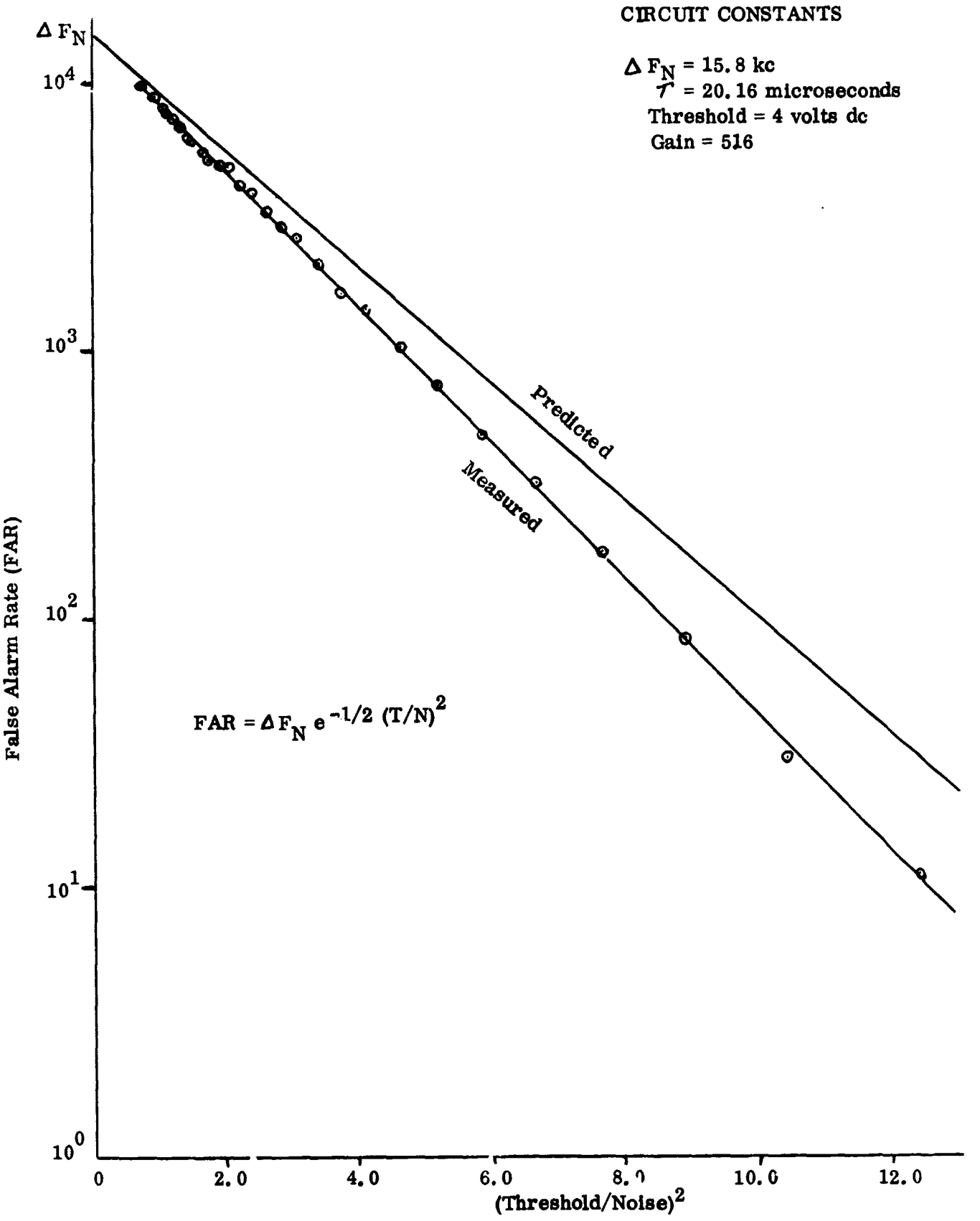

Also, the threshold (T) was found to vary somewhat under load conditions. In operation, it was found that the coincidence circuit added a small delay time to the individual threshold circuits. These subtle errors could shift the results enough so as to produce those differences obtained between the predicted and measured data. It is to be noted that predicted rates are always higher than those measured.

The measured and predicted ROC, as shown in Fig. 10, agreed satisfactorily. It appears that for very small T/N values, the percent increase in the number of coincidences declined because each circuit is in coincidence for longer periods of time. During this "coincidence time", the counter could not register new pulses. Typically, this occurs when a large amplitude noise signal coincides with several closely spaced lower amplitude signals. This counter could only sense the number of pulses and not their duration.

Figure 11 illustrates the effect of employing a pulse discrimination circuit together with the threshold circuit. The false alarm rate is reduced considerably as can be seen by comparison with Figures 8 and 9. The relatively good agreement between the predicted and measured values of FAR indicate that the theory postulated in the previous section is valid. The slight difference in slopes of the two curves illustrates the sensitivity of FAR to the value of the threshold voltage.

IV. CONCLUSIONS

The results presented in the preceding pages indicate that we can predict the effect of noise on the false alarm rate. This capability will allow us to determine the value of the threshold to noise ratio which is necessary to obtain any desired false alarm rate. This knowledge is needed in order to determine the sensitivity to which the circuit must be designed.

The next logical step in the development of the Sisyphus system is to consider the effect of noise on the measurement of transit times and differential times. These effects can be determined by superimposing noise on a signal of known width and then measuring the width of this pulse. The error in differential times, i.e., error in time between pulses, can be determined in a similar manner. This error analysis will be the subject of a separate report.

Figure 10. Rate of Coincidence (ROC)

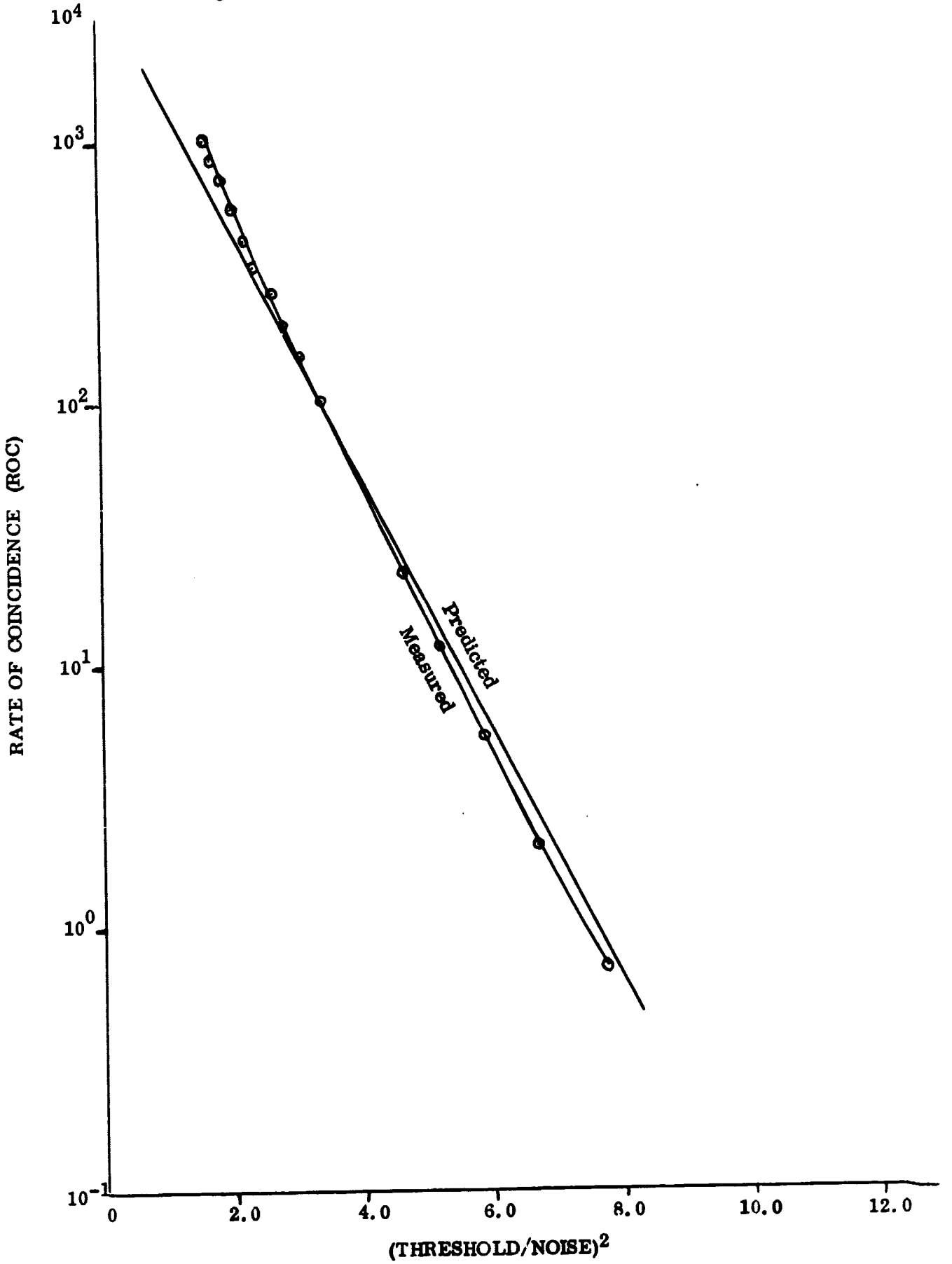

FALSE ALARM RATE WITH PULSE DISCRIMINATION

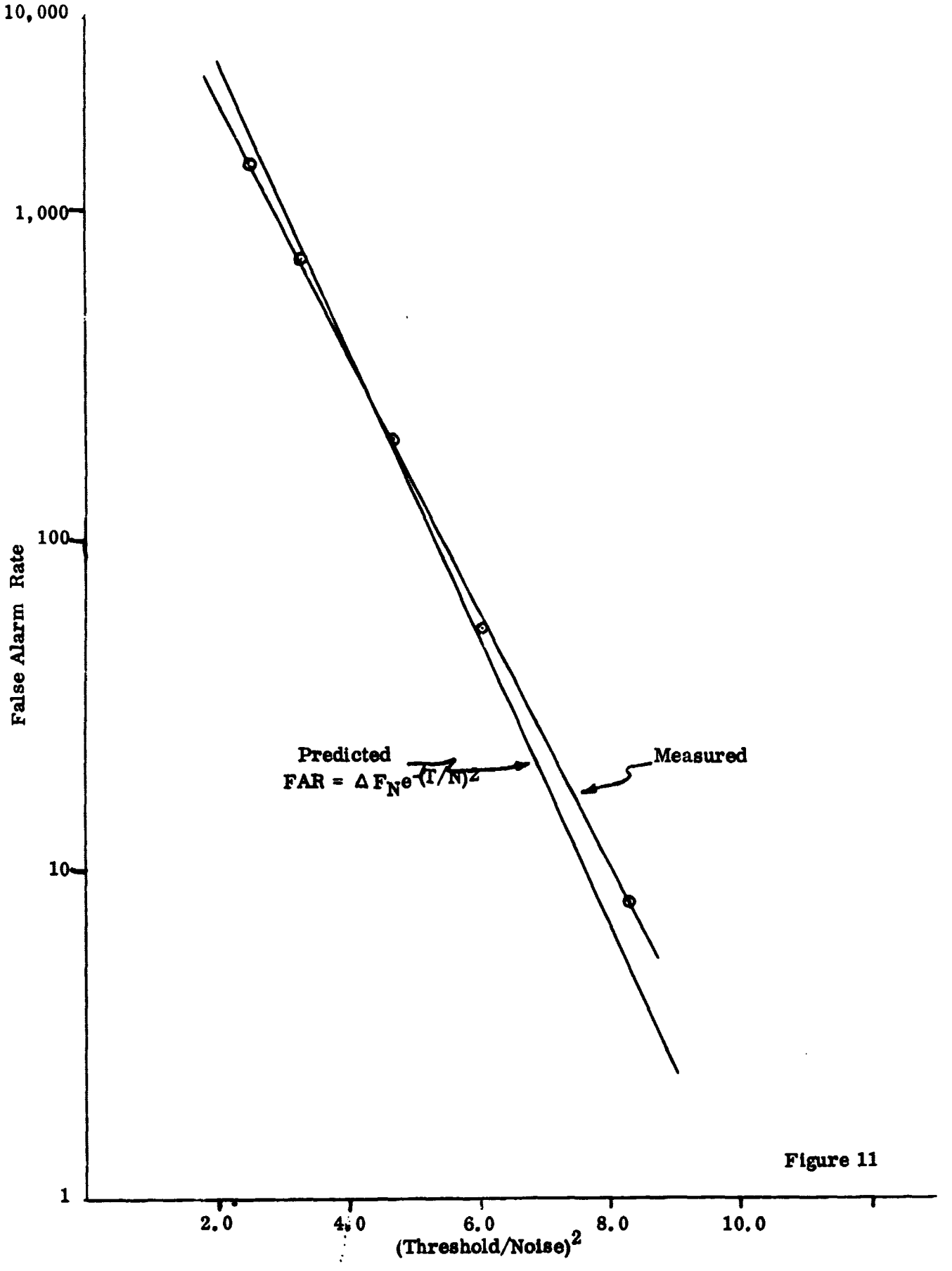

Figure 11

VI. REFERENCES

1. Skolnik, Merrill I., Introduction to Radar Systems (McGraw-Hill, New York, 1962).

2. Bissett-Berman Corp., Research on Non-Sequential Scanner for Surveillance Application, Confidential Report, 1965.

3. Faran, J. J., Jr., Random-Noise Generators, Experimenter, Vol. 42, No. 1, General Radio Co., January 1968.

4. Schwartz, Mischa, Information Transmission Modulation and Noise (McGraw-Hill, New York, 1959).

5. Skolnik, M., op cit.

6. Soberman, R. K., Meteoroid Astronomy in Deep Space and Supplement, GE Document No. N-10788, 1967.

SISYPHUS SIGNAL AND NOISE ERROR ANALYSIS

I. INTRODUCTION

The Sisyphus Detection System obtains information concerning the range and velocity of meteoroids by measuring their transit times through the fields of view of three independent, non-imaging optical subsystems. The success of the system depends upon its ability to produce reliable values for the measured transit times. However, since the system has a finite response time and since the measurements will be made in the presence of background noise it is inevitable that the information returned will be in error to some degree. It is therefore necessary to determine the values of threshold to noise and signal to threshold which will minimize these errors and still allow an adequate amount of data to be obtained. Also, given specific values for the above parameters we must possess the ability to determine the reliability of the data returned.

The errors which should be considered are of two types, namely, the error in the pulse width and the error in the differential times between the pulses of any two subsystems. The errors will be caused by the previously mentioned factors of finite rise time and the presence of noise. An additional source of error may result if the gains of any two pulses are not equal and thus the actual differential times would be altered.

A theoretical analysis of these potential errors is presented in the following pages. For convenience and clarity, the effect of the finite response time is treated first and then the effects of noise and variable gain are added to complete the theoretical study. Experimental verification of the theoretical results is presented in the final pages.

II. THEORETICAL ANALYSIS

A. Noise-Free Considerations

1. Errors in Pulse-width

The analysis which follows assumes that an exponential rise and decay is appropriate for the pulse form, as is shown in Figure 1.

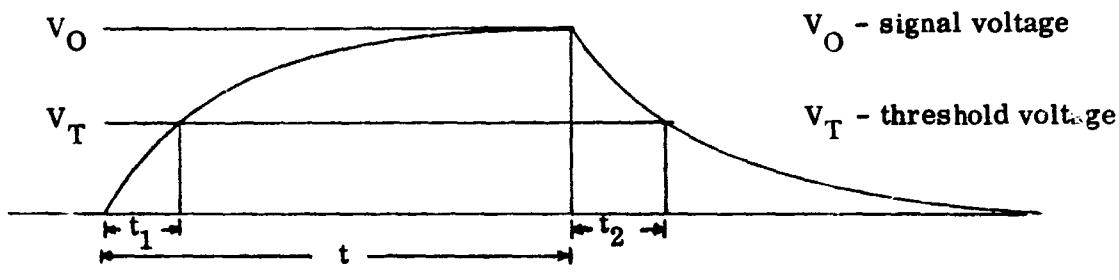

Figure 1

The time which we want to accurately determine is denoted by t. However, due to the non-zero rise-time of the circuit, the threshold voltage will not be reached at t=0 but at some later time (threshold-time) t_1. This limitation on the circuit thus causes our measured value for the lead threshold-time to be too large. Similarly, the trailing edge of the pulse will cross the threshold at a time $t + t_2$ which will also be larger than desired. The total measured width of the pulse will then be given by $t + t_2 - t_1$ which is in error by the amount $t_2 - t_1$. We must, therefore, obtain an expression for this error as a function of known variables.

If we consider the equations for the voltage as a function of time we have

$$V = V_o (1 - e^{-t/\tau}) \qquad (1)$$

from which we obtain, for the leading edge,

$$\frac{t_1}{\tau} = -\ln (1 - V_{T/V_o}) \qquad (2)$$

where τ is the time constant of the circuit. We have the analogous expression for the trailing edge, namely,

$$\frac{t_2}{\tau} = -\ln (V_{T/V_o}). \qquad (3)$$

Subtracting Eq. (2) from Eq. (3) yields

$$\frac{t_2 - t_1}{\tau} = \ln (1 - V_{T/V_o}) - \ln (V_{T/V_o}) \qquad (4)$$

Thus, we see that the pulse-width error is a function of the ratio (signal voltage/threshold voltage), V_o/V_T. The curves shown in Figure 2 illustrate this functional relationship. Note that the error is given in terms of the time constant, τ.

Also shown in Figure 2 is the case where the lead threshold is twice as large as the trailing threshold. This case of unequal thresholds may be used to eliminate the "dropout problem," i.e., when a signal is caused to fall below

EFFECT OF GAIN ON MEASURED PULSE WIDTH

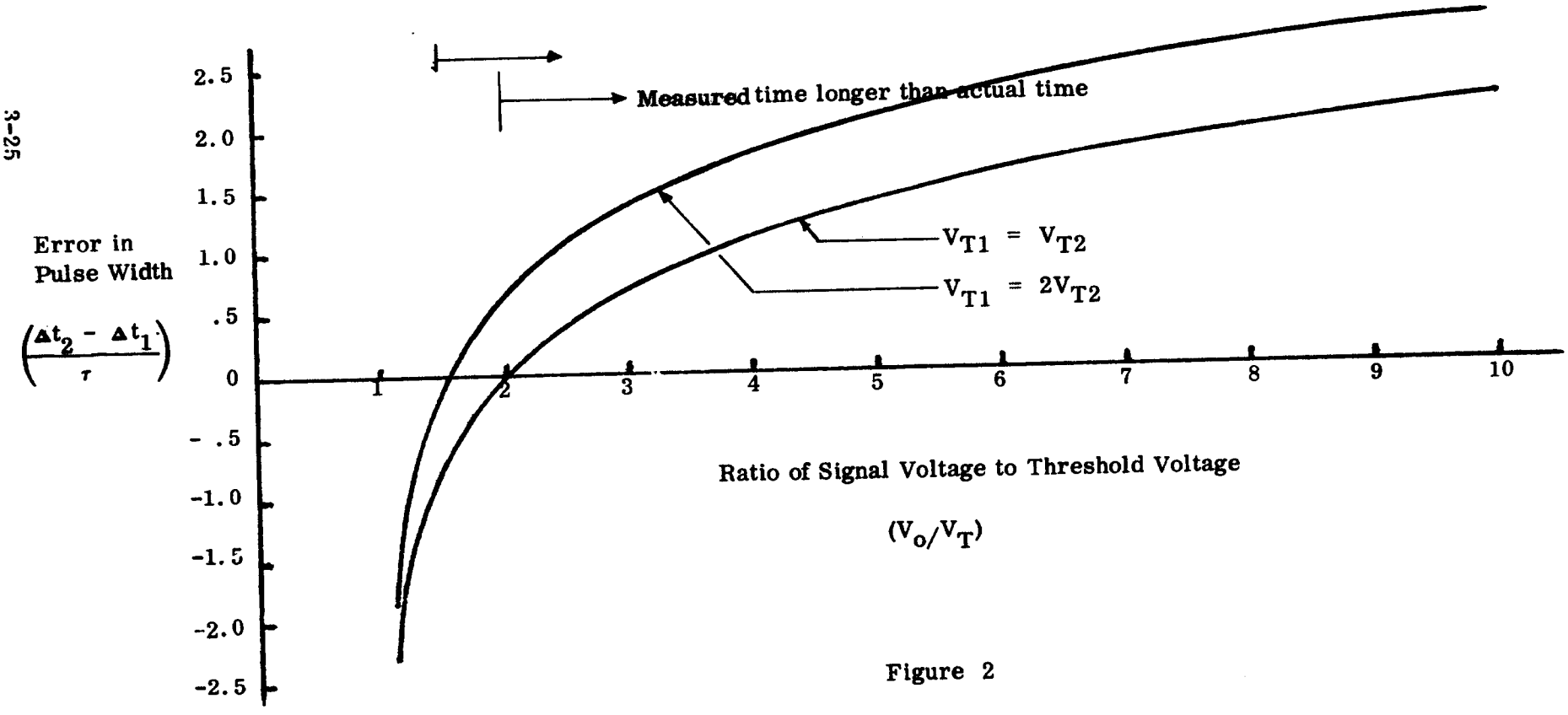

Figure 2

the threshold prematurely due to background noise. If dropout did occur the measured time for the pulse-width would be too small. Since the occurrence of "dropout" is difficult to detect and to compensate for the probability of its occurrence should be minimized.

2. Errors in Differential Times

Determination of the pulse-to-pulse error can be simplified by considering the change in threshold time produced by a variation in the gain. This difference is the error in the differential time measurements. We should, therefore, determine the change in threshold time as a function of the variation in gain. The parameters of interest are illustrated in Figure 3.

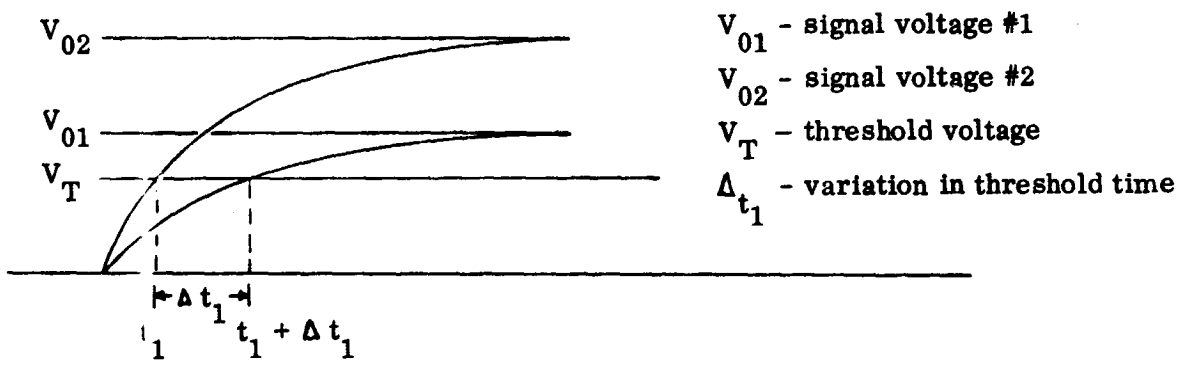

Figure 3

From Figure 3 we see that we must obtain an expression for Δt_1, (since it represents the variation in threshold-time). For any given threshold voltage, V_T, we have the expressions

$$V_T = V_{o1} (1-e^{-t_1/\tau}) \qquad (5)$$

and

$$V_T = V_{o2} (1-e^{-(t_1 + \Delta t_1)/\tau}) \qquad (6)$$

Manipulation of Eqs. (5) and (6) give us the results

EFFECT OF GAIN ON
PULSE TO PULSE ERROR

Noise Voltage = 0

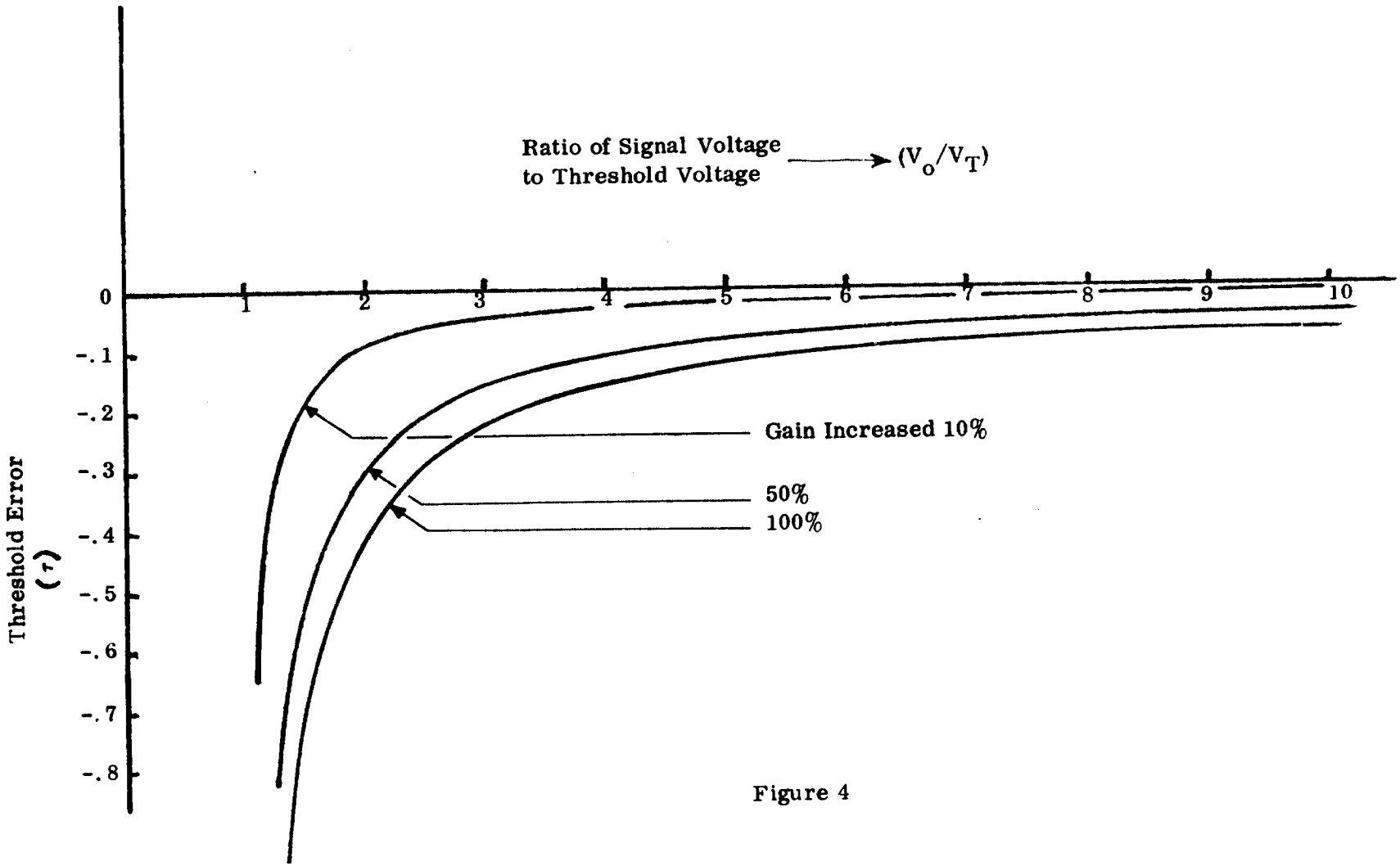

Figure 4

$$\frac{t_1}{\tau} = -\ln (1 - V_{T/V_{o1}}) \qquad (7)$$

and

$$\frac{t_1 + \Delta t_1}{\tau} = -\ln (1 - V_{T/V_{o2}}) \qquad (8)$$

Subtracting Eq. (7) from Eq. (8) provides us with the desired expression for Δt_1, namely,

$$\frac{\Delta t_1}{\tau} = \ln (1 - V_{T/V_{o1}}) - \ln (1 - V_{T/V_{o2}}). \qquad (9)$$

Thus, by varying the ratio V_{T/V_o} we can determine the behavior of Δt_1 for various values of $V_{o2/V_{o1}}$. The results of these calculations are shown by the curves in Figure 4. If we assume that $V_{o/V_T} = 2.$ is a typical value for the signal to threshold ratio, we see that a 100% variation in the gain produces an error of $.4\tau$ in the measured differential time.

B. Noise Considerations

1. Errors in Pulse Width

The previous analyses have assumed that we have been working with noise free circuits. At this point we shall consider the effect of white noise on the leading and trailing edges and thereby determine the pulse width errors.

It has been shown (Reference 1) that the noise in a circuit can be approximated by its constant rms value and added to the signal. On this basis our pulse (with noise) will be as shown in Figure 5.

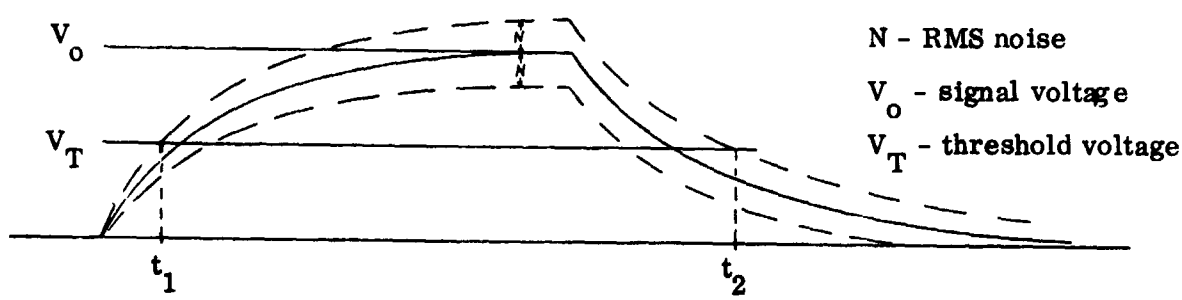

Figure 5

Our equations for the potential will thus have the form

$$V = V_o (1-e^{-t_{1/\tau}}) \pm N \qquad \text{(leading edge)} \quad (10)$$

and

$$V = V_o e^{-t_{2/\tau}} \pm N. \qquad \text{(trailing edge)} \quad (11)$$

Since we want the worst case we must use the expressions for the potentials in which the rms noise is added to both the trailing and leading edge of the pulse. Our expressions for the threshold times then become

$$\frac{t_1}{\tau} = -\ln (1- {}^{V_{T/V_o}} + {}^{N/V_o}) \qquad (12)$$

and

$$t_{2/\tau} = -\ln ({}^{V_{T/V_o}} - N/V_o). \qquad (13)$$

Combining eqs. (12) and (13) gives us

$$\frac{t_2 - t_1}{\tau} = \ln (1- {}^{V_{T/V_o}} + {}^{N/V_o}) - \ln ({}^{V_{T/V_o}} - {}^{N/V_o}) \qquad (14)$$

as the expression for the pulse width error in the presence of noise. In Figure 6 the pulse width error in the presence of noise is shown as a function of V_o/V_T for a (threshold/noise) ratio of 5. In order to illustrate the effect of noise more clearly, the error without noise is again presented.

2. Errors in Differential Times

As before we can determine the pulse-to-pulse errors by considering only the errors in the leading edge measurements as is illustrated in Figure 7.

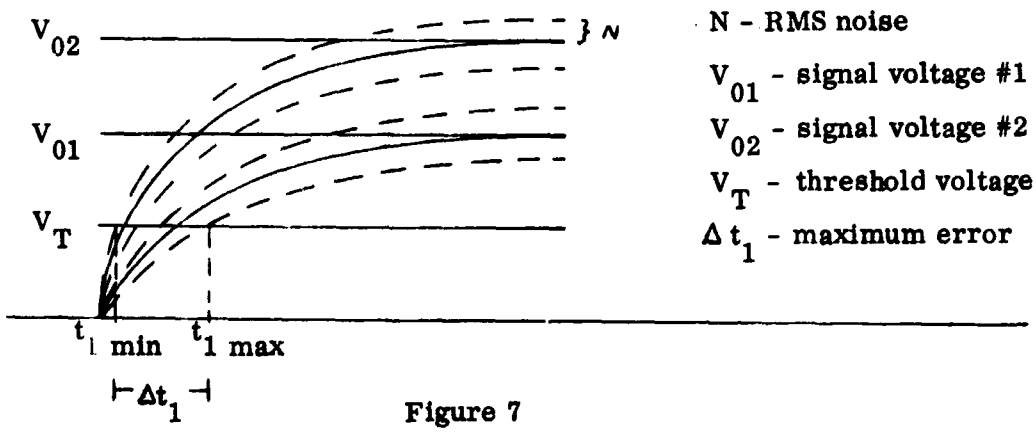

Figure 7

EFFECT OF GAIN ON MEASURED PULSE WIDTH

$$\frac{\text{Threshold Voltage}}{\text{Noise Voltage}} \left(\frac{V_T}{N}\right) = 5.0$$

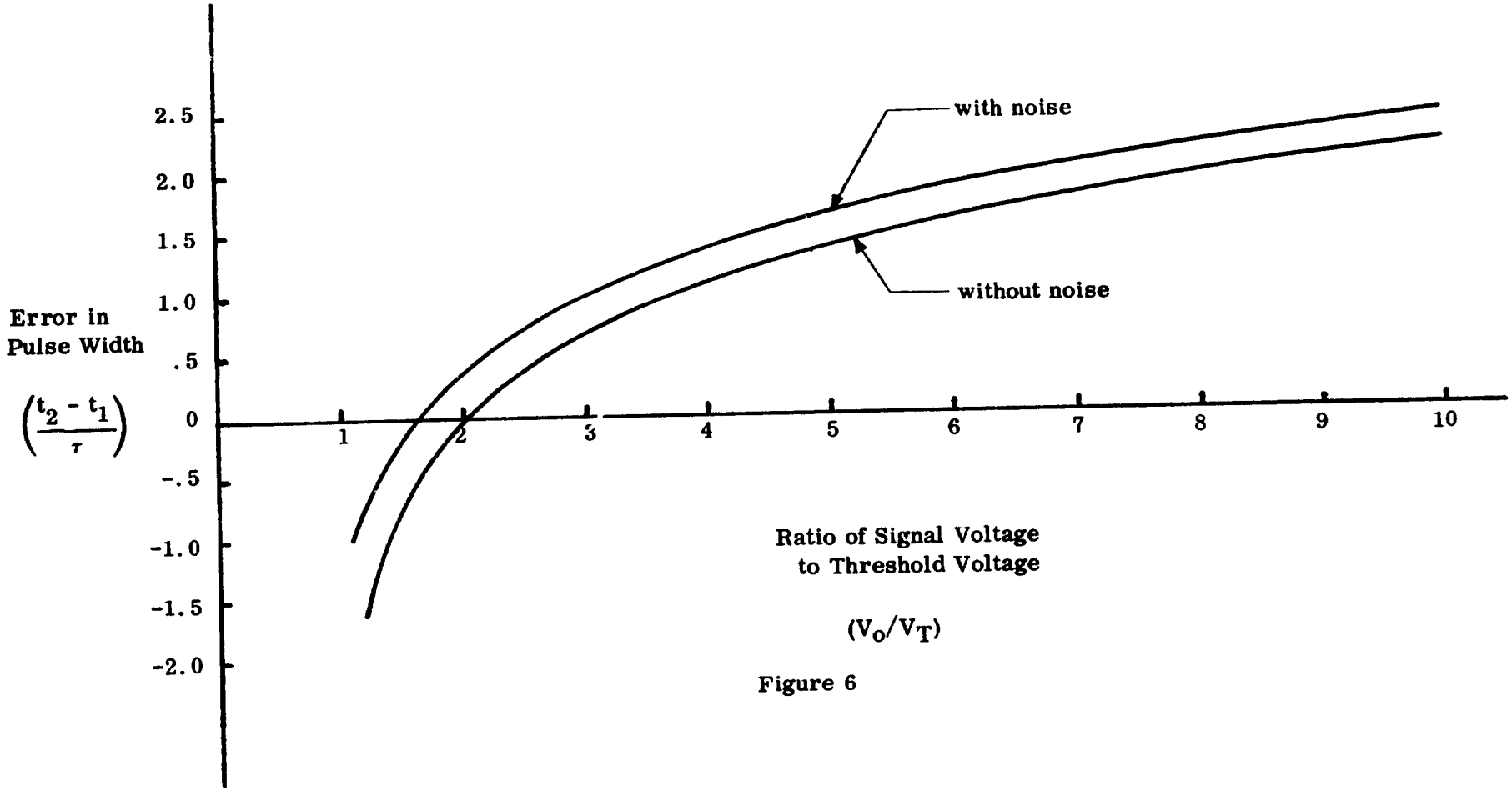

Figure 6

The quantity Δt_1 represents the maximum rms error which can occur in measuring the threshold-time. If we determine an expression for Δt_1, in Figure 7, it will represent a worst case analysis of the problem. Our expression for the potential now has the form

$$V_T = V_{o1} (1-e^{t_{1\,max}/\tau}) - N \qquad (15)$$

which yields

$$\frac{t_{1\,max}}{\tau} = -\ln (1- {}^{N}/_{V_{o2}} - {}^{V_T}/_{V_{o1}}). \qquad (16)$$

Similarly, we have

$$\frac{t_{1\,min}}{\tau} = -\ln (1 + {}^{N}/_{V_{o2}} - {}^{V_T}/_{V_{o2}}). \qquad (17)$$

Thus, the maximum rms error which could be obtained in measuring the threshold-time of a pulse with variable gain in the presence of noise is given by

$$\frac{t_{1\,max} - t_{1\,min}}{\tau} = \ln (1 + {}^{N}/_{V_{o2}} - {}^{V_T}/_{V_{o2}}) - \ln (1- {}^{N}/_{V_{o1}} - {}^{V_T}/_{V_{o1}}) \qquad (18)$$

The magnitude of this error can be examined as a function of the three ratios ${}^{V_{o1}}/_{V_{o2}}$, ${}^{V_T}/_{N}$, and ${}^{V_o}/_{V_T}$. The results of such a study are shown in Figures 8 and 9.

III. EXPERIMENTAL VERIFICATION OF THEORY

In order to determine the validity of the theoretical predictions, an electrical circuit capable of simulating actual signal to noise problems was constructed. The circuit, shown in block form in Figure 10, was essentially the same as that used previously in determining false alarm rates (FAR) for the system (Ref. 2). The only modification was the addition of a pulse generator, which provided the signal input.

The noise signal was generated by light emission to a photomultiplier tube. The output of the photomultiplier was then added to a signal from the pulse generator

EFFECT OF GAIN ON PULSE TO PULSE ERROR

$$\frac{\text{Threshold Voltage}}{\text{Noise Voltage}} \left(\frac{V_T}{N}\right) = 3$$

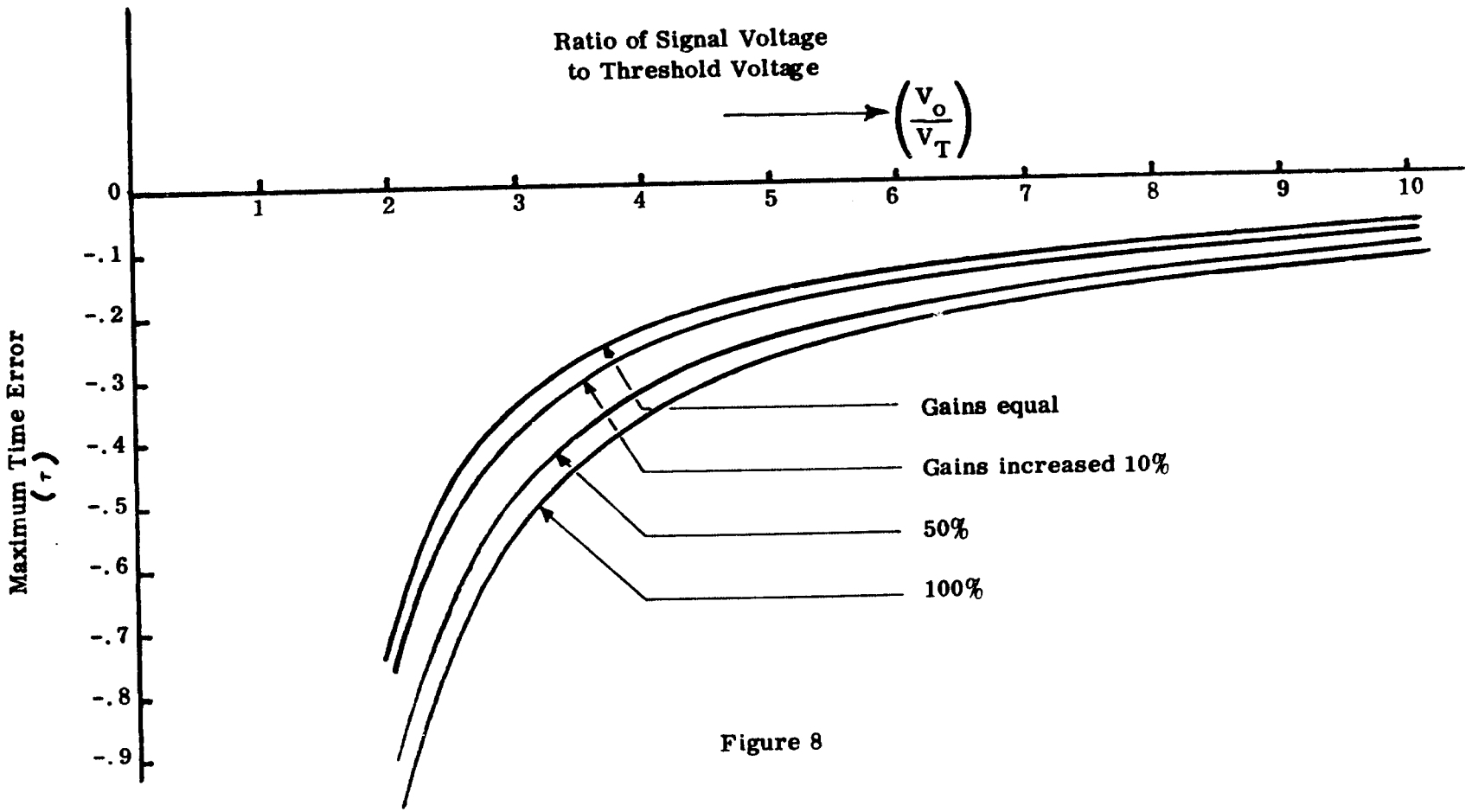

Figure 8

EFFECT OF GAIN ON PULSE TO PULSE ERROR

$$\frac{\text{Threshold Voltage}}{\text{Noise Voltage}} \left(\frac{V_T}{N}\right) = 5$$

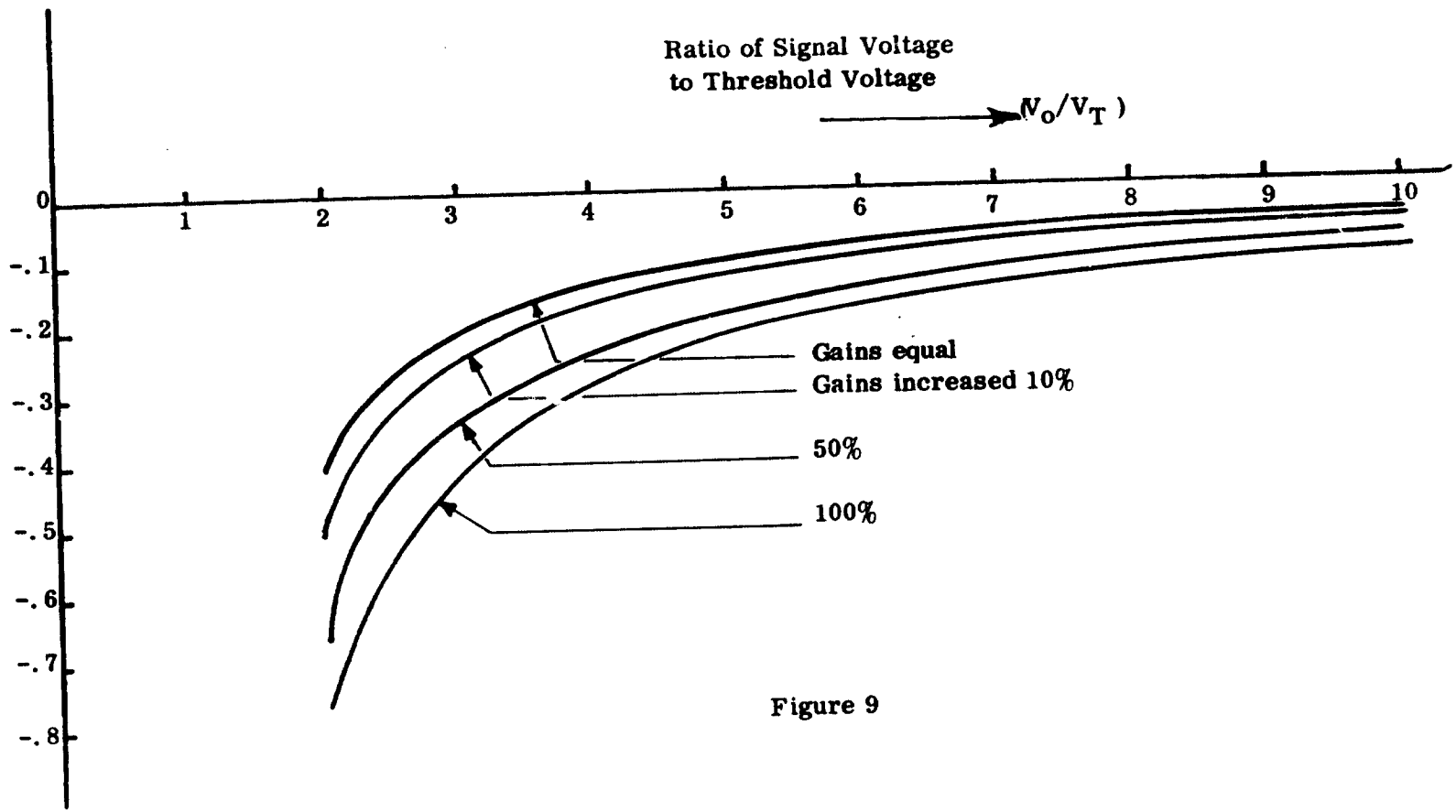

Figure 9

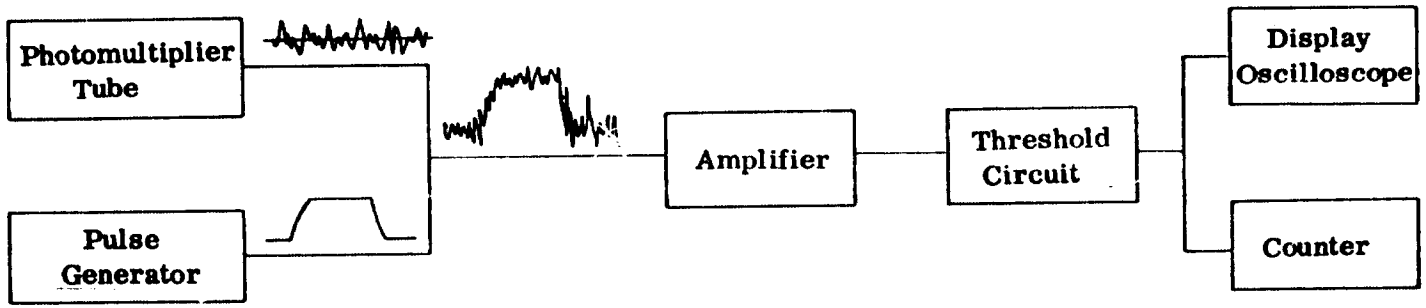
Photomultiplier Tube
Pulse Generator
Amplifier
Threshold Circuit
Display Oscilloscope
Counter

Figure 10

to produce a signal in the presence of noise. This output was then amplified and used to make the signal to noise measurements.

The threshold voltage was preset at a constant value of 4 vdc. Then by varying the rms noise voltage the ratio of (threshold/noise) could be controlled. The value of V_T/N will determine the false alarm rate as was shown in Ref. 2. It should be noted that a high V_T/N ratio corresponds to a low false alarm rate, e.g. if $V_T/N = 5$ then FAR $\simeq$ .6/sec. The value of (signal/noise) can be controlled by adjusting the amplitude of the pulse generator. It is, therefore, possible to obtain any set of conditions desired.

In order to provide experimental verification of our theoretical results we made several measurements in the most sensitive region of the curve. For each value of V_o/V_T several ($\sim$50) readings were taken for the pulse width and the standard deviation was calculated (Table 1). In this case the standard deviation is actually the deviation from the pulse-width error without noise. Thus, if these points are plotted they should fall on the theoretical curve for pulse-width error with noise. As is shown in Fig. 11, there is close agreement between the predicted and actual values. The accuracy of the theory seems to increase with larger values of V_o/V_T. The significance of Fig. 11 is that 68% of the pulse-width measurements will have errors which lie within the dashed boundaries.

Similar measurements were made for the pulse-to-pulse errors (Table 2) with the results shown in Fig. 12 for the specific value of $V_T/N = 5$. Again we see that the experimental and theoretical values are in close agreement.

PULSE WIDTH ERROR RANGE (1σ)

$$\frac{\text{Threshold Voltage}}{\text{Noise Voltage}} \left(\frac{V_T}{N}\right) = 5.0$$

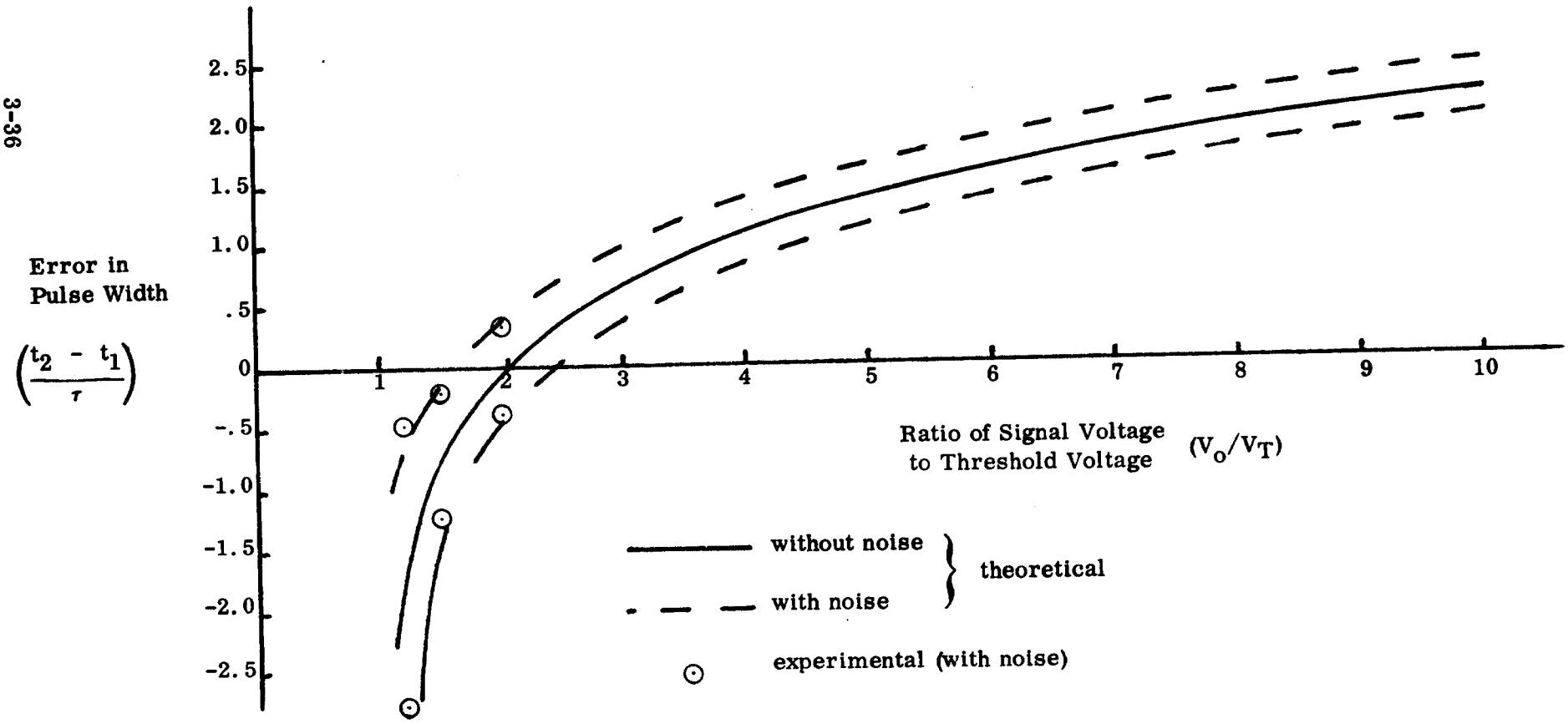

Figure 11

PULSE TO PULSE ERROR RANGE (1σ)

$$\frac{\text{Threshold Voltage}}{\text{Noise Voltage}} \left(\frac{V_T}{N}\right) = 5.0$$

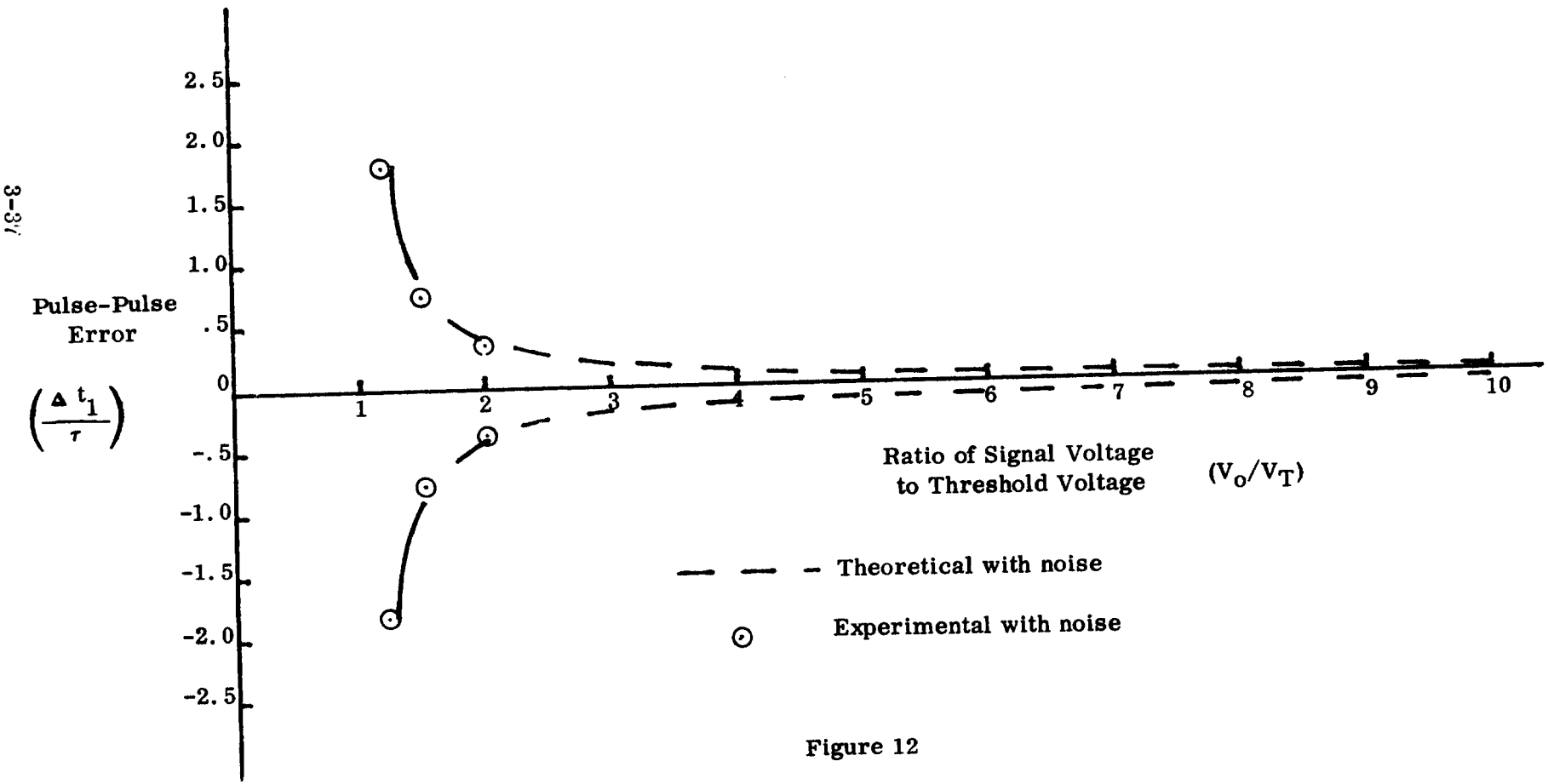

Figure 12

*TABLE 1

Pulse-width Errors

V_o/V_T (signal/threshold)	Theoretical** RMS Error	Experimental RMS Error
1.2	$1.05\tau = 15.75$ μ-sec.	17.43 μ-sec
1.5	$.55\tau = 8.25$ μ-sec.	7.64 μ-sec
2.0	$.4\tau = 6.00$ μ-sec.	5.95 μ-sec.

*TABLE 2

Pulse-to-Pulse Errors

V_o/V_T	Theoretical** RMS Error	Experimental RMS Error
1.2	-------	27.36 μ-sec.
1.5	$.85\tau = 12.75$ μ-sec	11.37 μ-sec.
2.0	$.4\tau = 6.00$ μ-sec	5.41 μ-sec.

** τ = time constant = 15μ s

*Note that (RMS Error)/τ is plotted in Figs. 11 & 12

IV. CONCLUSIONS AND SUMMARY

Although the experimental values obtained were limited in number, they were obtained for the most critical and sensitive portion of the curve. Since they correlated quite well throughout this region, it seems reasonable to assume that this close correspondence will continue for the remainder of the useable operating region.

We have therefore exhibited the capability of predicting the accuracy to which any time measurement can be made. Given the value of (threshold/noise) and (signal/threshold) it is possible to determine confidence limits on the error in the measurement. For example in Figures 11 and 12 we have shown the 68% confidence limits for the pulse-width error and pulse-to-pulse error.

The initial step in determining any error range is to define the expected false alarm rate, which in turn, will give us the (threshold/noise) ratio. It is then possible to generate the range of expected error as a function of (signal/threshold) and thus determine the reliability or accuracy of the data returned.

V. REFERENCES

1. Skolnik, M. I., Introduction to Radar Systems, pp. 462 - 465, (McGraw-Hill Book Company, Inc., New York, 1962).

2. Chaess, H., Threshold to Noise and Coincidence, Measurements for a New Meteoroid Detector, May, 1968.

APPENDIX 4

SISYPHUS ERROR ANALYSIS

I. Introduction

A parametric analysis has been performed to estimate the errors in particle range and velocity which may result from uncertainties in the measured parameters. The parameters to be measured and which will be considered in this study are the optical misalignment angles and the times of particle entrance and exit for each field of view.

Obviously, there exists an infinity of possible trajectories and any attempt to analyze more than one or two representative cases would indeed be a Sisyphustian task. Therefore, a "baseline trajectory " was established and the analysis was confined to considerations of this sample. Thus, it must be remembered that the results which are presented apply specifically only to the baseline trajectory, but will illustrate trends and relative errors between parameters which can be applied to other cases.

II. Instrument and Trajectory Information

A. Instrument Parameters

Since all necessary information can be derived from measurements made with a three-cone system, the analysis was performed with three optics arranged such that the apices of the conical fields of view were at the vertices of an equilateral triangle. The separation distance between individual optics was 8.5 inches, and the total field of view of each optic was 7.8^{o}. These dimensions are consistent with those being used for the Pioneer system, except that any three

cones chosen from the four-cone system of Pioneer will be at the vertices of a isosceles right triangle whose legs are 8.5 inches, and consequently, one separation distance will be greater than 8.5 inches (~12 inches). It must also be pointed out that four optics provide four independent solutions, yielding an improvement in accuracy of a factor of 2.

In order to have a realistic system we must assume that the optics are misaligned, i.e., the three optical axes are not mutually parallel. It is estimated that the axes can be aligned to within four milliradians. Therefore, a nominal misalignment of 4 milliradians will be used throughout the analysis. The angles used to describe the misalignment are illustrated in Figure 1.

B. Trajectory Parameters

An attempt was made to choose a particle trajectory which represents a "general" case, i.e., transit times are not maximum, differential times are all unequal and the velocity components are all non-zero. The parameters of such a trajectory are shown in Table 1, along with the instrument parameters for completeness. Figure 2 illustrates the path of the particle through the three-cone system in the aligned and misaligned case.

The first cone entered by the particle is designated cone number one. If the triangle formed by the line joining the apices of the three cones is traversed in a clockwise direction as seen looking into the detector, the next apex encountered will be designated as the apex of cone 2. The remaining cone is then cone 3. The coordinate axes for the system are centered at the apex of cone 1 with the positive X_2 axis extending to the apex of cone 2. The positive X_3 axis coincides

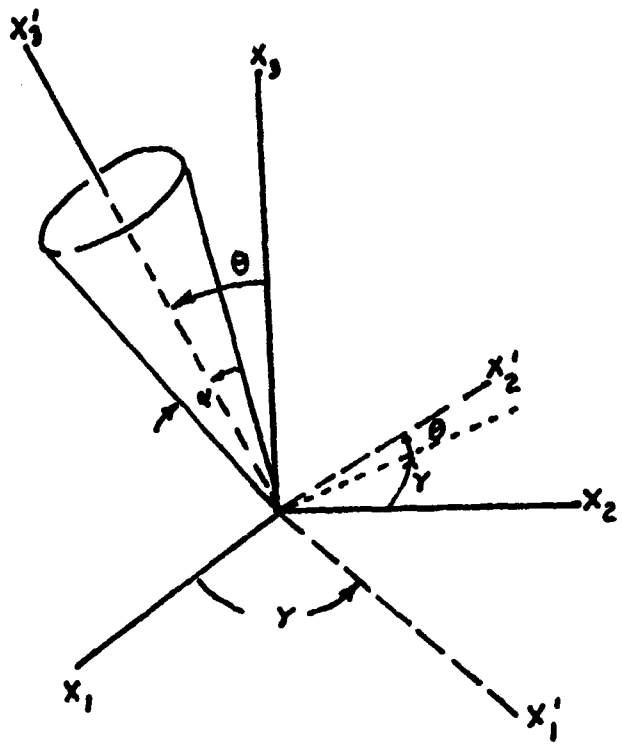

Figure 1. Illustration of the angles(θ,γ) used to define the optical misalignment.

Table 1

Trajectory Parameters:

Particle Velocity		20 km/s
Velocity Component	V_1	13.15 km/s
Velocity Component	V_2	14.14 km/s
Velocity Component	V_3	4.84 km/s

Entrance angle (see Figure 1):

For Range = 10 m	200^{o}
For Range = 100m	223^{o}

System Parameters:

Separation Distance of Optics	8.5 in.
Total Field of View	7.8^{o}

Misalignment Angles:

θ_2	4 m rad
γ_2	π
θ_3	4 m rad
γ_3	$\pi/4$

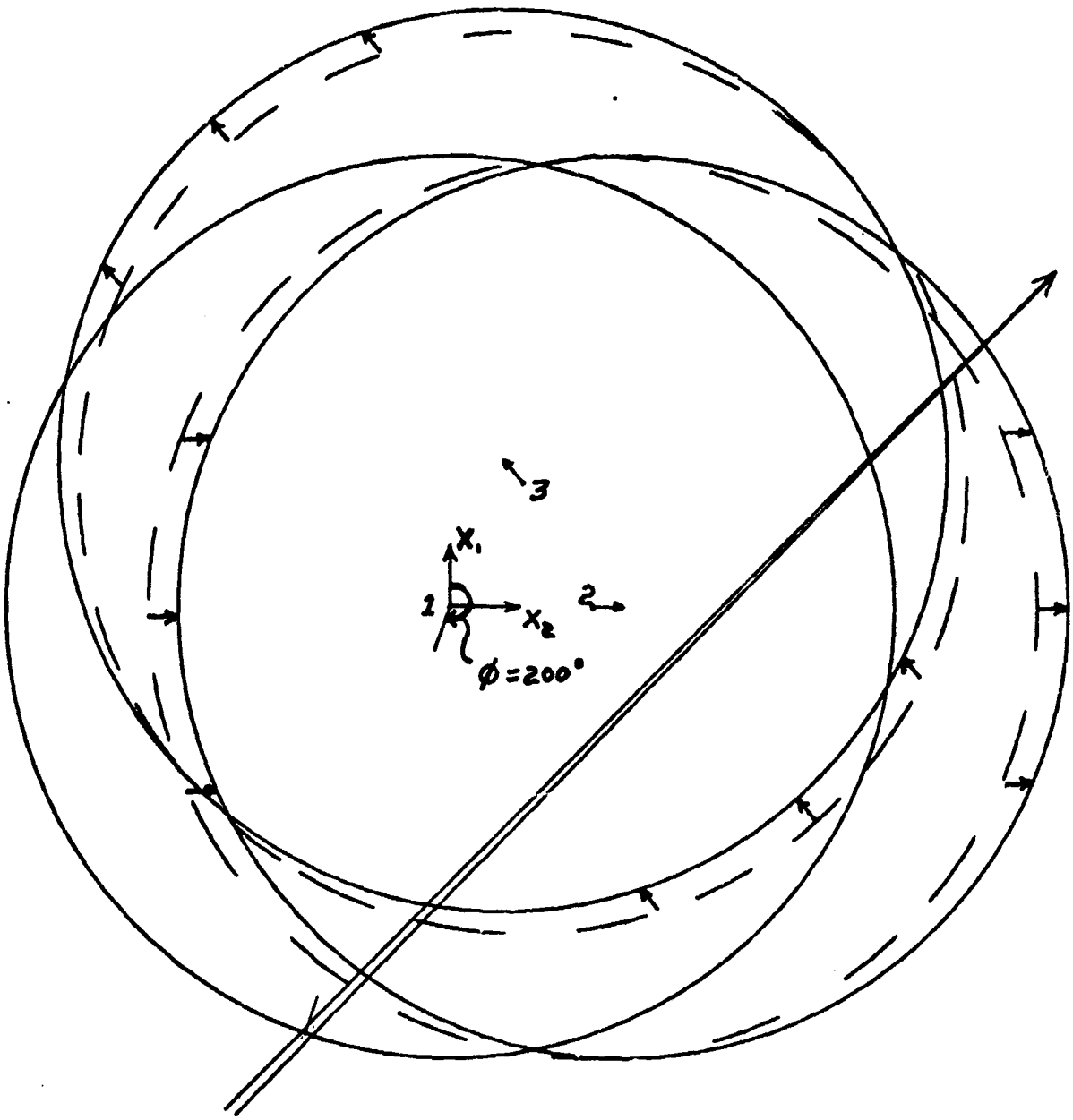

Figure 2. Trajectory through aligned (dashed) and misaligned (solid) fields of view at a range of ~10 meters. Arrows indicate direction of misalignment.

with the optical axis of cone 1 and the X_1 axis completes a right-handed orthogonal coordinate system with X_2 and X_3.

III. Method of Analysis

In order to perform the desired analysis of the system, the correct entrance and exit times had to be generated for the trajectory to be studied. It was to meet this requirement that the computer program "MISTIMES" was written. Using the set of system and trajectory parameters given in Table 1, the set of times (Tij) listed in Table 2 was generated. The subscript i = 1, 2, or 3 identifies the cone; the subscript j = 1 or 2 denotes an entrance or exit, respectively.

The usual procedure for determining the range and three velocity components was first to assume that the system was aligned and obtain an estimated set of solutions using the "SISYPHUS" program. This estimate was then used as the starting point for the iterative procedure employed in determining the solutions for a misaligned system using the "MISSYS" program. However, it was found that when the difference between the estimate and the correct solution was greater than about 50% of the correct solution, erroneous values were returned for the range and the velocity components. It was also found that any set of estimates which was within 50% of the correct values would consistently return the same set of answers, namely the correct set. If, on the other hand, different estimates returned different sets of solutions, the correct set was never among them. Thus, when a variety of estimated solutions consistently yield the same results. the correct solution has been obtained. It was also observed that errors in the estimated range had he

Table 2

Range = 10 m:

$T_{11} = 0.0$	$T_{12} = 63.95\ \mu s$
$T_{21} = 6.44\ \mu s$	$T_{22} = 77.00\ \mu s$
$T_{31} = 13.71\ \mu s$	$T_{32} = 71.43\ \mu s$

Range = 100 m:

$T_{11} = 0.0$	$T_{12} = 714.93\ \mu s$
$T_{12} = 21.15\ \mu s$	$T_{22} = 740.16\ \mu s$
$T_{13} = 12.27\ \mu s$	$T_{32} = 722.42\ \mu s$

greatest influence on the results obtained by the iterative procedure. Finally, the values of the entrance angle obtained from SISYPHUS were found to be acceptable estimates in most cases.

Currently, the estimates must be chosen by the analyst, but it will obviously be advantageous to incorporate this task into the computer program. When this program modification is completed the computer will choose estimates until the same set of values is consistently returned.

Using the three computer programs, MISTIMES, SISYPHUS, and MISSYS (see Section VII) the following questions were answered for the trajectory and system parameters listed in Table 1:

Assuming correct misalignment (values in table 1) -

1. What is the effect of a change in one exit time?
2. What is the effect of a change in all exit times?
3. What is the effect of a change in the entrance and exit times of one channel (constant transit time)?
4. What is the effect of a change in the pulse width of 1 channel?
5. What is the effect of a change in the pulse width of 2 channels?

Assuming correct times (values in table 2) -

6. What is the effect of a change in the misalignment angles?
7. What is the maximum misalignment angle which can be tolerated?

IV. Results of the Analysis

The assumed errors in the entrance and exit times were varied from 0.1μs

to 1.6 μs; the effect of these errors on the range and the three velocity components is illustrated graphically in Figures 3 through 8. Figures 3 and 4 show the effect of varying first one and then all three exit times. When only one exit time is changed, an error is introduced into the exit differential (time between exits from two successive cones) which results in large error in V_3 (the axial velocity). However, if all three exits are changed equally (Figure 4) the differentials remain unaffected and the corresponding errors are very small.

The curves in Figure 5 illustate the effect of changing the entrance and exit times of one channel such that the transit time will remain constant. Since we are again changing the differential times, a large error is observed in V_3 (as expected).

The results shown in Figures 6 and 7 correspond to the physical case of too high (or too low) a threshold setting, which would result in the measured transit time being too short (or too long). Once again, the errors are quite well behaved with the exception of V_3. It should be noted that in all cases (Figures 3 - 7) the errors in V_3 and range are somewhat less at the 100 m distance than at 10 m. This improvement is due to the divergent misalignment which increases the differentials at the larger range, thus reducing the percentage error in differential time. All results presented up to this point have assumed that the misalignment angles are accurately known.

If it is now assumed that the times are correctly measured, what error will be introduced by an uncertainty in the misalignment angles? This question is answered by the curves of Figure 8 which show that measurements at large ranges are affected much more than those at close range. This is quite reasonable since

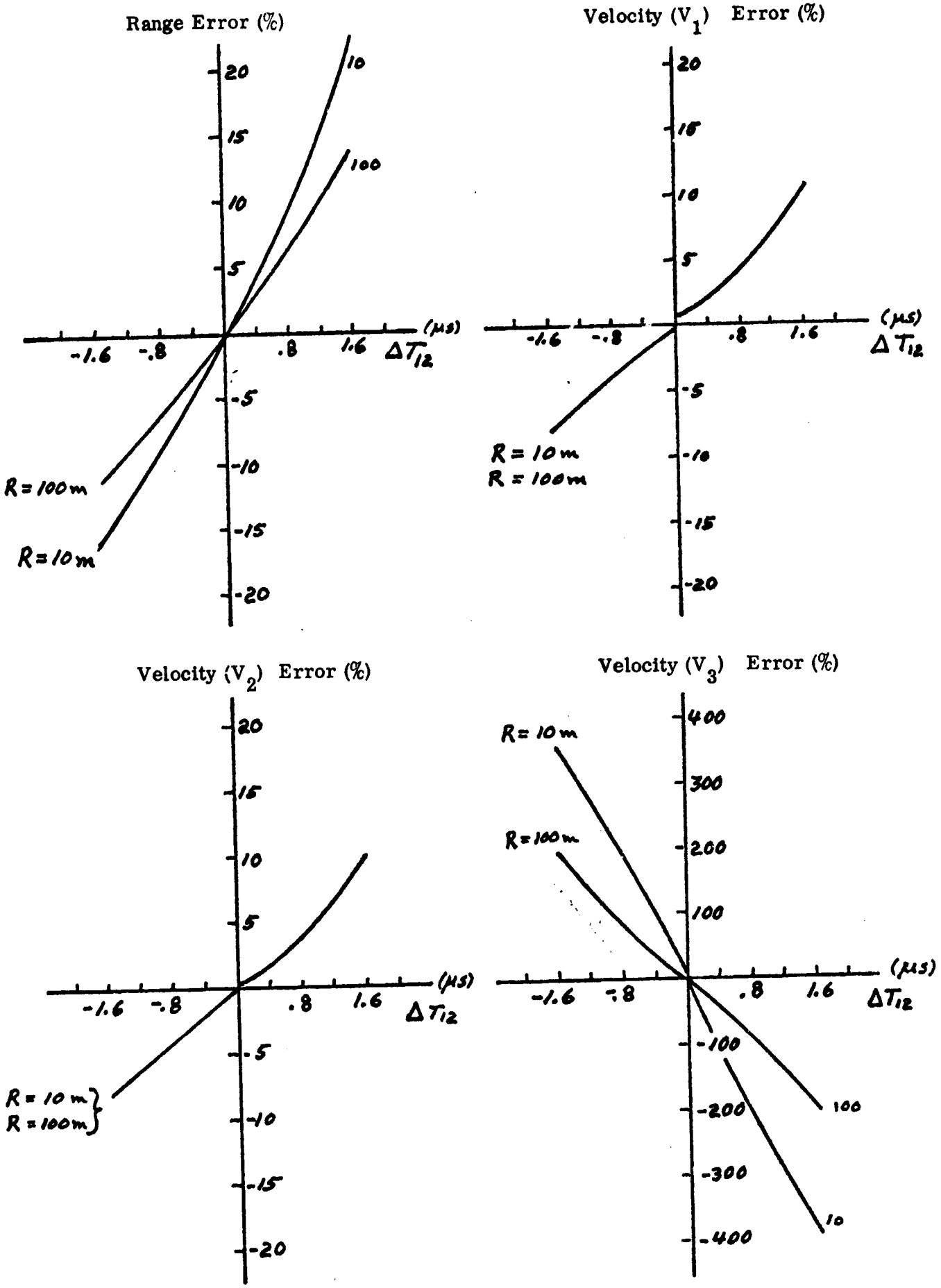

Figure 3. Effect of changing channel 1 exit time

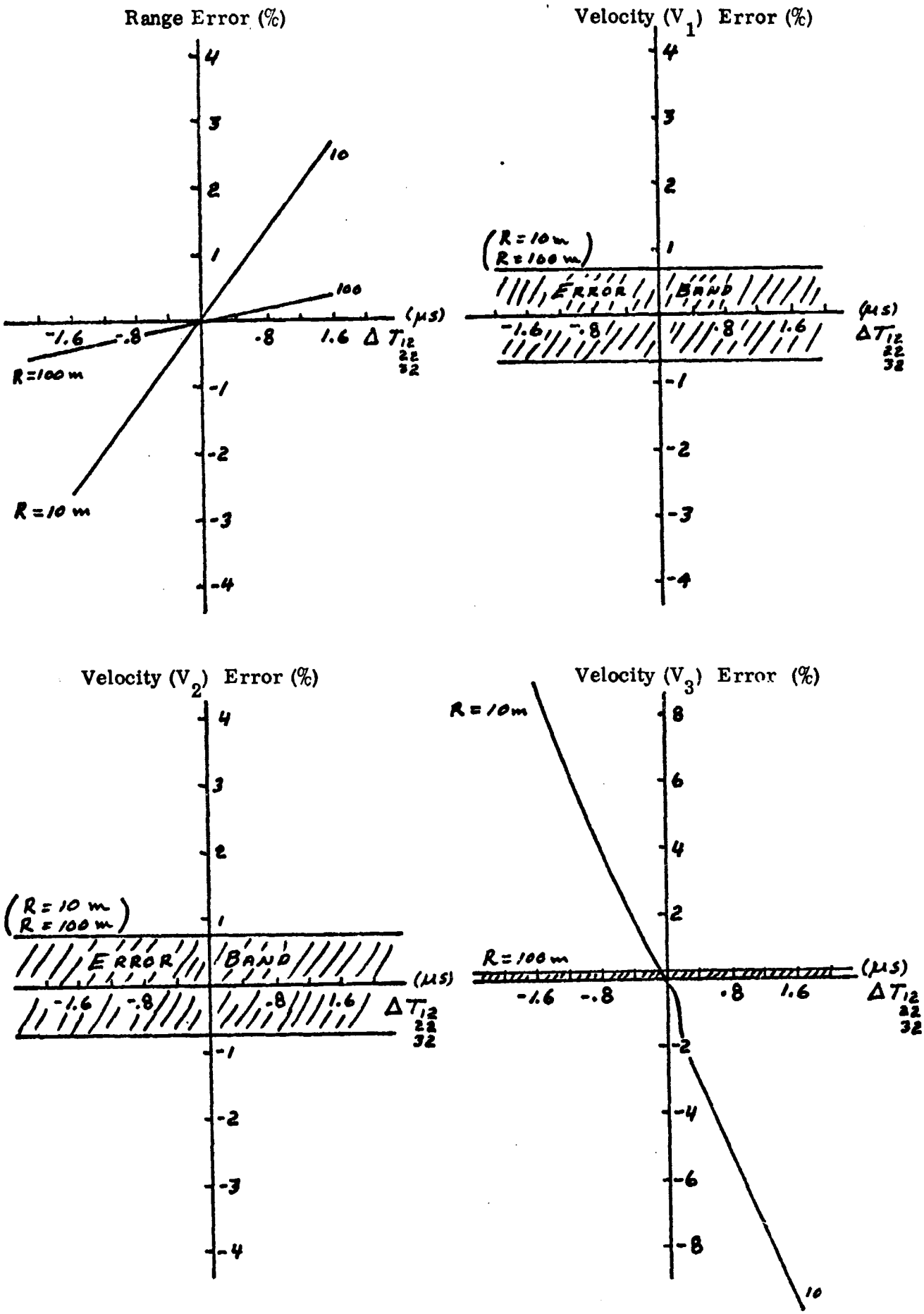

Figures 4. Effect of changing exit times of all channels.

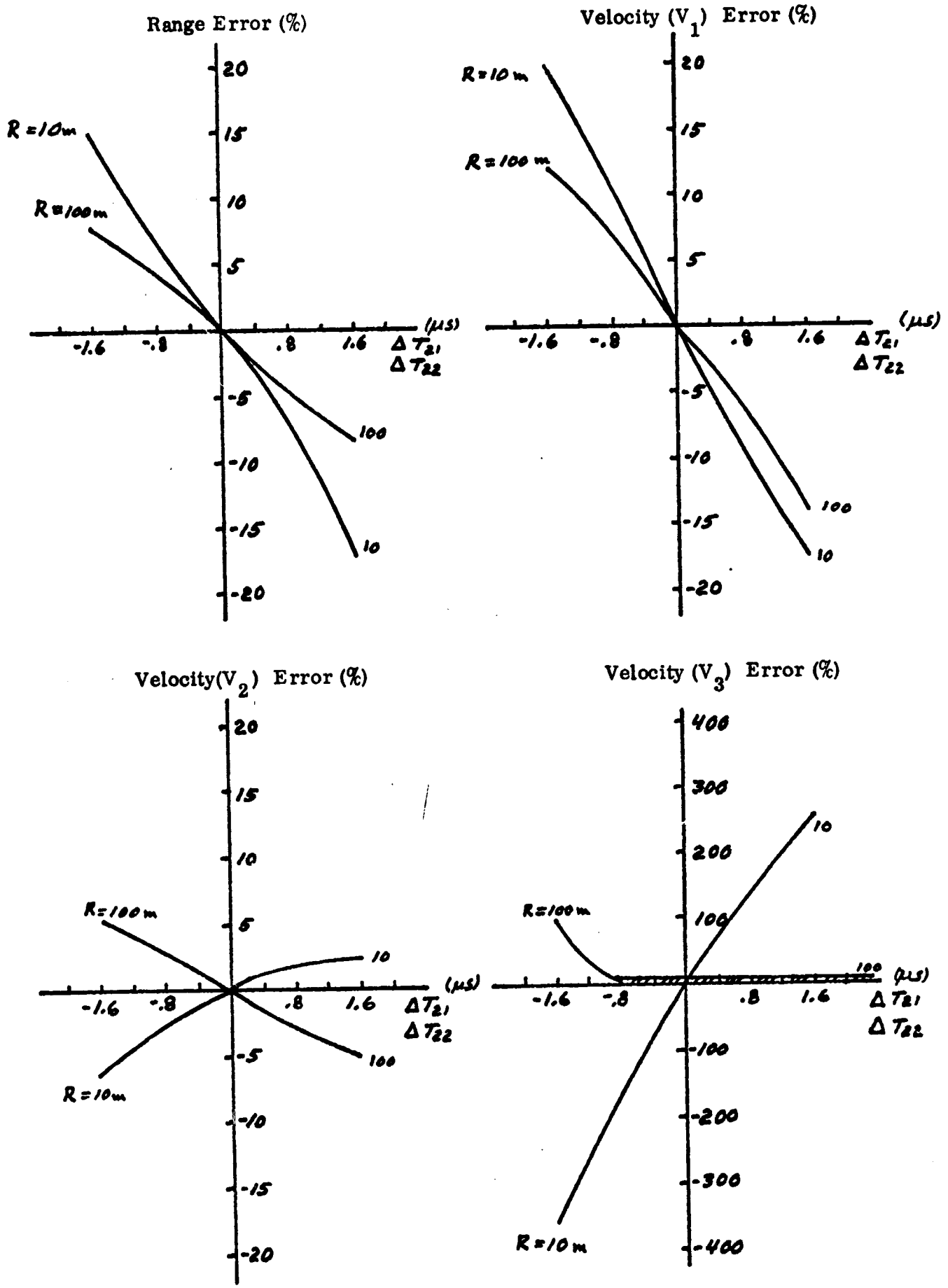

Figure 5. Effect of changing entrance and exit time of channel 2 (transit time remain constant)

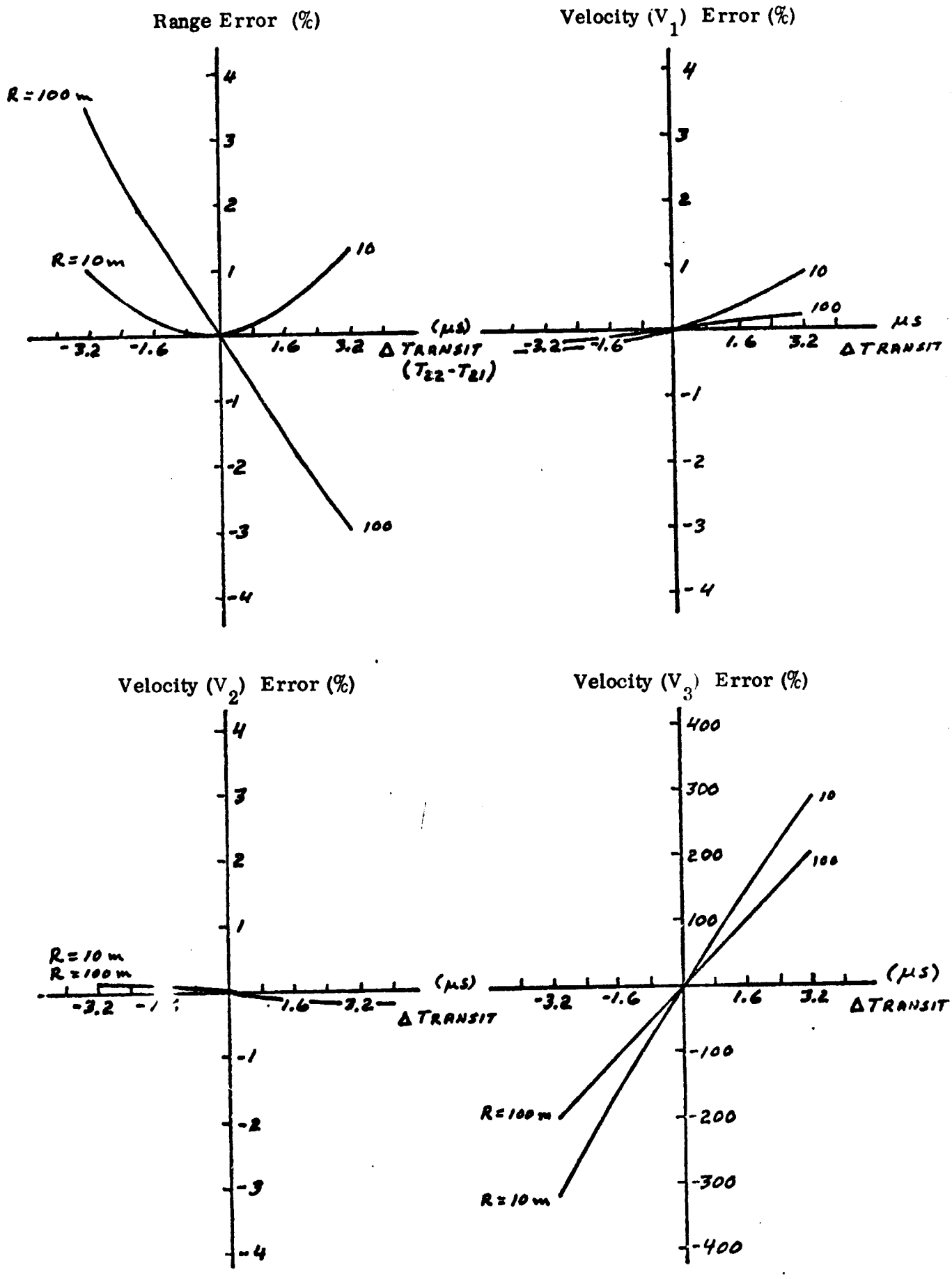

Figure 5. Effects of changing transit time of channel 2.

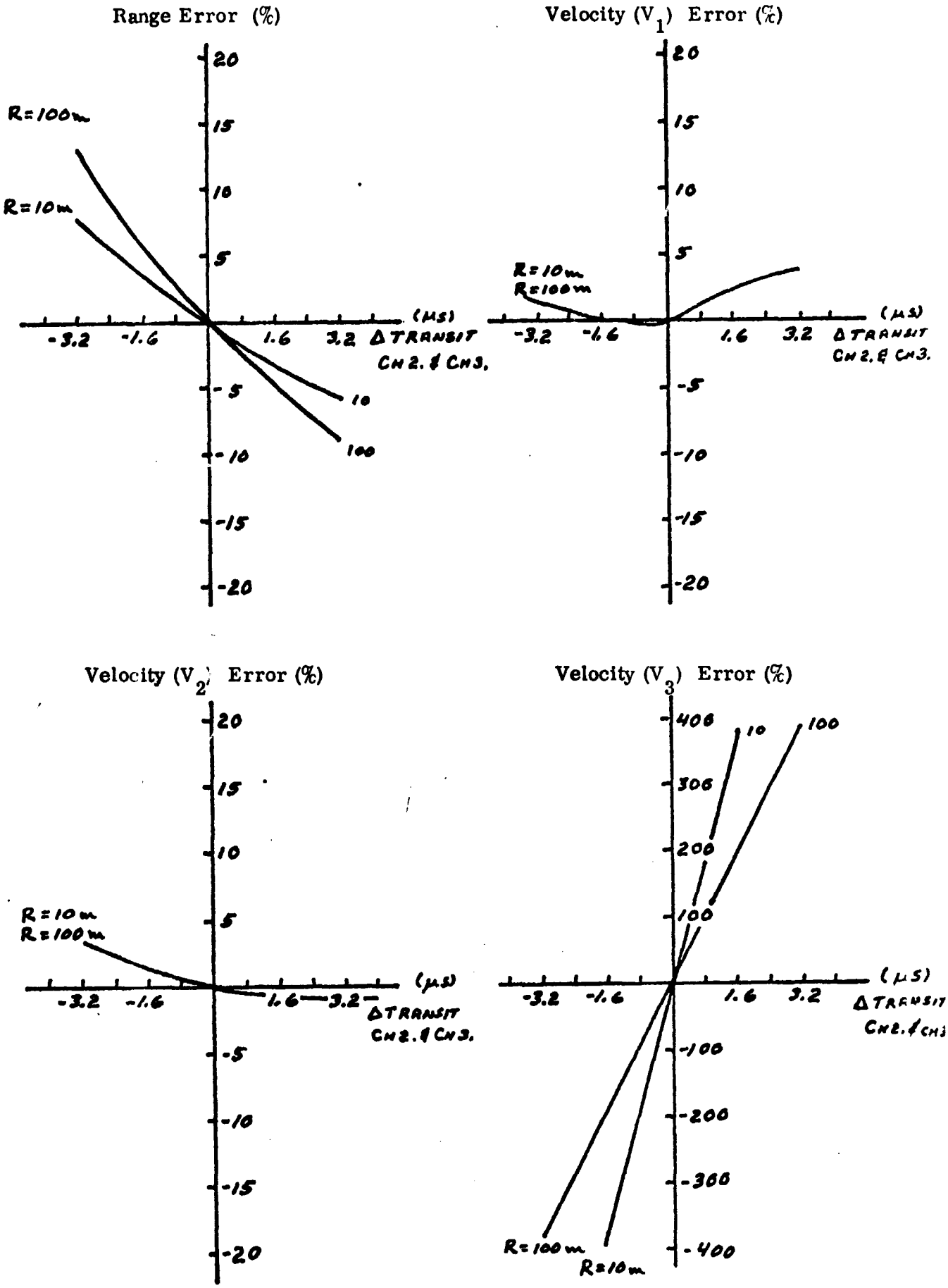

Figure 7. Effect of changing transit time of channels 2 and 3.

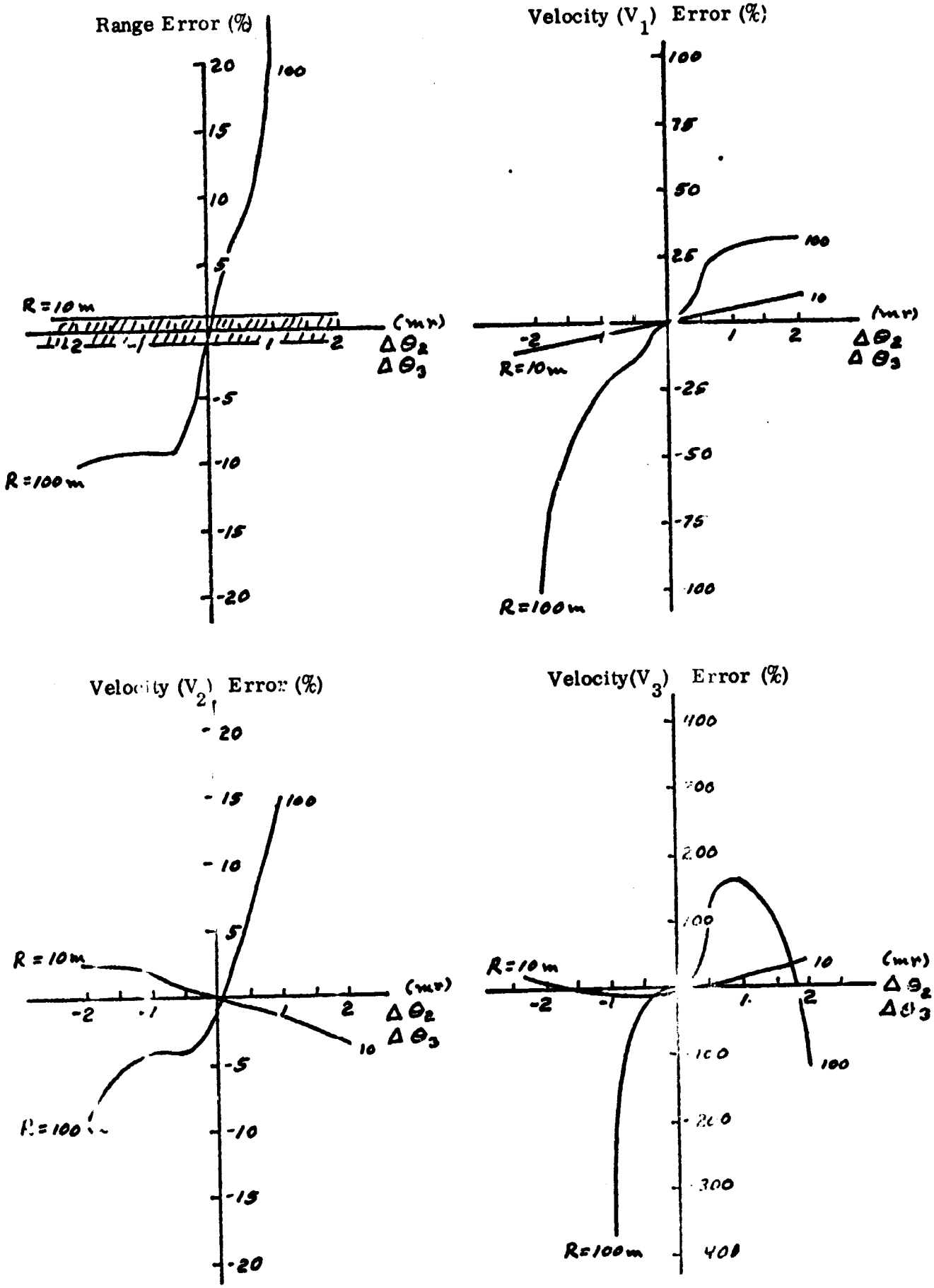

igu 8. Effect of changing the misalignment angles (θ_2 & θ_3)

any misalignment error is magnified as the range increases, and the effect is similar to that caused by an uncertainty in the differential time. However, if the misalignment is accurately known, angles of up to one degree can be compensated for by using the MISSYS program.

In light of the preceding discussion what type of accuracy can be expected from the current Sisyphus system? The electronics of the present system will be capable of measuring the times to within $\pm$ 0.4 μs, and it is expected that accuracies of $\pm$ 0.1 mr, will be obtained on the misalignment measurements. Assuming that the trends indicated by Figures 3 to 8 are realistic, the errors in range should not exceed 5%, while a smaller error (approximately 2.5%) can be expected in the radial velocity components. The axial velocity component, however, may be in error by a factor of 2.

V. Recommendations for Improving Accuracy

It is apparent that the most critical parameter is the differential time. An obvious method of reducing the percentage error in this measurement is to increase the separation distance between the optical systems. It is felt that the present separation distance of 8.5 inches can easily be increased by a factor of four. This modification together with an improved accuracy in the time measurement (to perhaps $\pm$ .2 μs) would result in an overall improvement factor of 8. Thus, the errors in the measured axial velocity component could be reduced to approximately 10% while errors in the other measured parameters would be reduced by a smaller amount. These improvements will require an increase in size and weight over the specified Asteroid/Meteoroid Detector package as used on the Pioneer vehicles.

VI. Breadboard Error Analysis

During the testing of the Sisyphus breadboard, a large error was obtained for the axial velocity component while acceptable values were returned for the other parameters. This large error was primarily due to the limitations of the spherical optics used in the system. The specific limitations and their effects are:

1. Poor definition of the field of view which introduced uncertainties in the measured entrance and exit times.
2. Poor definition of the field of view which introduced uncertainties in the alignment.

The edge of the field of view could only be measured to $\pm$ 0.2 inch, which, for a light spot of 2 mm diameter, traveling at a velocity of 20 km/s, would result in a time uncertainty of approximately $\pm$ 0.2 μ s. Thus, the uncertainty in any differential time measurement could have been as much as $\pm$ .4 μ s. Similarly, the misalignment measurement would be in error by $\pm$ 0.2 inch,which, at a range of approximately 200 inches,translates into an error of $\pm$ 1 mrad.

Referring to Figures 3 - 8, it can be seen that these large uncertainties would, indeed, produce a correspondingly large error in the axial velocity. Thus, the observered deviation of V_3 from the correct value by a factor of 3 is not unexpected. The optics used in the Pioneer system are expected to improve the imaging characteristics by a factor of 3 which will reduce the inaccuracies in time and misalignment measurement.

VII. Programs

The following pages contain the programs which have been used in carrying out the error analysis of the misaligned Sisyphus solution:

```
$LIST SISYPHUS

04/27/70  23.388

00010 *      THE "SISYPHUS" PROGRAM GIVES THE SOLUTION FOR AN ALIGNED
00020 *      SISYPHUS HAVING AN EQUILATERAL BASE.
00030 *      ....INPUTS:
00040 *             ALFA - CONE HALF ANGLE IN DEGREES
00050 *             EL - CONE SEPARATION DISTANCE
00060 *             TAU(I,J) - TIME OF ENTRANCE (J=1) OR EXIT (J=2)
00070 *                        AT THE I-TH CONE
00080 *      ..........................................................
00090        DIMENSION TAU(3,2),H(3,2),COF(4),ETAT(3),CSI(3),V(3)
00100        NAMELIST/DATAS/ALFA,EL/TIMES/TAU
00110        READ DATAS
00120        ALFA=3.14159*ALFA/180.0
00130        READ TIMES
00140        TNAL = TAN(ALFA)
00150        DO 90 J=1,3
00160        DO 89 K=1,2
00170 89     H(J,K)=(TAU(J,K)-TAU(1,1))/TNAL
00180 90      CONTINUE
00190        A=(H(2,1)+H(2,2)-H(1,2))/H(1,2)
00200        B=(H(3,1)+H(3,2)-H(1,2))/H(1,2)
00210        F=4.*H(2,1)*H(2,2)/H(1,2)**2
00220        G=4.*H(3,1)*H(3,2)/H(1,2)**2
00230        D=EL/TNAL
00240        P1=(2.*B-A)*G+(2.*A-B)*F
00250        P2=A+B+3.
00260        P3=4./3.*(A**2-A*B+B**2)
00270        P4=F**2-F*G+G**2
00280        P5=G+F
00290        VD=2.*D/(P3*H(1,2))
00300        CNF=-(B*F-A*G)**2
00310        COF(1)=((1./3.)*(P1-P2*P3)**2)/CNF
00320        COF(2)=(P1**2-4./3.*P1*P2*P3-P3*P4+1./3.*(P2*P3)**2
00330 &      +P5*P3**2-P3**3)/CNF
00340        COF(3)=(P1**2-2./3.*P1*P2*P3-2.*P3*P4+P5*P3**2)/CNF
00350        COF(4)=1.
00360        CALL DOWNH(COF,3,ETAT,CSI)
00370        DO 111 I=1,3
00380        IF(CSI(I)) 105,111,105
00390 105    ETAT(I)=-1.
00400 111    CONTINUE
00410        K=0
00420        IF (ETAT(1)) 120,120,115
00430 115    ETA=ETAT(1)
00440        K=1
00450 120    IF(ETAT(2))130,130,125
00460 125    IF(K) 127,127,899
00470 127    ETA=ETAT(2)
00480        K=1
00490 130    IF(ETAT(3))140,140,135
00500 135    IF(K) 137,137,899
```

```
00510 137    ETA=ETAT(3)
00520        K=1
00530 140    IF(K) 896,896,142
00540 142    ET=ETA+1.
00550        V(1)=VD*(2.*B-A)*ET/SQRT(3.)
00560        V(2)=VD*A*ET
00570        Q=P1*ET-P2*P3
00580        IF (Q) 150,160,170
00590 150    V(3)=VD*SQRT(P3*ET*ETA)
00600        GO TO 180
00610 160    V(3)=0.
00620        GO TO 180
00630 170    V(3)=-VD*SQRT(P3*ET*ETA)
00640 180    CONTINUE
00650        IF(V(3))190,200,190
00660 190    CSLM=(SQRT(3.)*((2.*G-F)*ET-P3)*V(3))/(2.*VD*ET*Q)
00670        SNLM=(3.*(F*ET-P3)*V(3))/(2.*VD*ET*Q)
00680        HLAM=ATAN2(SNLM,CSLM)
00690        GO TO 210
00700 200    C1=(2.*G-F)*ET-P3
00710        C2=F*ET-P3
00720        C3=-C2*SQRT(3.)
00730        C4=-C1
00740        IF(C1)204,206,204
00750 204    HLAM=ATAN2(C3,C4)
00760        GO TO 210
00770 206    IF(-C2)207,898,208
00780 207    HLAM=-3.14159/2.
00790        GO TO 210
00800 208    HLAM=3.14159/2.
00810 210    CONTINUE
00820        Q2=V(1)*CSLM+V(2)*SNLM-V(3)
00830        IF(Q2) 220,897,220
00840 220    R11=-(V(1)**2+V(2)**2-V(3)**2)*H(1,2)/(2.*Q2)
00850        V(3)=V(3)/TNAL
00860        HLAM = HLAM*180./3.14159
00870        PRINT:"       RANGE          SIN(PHI)         COS(PHI)"
00880        PRINT:R11,SNLM,CSLM
00890        PRINT:"          V1               V2               V3"
00900        PRINT:V(1),V(2),V(3)
00905        PRINT 3
00907      3 FORMAT (///)
00910        GO TO 700
00920 896    PRINT:"THERE ARE NO POSITIVE ROOTS"
00930        GO TO 700
00940 897    PRINT:"THE ENTRANCE RANGE IS INFINITE"
00950        GO TO 700
00960 898    PRINT:"ERROR--BOTH SINE AND COSINE ARE ZERO"
00970        GO TO 700
00980 899    PRINT:"THERE ARE NO POSITIVE ROOTS"
00990 700    STOP
01000        END
```

```
$LIST MISTIMES

04/27/70  23.668

00010 *   THE PROGRAM "MISTIMES" WILL CALCULATE THE ENTRANCE AND
00020 *   EXIT TIMES FOR A PARTICLE PASSING THROUGH THE MISALIGNED
00030 *   SISYPHUS SYSTEM WHEN THE SYSTEM AND TRAJECTORY PARAMETERS
00040 *   ARE KNOWN.  THE INPUTS ARE:
00050 *
00060 *      V1 (VELOCITY COMPONENT--M/S)
00070 *      V2 (VELOCITY COMPONENT--M/S)
00080 *      V3 (VELOCITY COMPONENT--M/S)
00090 *      R  (PARTICLE RANGE--M)
00100 *      DA (APERTURE SEPARATION--M)
00110 *      ALFA (OPTICAL FIELD OF VIEW,HALF ANGLE--DEGREES)
00120 *      PHI (ENTRANCE ANGLE--DEGREES)
00130 *      LAM (ANGLE BETWEEN OPTICS--DEGREES)
00140 *      TH2,GAM2,TH3,GAM3 (MISALIGNMENT ANGLES--RADIANS)
00150 *
00160        REAL LAM
00170        DIMENSION X(3),T(2),U(2)
00180        PRINT: "ENTER V1,V2,V3,R"
00190        READ: V1,V2,V3,R
00200        PRINT: "ENTER DA,ALFA,PHI,LAM"
00210        READ: DA,ALFA,PHI,LAM
00220        ALFA=3.14159*ALFA/180.0; PHI=3.14159*PHI/180.0
00230        LAM=3.14159*LAM/180.0
00240        PRINT: "ENTER TH2,GAM2,TH3,GAM3"
00250        READ: TH2,GAM2,TH3,GAM3
00260        F1=TAN(ALFA); F2=COS(ALFA); F3=SIN(ALFA); F4=SIN(GAM2)
00270        F5=COS(GAM2); F6=SIN(TH2); F7=COS(TH2); F8=COS(PHI)
00280        F9=SIN(PHI); F10=SIN(-GAM3); F11=SIN(TH3); F12=COS(TH3)
00290        F13=COS(-GAM3); F14=SIN(GAM3); F15=COS(GAM3)
00300        F16=SIN(LAM); F17=COS(LAM); F18=SIN(-GAM2)
00310        F19=COS(-GAM2)
00320        YL=DA; YM=DA
00330        B1=-(V1**2+V2**2)+(V3*F1)**2
00340        C1=-2.*R*F3*(V1*F8+V2*F9)+2.*R*F2*V3*F1**2.
00350        D1=F1**2.*(R*F2)**2.-(R*F3)**2.
00360        X(1)=D1; X(2)=C1; X(3)=B1
00370        CALL DOWNH(X,2,T,U)
00380        T11=AMIN1(T(1),T(2)); T12=AMAX1(T(1),T(2))
00390        A11=R*(-F3*F8*F10*F11+F3*F9*(-F11*F13)+F2*F12)
00400        B11=(V1*F14-V2*F15)*F11+V3*F12
00410        C11=-YM*F11*(F16*F14-F17*F15)
```

```
00420       A12=F3*F8*F13-F3*F9*F10
00430       B12=V1*F15+V2*F14
00440       C12=-YM*(F16*F15+F14*F17)
00450       A13=F3*F8*F10*F12+F3*F9*F12*F13+F2*F11
00460       B13=-((V1*F14-V2*F15)*F12-V3*F11)
00470       C13=YM*F12*(F16*F14-F15*F17)
00480       D11=A11+C11
00490       D12=R*A12+C12
00500       D13=R*A13+C13
00510       D1=(D11*F1)**2-D12**2-D13**2
00520       B1=(B11*F1)**2-B12**2-B13**2
00530       C1=2.*D11*B11*F1**2.-2.*(D12*B12+D13*B13)
00540       X(1)=D1; X(2)=C1; X(3)=B1
00550       CALL DOWNH(X,2,T,U)
00560       T31=AMIN1(T(1),T(2)); T32=AMAX1(T(1),T(2))
00570       A21=R*(-F3*F8*F18*F6+F3*F9*(-F6*F19)+F2*F7)
00580       B21=(V1*F4-V2*F5)*F6+V3*F7
00590       C21=YL*F5*F6
00600       A22=F3*F8*F19-F3*F9*F18
00610       B22=V1*F5+V2*F4
00620       C22=-YL*F4
00630       A23=F3*F8*F18*F7+F3*F9*F7*F19+F2*F6
00640       B23=-((V1*F4-V2*F5)*F7-V3*F6)
00650       C23=-YL*F5*F7
00660       D21=A21+C21
00670       D22=R*A22+C22
00680       D23=R*A23+C23
00690       D2=(D21*F1)**2-D22**2-D23**2
00700       B2=(B21*F1)**2-B22**2-B23**2
00710       C2=2.*D21*B21*F1**2.-2.*(D22*B22+D23*B23)
00720       X(1)=D2; X(2)=C2; X(3)=B2
00730       CALL DOWNH(X,2,T,U)
00740       T21=AMIN1(T(1),T(2)); T22=AMAX1(T(1),T(2))
00750       PRINT: "T11=",T11,"   T12=",T12
00760       PRINT: "T21=",T21,"   T22=",T22
00770       PRINT: "T31=",T31,"   T32=",T32
00780       PRINT 20
00790    20 FORMAT (///)
00800       STOP
00810       END
```

```
$LIST MISSYS

04/27/70  23.056

00010 *      THE "MISSYS" PROGRAM GENERATES THE SOLUTION FOR THE
00020 *      MISALIGNED SISYPHUS USING THE SECANT METHOD FOR
00030 *      SOLUTION OF NON-LINEAR EQUATIONS. AN INITIAL ESTIMATE
00040 *      OF THE VARIABLES (RANGE,X(1)),(SIN(PHI),X(2)),(COS(PHI),
00050 *      X(3)),(V1,X(4)),(V2,X(5)),AND (V3,X(6)) IS REQUIRED. THIS
00060 *      ESTIMATE CAN BE OBTAINED FROM THE ALIGNED SISYPHUS
00070 *      SOLUTION USING THE "SISYPUS" PROGRAM.
00080 *      ....INPUTS:
00090 *            ALFA - CONE HALF ANGLE IN DEGREES
00100 *            XLL - CONE SEPARATION DISTANCE
00110 *            TH2,GAM2,TH3,GAM3 - CONE MISALIGNMENT IN RADIANS
00120 *            TIJ - TIME OF ENTRANCE (J=1) OR EXIT (J=2) AT
00130 *                  THE I-TH CONE
00140 *            NI - NUMBER OF INTERATIONS
00150 *            CC - CONVERGENCE CRITERIA
00160 *      ..........................................................
00170        COMMON XLL,T12,T21,T22,T31,T32,A1,A2,A3,A4,A5,
00180 &      A6,A7,A8,A9,A10,A11,B1,B2,B3,B4,B5,B6,B7,B8,B9,B10,B11,B12,
00190 &      B13,B14,B15,B16,C1,C2,C3,C4,C5,C6,C7,C8,C9,C10,C11,C12,C13
00200        EXTERNAL EVAL
00210        DIMENSION X(7),F(7),Q(7),Z(7),S(7),G(7,7),Y(7,7)
00220        NAMELIST/CONFIG/ALFA,XLL,TH2,GAM2,TH3,GAM3/
00230 &      TIMES/T11,T12,T21,T22,T31,T32/ESTIM/X/INTER/NI,CC
00235        READ INTER
00240        READ CONFIG
00245        ALFA=ALFA*3.14159/180.
00250        READ TIMES
00260        READ ESTIM
00280        T12=T12-T11
00290        T21=T21-T11
00300        T22=T22-T11
00310        T31=T31-T11
00320        T32=T32-T11
00340        A1=SIN(ALFA)
00350        A2=COS(ALFA)
00360        A3=A1/A2
00370        A4=SIN(TH2)
00380        A5=COS(TH2)
00390        A6=SIN(GAM2)
00400        A7=COS(GAM2)
00410        A8=SIN(TH3)
00420        A9=COS(TH3)
00430        A10=SIN(GAM3)
00440        A11=COS(GAM3)
00450        B1=A1*A3*A8*A10
```

```
00460         B2=A1*A3*A8*A11
00470         B3=A2*A3*A9
00480         B4=A3*A8*A10
00490         B5=A3*A8*A11
00500         B6=A3*A9
00510         B7=A3*A8
00520         B8=A1*A11
00530         B9=A1*A10
00540         B10=A1*A10*A9
00550         B11=A1*A9*A11
00560         B12=A2*A8
00570         B13=A9*A10
00580         B14=A9*A11
00590         B15=XLL/2.*(A11-SQRT(3.)*A10)
00600         B16=XLL/2.*(SQRT(3.)*A11+A10)
00610         C1=A1*A3*A4*A6
00620         C2=A1*A3*A4*A7
00630         C3=A2*A3*A5
00640         C4=A3*A4*A6
00650         C5=A3*A4*A7
00660         C6=A3*A5
00670         C7=A1*A7
00680         C8=A1*A6
00690         C9=A1*A5*A6
00700         C10=A1*A5*A7
00710         C11=A2*A4
00720         C12=A5*A6
00730         C13=A5*A7
00740         N=6
00750         CALL SECANT(N,NI,CC,FM,X,F,Q,Z,S,G,Y,7,EVAL,IERR)
00760         IF(IERR.EQ.1)GO TO 100
00770         IF(IERR.EQ.2)GO TO 200
00780         PRINT:"NORMAL  RETURN"
00790         PRINT 600
00800         PRINT:"      RANGE          SIN(PHI)         COS(PHI)"
00810         PRINT:X(1),X(2),X(3)
00820         PRINT:"         V1              .V2              V3"
00830         PRINT:X(4),X(5),X(6)
00840         PRINT70
00850         PRINT:(F(I),I=1,N)
00860         GO TO 800
00870 100     PRINT:"MATRIX INVERSION HAS DETERIORATED"
00880         PRINT:600
00890         PRINT:"      RANGE          SIN(PHI)         COS(PHI)"
00900         PRINT:Z(1),Z(2),Z(3)
```

```
00910         PRINT:"          V1                V2                V3"
00920         PRINT:Z(4),Z(5),Z(6)
00930         PRINT 700
00940         PRINT:(F(I),I=1,N)
00950         GO TO 800
00960 200     PRINT:"MAXIMUM NUMBER OF INTERATIONS EXCEEDED"
00970         PRINT 600
00980         PRINT:"       RANGE           SIN(PHI)          COS(PHI)"
00990         PRINT:X(1),X(2),X(3)
01000         PRINT:"          V1                V2                V3"
01010         PRINT:X(4),X(5),X(6)
01020         PRINT 700
01030         PRINT:(F(I),I=1,N)
01035         PRINT 6
01037       6 FORMAT (///)
01040 600     FORMAT(//" SOLUTION VECTOR"//)
01050 700     FORMAT(//" FUNCTION VECTOR"//)
01060 800     STOP
01070         END
01080         SUBROUTINE EVAL(F,X)
01090         COMMON XLL,T12,T21,T22,T31,T32,A1,A2,A3,A4,A5,
01100 &       A6,A7,A8,A9,A10,A11,B1,B2,B3,B4,B5,B6,B7,B8,B9,B10,B11,B12,
01110 &       B13,B14,B15,B16,C1,C2,C3,C4,C5,C6,C7,C8,C9,C10,C11,C12,C13
01120         DIMENSION X(7),F(7)
01130         F(1)=X(2)**2+X(3)**2-1.
01140         F(2)=2.*X(1)*A1*(X(3)*X(4)+X(2)*X(5)-X(6)*A3)
01150 &       +(X(4)**2+X(5)**2-X(6)**2*A3*A3)*T12
01160         F(3)=(X(1)*(X(3)*B1-X(2)*B2+B3)+T31*(X(4)*B4-X(5)*B5
01170 &       +X(6)*B6)+B7*B15)**2-(X(1)*(X(3)*B8+X(2)*B9)
01180 &       +T31*(X(4)*A11+X(5)*A10)-B16)**2-(X(1)*(-X(3)*B10
01190 &       +X(2)*B11+B12)-T31*(X(4)*B13-X(5)*B14-X(6)*A8)
01200 &       -A9*B15)**2
01210         F(4)=(X(1)*(X(3)*B1-X(2)*B2+B3)+T32*(X(4)*B4-X(5)*B5
01220 &       +X(6)*B6)+B7*B15)**2-(X(1)*(X(3)*B8+X(2)*B9)+T32*(X(4)*A11
01230 &       +X(5)*A10)-B16)**2-(X(1)*(X(3)*(-B10)+X(2)*B11+B12)
01240 &       -T32*(X(4)*B13-X(5)*B14-X(6)*A8)-A9*B15)**2
01250         F(5)=(X(1)*(X(3)*C1-X(2)*C2+C3)+T21*(X(4)*C4-X(5)*C5
01260 &       +X(6)*C6)+XLL*C5)**2-(X(1)*(X(3)*C7+X(2)*C8)+T21*(X(4)*A7
01270 &       +X(5)*A6)-XLL*A6)**2-(X(1)*(-X(3)*C9+X(2)*C10+C11)
01280 &       -T21*(X(4)*C12-X(5)*C13-X(6)*A4)-XLL*C13)**2
01290         F(6)=(X(1)*(X(3)*C1-X(2)*C2+C3)+T22*(X(4)*C4-X(5)*C5
01300 &       +X(6)*C6)+XLL*C5)**2-(X(1)*(X(3)*C7+X(2)*C8)+T22*(X(4)*A7
01310 &       +X(5)*A6)-XLL*A6)**2-(X(1)*(X(3)*(-C9)+X(2)*C10+C11)
01320 &       -T22*(X(4)*C12-X(5)*C13-X(6)*A4)-XLL*C13)**2
01330         RETURN
01340         END
```